

Photosynthetic Light Reactions at the Gold Interface Kamran, M.

Citation

Kamran, M. (2014, May 7). *Photosynthetic Light Reactions at the Gold Interface*. Casimir PhD series, Delft-Leiden. Retrieved from https://hdl.handle.net/1887/25580

Version: Not Applicable (or Unknown)

License: <u>Leiden University Non-exclusive license</u>

Downloaded from: https://hdl.handle.net/1887/25580

Note: To cite this publication please use the final published version (if applicable).

Cover Page



Universiteit Leiden



The handle http://hdl.handle.net/1887/25580 holds various files of this Leiden University dissertation

Author: Kamran, Muhammad **Title:** Photosynthetic light reactions at the gold interface

Issue Date: 2014-05-07

Photosynthetic Light Reactions at the Gold Interface

Proefschrift

ter verkrijging van de graad van Doctor aan de Universiteit Leiden, op gezag van Rector Magnificus prof.mr. C.J.J.M. Stolker, volgens besluit van het College voor Promoties te verdedigen op woensdag 7 mei 2014 klokke 13:45 uur

door

Muhammad Kamran geboren te Rawalpindi, Pakistan in 1981

Promotiecommissie:

Promotor: Prof. dr. T.J. Aartsma Universiteit Leiden

Co-promotor: Dr. R.N. Frese Vrije Universiteit, Amsterdam

Overige Leden: Prof. dr. E.R. Eliel Universiteit Leiden

Prof. dr. G.W. Canters Universiteit Leiden

Prof. dr. ir. T.H. Oosterkamp Universiteit Leiden

Prof. dr. J. Matysik University of Leipzig, Germany

Dr. M. Jones University of Bristol, UK

Dr. H.J. van Gorkom Universiteit Leiden

Casimir PhD series, Delft-Leiden 2014-12

ISBN: 978-90-8593-187-4

Financial support for this project was provided by the Higher Education Commission (HEC) of Pakistan in the form of a student fellowship.

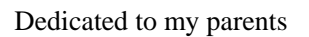


Table of Contents

1.	Intro	oduction	1
	1.1	Interfacing	2
		1.1.1 This work	3
	1.2	Photosynthesis	4
		1.2.1 Bacterial photosynthesis	4
		1.2.2 Light harvesting 2 (LH2) complex	6
		1.2.3 The RC-LH1 complex	8
		1.2.4 Reaction center (RC) complex	10
		1.2.5 RC mutants	11
		1.2.6 2D crystals of LH2 and RC-LH1 complexes	11
	1.3	Experimental techniques	12
		1.3.1 Atomic Force Microscopy (AFM)	12
		1.3.2 Conductive Atomic Force Microscopy (C-AFM)	13
		1.3.3 Langmuir Blodgett deposition	14
		Photoelectrochemistry	18
	Ref	erences	20
2.	Ele	ctron tunneling and electron transfer of 2D crystals	
	of F	RC-LH1 complexes on a gold electrode	25
	2.1	Introduction	26
	2.2	Materials and methods	30
	2.3	Results	33
		2.3.1 2D crystals of LH2	34
		2.3.2 2D crystals of RC-LH1	37
		2.3.3 Light induced electron transfer	40
	2.4	Discussion	44
	2.5	Conclusion	48
	Ref	erences	49
3.	Pho	otosynthetic protein complexes as bio-photovoltaic	
		ding blocks with a high internal quantum efficiency	55
	3.1	Introduction	57
		Materials and methods	59
	·-	3.3.1 Photocurrent measurements	61
	3.3	Results and discussion	61
		Conclusion	66
		erences	66
		S Supporting Information	71

4 .	Role of co-factors in electron tunneling in bacterial RCs on a bare gold electrode		
	4.1 Introduction	81	
	4.2 Materials and methods		
	4.3 Results	86	
	4.3.1 Monolayers of RC-containing membrane fragments	87	
	4.3.2 Monolayers of RC variants	92	
	5.0 Discussion		
	6.0 Conclusion	99	
	References	99	
	Summary	103	
	Samenvatting	107	
	Acknowledgments	111	
	Curriculum Vitae	113	

CHAPTER 1

Introduction

1.1 Interfacing

Biomolecular components are being explored as building blocks for materials and devices for a variety of purposes, at a rapidly increasing rate. This development is gaining momentum because it is at the core of bionanotechnology which is a major focus of current research across the globe. Significant research activities in this field are aimed at the integration of macromolecules of biological origin with electronic circuits, based on the assumption that this will ultimately provide the elementary basis for the design of novel bioelectronic devices. Redox-active proteins and enzymes in particular have a natural propensity for interaction by exchange of electrons. Recent applications of photosensitive enzymes and proteins, for example, have shown their potential in solar energy conversion, optical memories, optical bioswitches, electronic gates and biological actinometers. The scope of interfacing can be extended to three dimensions to enhance functional sensitivity and selectivity. Use of biocomponents for the construction of functionalized electronic devices may in principle offer advantages compared to classical semi-conductor technology, such as

- * miniaturisation down to nanometer scale and even single molecule level,
- * extreme sensitivity and specificity both with respect to external stimuli and with respect to enzymatic conversion.
- * self organising and self-repair capacity,
- * versatility of engineering by modern molecular genetic and biochemical methods *in vivo* and *in vitro*, in addition to solid state chemical/physical techniques.
- * selectivity based on function or shape, also in a non-enzymatic sense.

There are significant complicating factors, however, that need to be addressed, as well as interfacing problems that must be solved, in order to be able to take full advantage of the technology that is available. In particular, direct electrical communication between enzyme and electrode is often prohibited, since the active site at which catalytic transformation occurs is buried deep in the protein, and there may be no natural relay system (a series of electron-transfer centers, each separated by 15Å or less) to mediate electrons to and from the surface. In effect, the active site is then electrically isolated from the electrode by the protein matrix. Furthermore, direct modification of electrically conducting support by proteins

often leads to denaturation of the protein layer that is in direct contact with the electrode. Because electron tunneling depends on distance and medium, it is essential to control alignment and orientation of the redox enzyme with respect to the conductive support. Even if there is surface exposure of the active site (unlikely) or a relay center, the protein orientation may be unfavorable for direct electron exchange with the electrode.

The interfacing of biomolecules to substrates such as metal electrodes is, therefore, a central issue in bionanoscience. Typically, a bioelectronic device, e.g., a biosensor or a biofuel cell, consists of an assembly of redox-active proteins on a conducting electrode such that their biocatalytic activity can be transformed into a measurable output signal by electronic transduction. Direct coupling of the bioactive redox enzyme or protein to an electrode offers important advantages from a technological point of view in terms of efficiency, reactivity, specificity, selectivity and sensitivity. Much research is aimed at optimizing electrical contact, at biocompatibility of the interface, and at control over alignment and orientation of the surface-assembled biomolecules. To achieve further progress it is necessary to improve the protocols for immobilization and mono-layer formation of biomolecules on electrode surfaces. Furthermore, it may be advantageous to engineer a linker between the electrode and the biomolecules as a conduit for electrons, improving electrical contact.

1.1.1 This work:

In the project described in this thesis we studied a simple bio-electronic device for solar energy conversion by surface-assembly of photosynthetic pigment-protein complexes on a bare gold-electrode. Optical excitation of the photosynthetic pigments gives rise to charge separation in the so-called reaction center complex. Energy conversion is completed by subsequent electron transfer to the electrode, generating a light-induced electric current.

Such a device allows us to address a number of questions directly related to bioinspired solar energy conversion:

- How can biology be interfaced with electronic, mechanical and optical systems?
- Specifically, what is the energy conversion efficiency of such an optimized device?

- Does the intrinsic photostability of photosynthetic systems lead to enhanced performance?
- Can general design criteria for bio-inspired energy conversion be derived or tested?

1.2 Photosynthesis

Photosynthesis is a process of solar energy absorption and conversion into chemical form for storage by an organism, and to drive its metabolic activities. This process is responsible of sustaining life on earth. Photosynthesis is not only associated with plants but also with a large number of other organisms including phytoplankton, algae and photosynthetic bacteria which use the same process to utilize solar energy for cellular processes. Among all these species photosynthetic bacteria have often a relatively simple machinery for solar energy conversion. These organisms, therefore, have been extensively studied as model systems to understand the basics of solar energy absorption, energy transfer and organization of photosynthetic complexes in cell membranes¹⁻⁶. For the work described in this thesis we have used pigment-protein complexes and membrane fragments that were isolated and purified from purple photosynthetic bacteria.

1.2.1 Bacterial Photosynthesis

The components of the bacterial photosynthetic apparatus of purple bacteria are embedded in intracytoplasmic membranes and comprise two types of antenna complexes and a reaction center (RC) complex. They are assisted by the cytochrome *bc1* complex to drive light-induced, proton-coupled electron transfer across the membrane. The antenna complexes are membrane proteins which are referred to as light harvesting complex 1 (LH1) and light harvesting complex 2 (LH2).^{1,7-12} Both are ring-like structures, but the LH1 ring is bigger in size compared to LH2, and accommodates the RC complex in the center. The primary function of the antenna complexes is to capture solar energy and to "feed" the RC complex which utilizes the absorbed photon energy for charge separation. Light is absorbed by the pigments, bacteriochlorophyll *a* and carotenoid molecules, embedded in the antenna. The RC itself contains also light absorbing pigments but their rate of absorption is usually low compared to that of the antenna complexes¹³. Therefore, antenna complexes are very important for optimal energy capture by increasing the absorption cross section.

Figure 1 shows the arrangement of the pigments in the LH1 and LH2 rings. Note that the protein scaffold has been omitted from this figure. Intermolecular interactions are strong because the distances between neighboring pigments is small. This results in very efficient excited state energy transfer within and between the LH complexes as indicated in Figure 1.

The process of light absorption and excitation is optimized by a dense packing of the pigment-protein complexes in intracytoplasmic membrane. The RC-LH1 complex is surrounded by multiple LH2 complexes to increase the absorption cross section and to provide an efficient supply of energy to the RC. The solar energy absorbed by LH2 complex is transferred to neighboring LH2 or LH1 complexes on a picosecond time scale, from where it is funneled to the RC¹⁴. A dimer of bacteriochlorophylls in the RC, called the "special pair", is the terminal receiver of the absorbed solar energy. It is situated close to the periplasmic side of the

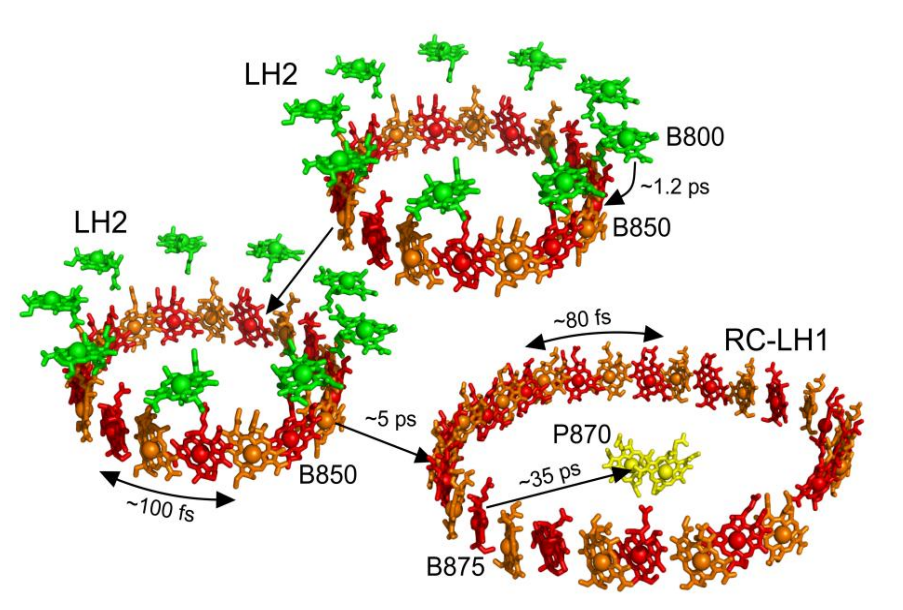


Figure 1: Schematic diagram of the pigment arrangement in a bacterial photosynthetic unit with time scale of energy transfer. Pigments contained in LH2 and LH1 antennas are responsible for the absorption of solar energy which then is transferred to the reaction center (RC) complex via neighboring LH2 and LH1 complexes at a time scale of few tens of picoseconds to initiate a charge separation reaction. The LH2 and RC-LH1 complexes are closely packed in the membrane for efficient functionality. Copyright Dr. M. Jones (Bristol University, UK), used with permission.

membrane. Upon excitation of the special pair a charge separation is induced in the RC, resulting in proton-coupled, trans-membrane electron transfer. A proton gradient gradient is formed across the membrane which drives ATP synthesis.

We utilized photosynthetic pigment protein complexes isolated from two different species of photosynthetic purple bacteria in our study namely, *Rhodobacter (Rb.)* sphaeroides and *Rhodopseudomonas (Rps.)* acidophila. The constituents of the photosystem of *Rb.sphaeroides* have been extensively studied and their structural models have been reported in the literature. This particular species has a very well developed mutagenesis which allows expression of membranes with different compositions of protein complexes, for example variants that contain only LH1, RC, or RC-LH1 complexes. It is also viable to make mutants with missing cofactors or one cofactor replaced with another, while specific residues can be manipulated by site directed mutagenesis. The organization of LH2 and RC-LH1 complexes in native membranes has been visualized by atomic force microscopy (AFM), but the position of the cytochrome *bc*1 complex and ATP synthase are not yet clearly known¹⁵.

1.2.2 Light harvesting 2 (LH2) complexes

The light harvesting complex 2 (LH2) is a membrane protein that is present in purple photosynthetic bacteria. It is a very important component for light absorption by the organism. The LH2 complex consists of two different peptides (α and β) which are arranged in the form of concentric cylinders embedded in the membrane. Bacteriochlorophyll (BChl) a and carotenoid molecules are the cofactors, sandwiched between these two cylinders and non-covalently attached to the protein scaffold. Depending on species the LH2 complex contains eight or nine copies of the $\alpha\beta$ subunit. ^{16,17}

The optical spectra of LH2 are characterized by two strong absorption bands at 850 nm and 800 nm, respectively, which are associated with two different binding sites for BChl a; the corresponding pigments are referred to as B800 and B850 (cf. Figure 1)¹⁸. These BChls are arranged such that the molecular plane of the B850 pigments is perpendicular and that of B800 parallel to the plane of the membrane. LH2 complexes also contain carotenoid molecules in addition to BChl a, which not only increases the absorption cross section of the molecule by absorbing in the visible wavelength region but they also play a very important role by quenching

singlet oxygen or its precursor, thus protecting the photosynthetic system from damage that results from reaction with these harmful species that are formed in the process. ¹⁹⁻²³

There is some variation in the peripheral antenna of different species of purple bacteria. For example, the LH2 complex from *Rhodospirillum molischianum* contains 8 $\alpha\beta$ subunits, while *Rps. acidophila* contains 9. ^{17,24} The LH2 antenna of *Rb. sphaeroides* is in this respect similar to that of *Rps. acidophila*. A high resolution crystal structure of the LH2 complex from *Rps. acidophila* has been reported in the literature ^{16,17}. The structure is schematically shown in Figure 2, with the α and β polypeptides represented as helical structures at the inner and outer perimeter of the ring, respectively. LH2 complexes of various species have also been investigated with high resolution AFM; sub-molecular resolution has been achieved by imaging the LH2 complexes in reconstituted lipid bilayers. ^{10,17,25} Various types of packing of LH2 complexes in artificial lipids have been observed. ^{26,27} In addition, LH2 complexes in native membranes have been visualized under physiological conditions. ^{10,25,28,29}

The ratio of the LH1 and LH2 antennas varies in different species of photosynthetic bacteria³⁰, while some of the species even do not contain LH2 complexes in which

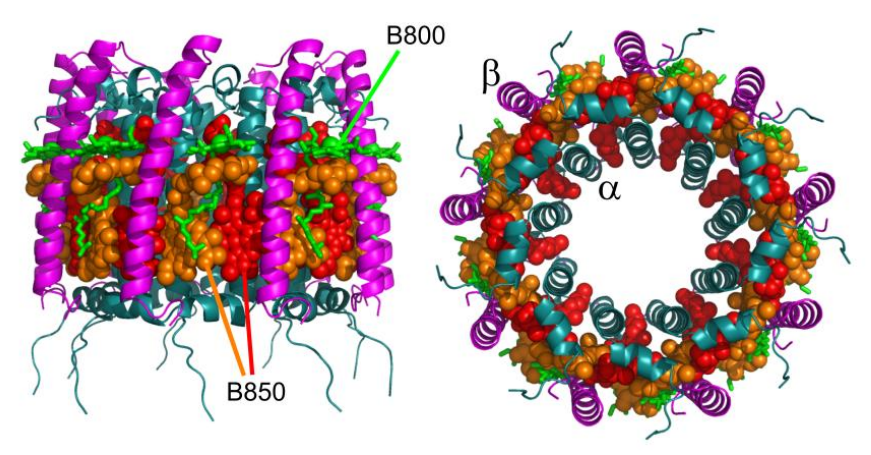


Figure 2: Schematic representation of LH2 complex of Rps. Acidophila (papiz et al., 2003). The right hand side is a top view, showing two concentric cylinders of α and β polypeptides which are indicated by the helical structures, with the cofactors being contained in between these cylinders. At the left is a side view of the LH2 complex; co-factors are shown in different colors for clarity. Copyright Dr. M. Jones (Bristol University, UK), used with permission.

case the function of light absorption and excitation transfer is performed by RC-LH1 complexes only. The ratio of LH2 and LH1 is also dependent on growth conditions of the cells,^{30,31} and it is strongly influenced by the light intensity and the presence of oxygen during growth. The cells grown under high light intensity contain less LH2 complexes compared to cells grown at low-light^{30,31}.

We studied electron tunneling properties of LH2 complexes from *Rps. acidophila* reconstituted in a lipid bilayer the results of which are described in chapter 2 of this thesis. Current voltage curves were recorded by utilizing conductive atomic force microscopy under different contact forces, and results were compared with current-voltage characteristics of RC-LH1 complexes.

1.2.3 Reaction Center-Light Harvesting 1 (RC-LH1) Complex

The RC-LH1 complex is at the core of the photosystem of purple bacteria. This complex is photosynthetically fully competent in terms of light absorption and charge separation in the absence of LH2^{32,33}. The LH1 antenna absorbs light energy in the near-infrared region of the spectrum, at 875 nm. The architecture of the LH1 complex is similar to that of LH2 but the LH1 ring has a bigger size to accommodate the RC, see Figure 3. The subunits of LH1 are heterodimers

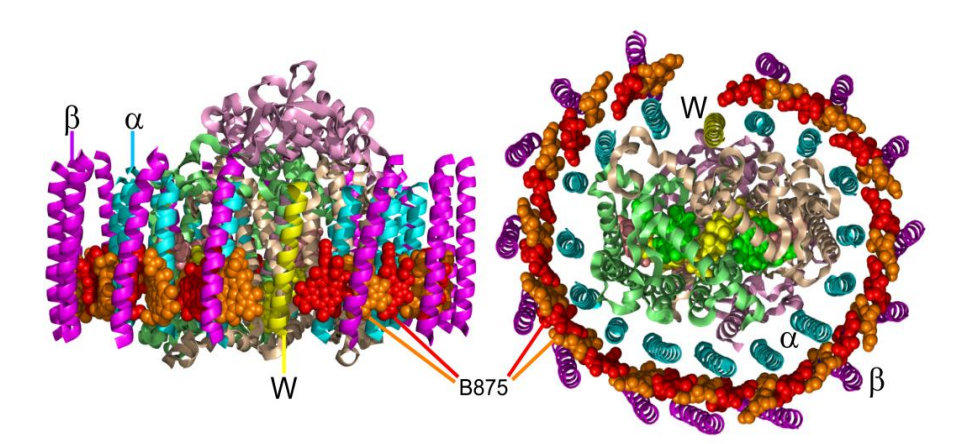


Figure 3: Side view (left) and top view (right) of the RC-LH1 complex. The co factors are sandwiched between the two concentric cylinders formed by the α and β peptides which are shown as helical structures. PufX is represented by a yellow color in the side view (W in the top view), replacing one pair of α , β peptides; this gap (W) provides a gateway for the mobility of the quinol. Copyright Dr. M. Jones (Bristol University, UK), used with permission.

comprised of two types of peptides, α and β . Like in LH2, the α and β polypeptides are arranged in the form of two concentric cylinders, α forming the inner and β the outer cylinder. LH1 contains around 15 pairs of α and β polypeptides. BChl a and carotenoid molecules are the cofactors in this protein complex. The BChl a molecules in LH1 are arranged in a ring, two per $\alpha\beta$ subunit, with the molecular plane perpendicular to the plane of the membrane. The high resolution crystal structure of RC-LH1 complex is not (yet) available; the most detailed structure is from *Rps. palustris* with a resolution of 4.8 Å. 34 In *Rb. sphaeroides* the RC-LH1 complex has a dimeric structure with two joint LH1-rings each containing one RC¹.

LH2 and RC-LH1 complexes are organized in two-dimensional (2D) networks with different packings depending on species^{1,31}. The solar energy absorbed by LH2 and LH1 complexes is transferred to the RC, where charge separation results in reduction of ubiquinone to quinol at the so-called Q_B site (see Figure 4). The exchange of quinol with the ubiquinone pool present in the lipid bilayer facilitates the next step in the cyclic electron transport, i.e. the reduction of cytochrome bc1. This exchange step implies that a mechanism must exist for quinol to pass the barrier formed by the LH1 complex: either the peptide ring should be flexible enough to let the quinol through or there should be an opening in the structure, i.e., a gap that allows the quinol to escape. The proposed gap in the LH1 ring was supported by the discovery of a protein, pufX, in Rb. sphaeroides, which was assumed to replace one of the αβ subunits in LH1^{35,36}. This conjecture was later confirmed by X-ray analysis³⁴. There is no structural information of RC-LH1 from Rps .acidophila so far but the spectral properties of the complex resemble those of Rps. palustris; probably both complexes can be described by the same structural model. 37-39 The structure model of RC-LH1 from Rps. palustris is depicted in figure 3. RC-LH1 complexes from different species have been visualized in native membranes by using high resolution AFM. This complex has been successfully reconstituted in artificial lipid bilayer while keeping it functionally intact. 32,40

1.2.4 Reaction Center (RC) complex

The RC complex has a key role in the photosynthetic system by converting and stabilizing the absorbed photon energy into a charge separated state which is reminiscent of the storage of charge in a battery. The RC complex of *Rb*. *sphaeroides* was the first membrane protein whose crystal structure was resolved. The RC of purple bacteria consists of three peptides, called L, M and

H, and ten cofactors. The cofactors include four BChl a molecules, two bacteriopheophytins (BPhe), two ubiquinones, a carotenoid molecule and a nonheme iron atom (see figure 4).

Charge separation is initiated in this compartment of the photosynthetic unit, where a BChl a dimer, the so called "special pair" or "primary donor", traps the solar energy harvested by the photosynthetic antenna complexes. Energy trapping is followed by charge separation through multiple electron transfer steps along the Abranch of the RC, ultimately resulting in reduction of the ubiquinone in the Q_B site. The RC complex has been intensively studied in isolated form as well as together with LH1 antenna by using various experimental techniques to explore the molecular basis of energy harvesting and electron transfer.

1.2.5 RC mutants

For the work described in this thesis we have also used mutants of *Rb. sphaeroides*. In particular, we have studied an antenna-deficient strain of this species which expresses only RCs. This strain was further modified by site-directed mutagenesis

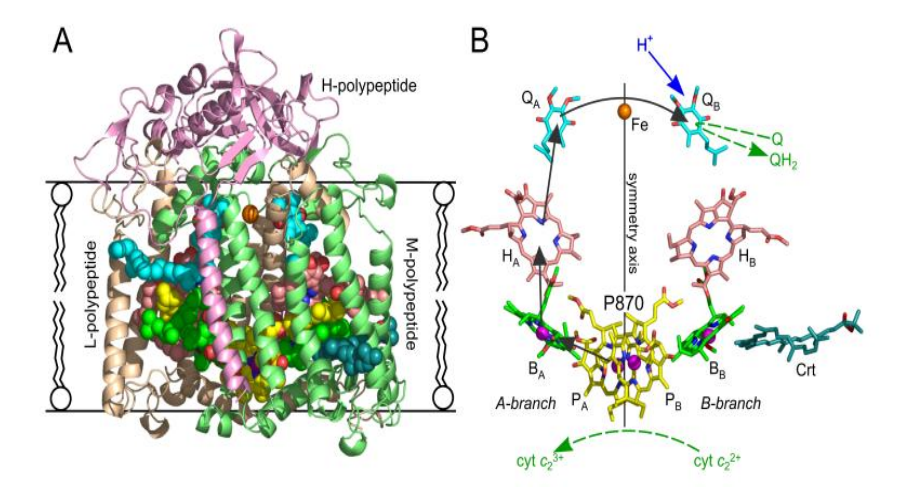


Figure 4: Side view of Reaction center complex and cofactors of the RC. (A) side view of the whole complex. (B) Side view of cofactors of reaction center. The charge separation is initiated at the dimer of bacteriochlorophylls denoted by PA and PB in the figure. The electron transfer takes place along the A-branch of the reaction center to get to QB site, from where it is transported to the periplasmic side of the membrane. Copyright Dr. M. Jones (Bristol University, UK), used with permission.

to engineer RCs with different cofactor composition, resulting in two mutants known as AM260W and AM149W. AM149W is a mutant in which the RC lacks the H_B cofactor, while in the AM260W mutant the Q_A cofactor is missing.

1.2.6 2D crystals of LH2 and RC-LH1 Complexes

2D crystallization provides a native-like environment to membrane proteins, which is desirable to keep them functionally and structurally intact. The method of making 2D crystals of membrane proteins is illustrated in figure 5. Membrane proteins are first dissolved in detergent, then mixed with lipid solution and subsequently the detergent is removed to get reconstituted proteoliposomes, which disrupt on the surface of the electrode to make 2D crystals of the membrane protein.⁴⁵

We studied LH2 and RC-LH1 complexes from *Rps.acidophila* embedded in lipid bilayer, where we used L-α-phosphatidylcholine, also called egg pc, as an artificial lipid. Prior to crystallization the RC-LH1 and LH2 complexes were solubilized in LDAO as detergent. The detergent was gradually removed by using polystyrene

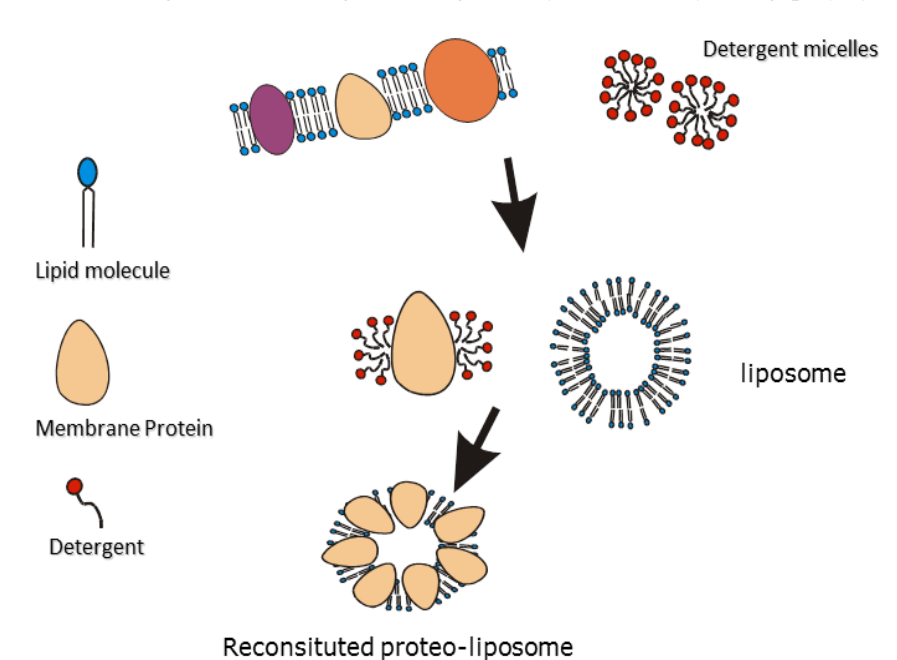


Figure 5: Schematic diagram of crystallization of membrane proteins. Membrane proteins are first dissolved in detergent, followed by addition of artificial lipid. Detergent is then removed to obtain reconstituted proteo-liposomes.

beads, also known as biobeads. A small volume of the lipid and protein mixture was used for efficient detergent removal.

1.3 Experimental techniques

1.3.1 Atomic Force Microscopy (AFM)

Atomic force microscopy (AFM) was initially a surface imaging technique for insulating materials. The working principle is based on bringing an oscillating probe (with sharp tip of a few nm radius mounted on a cantilever) in close proximity to the surface under investigation. Due to the forces between the tip and the surface the probe gets deflected, which is measured by a laser shining at the back side of the probe. The deflection of the reflected laser beam is then detected by a quadrant photodiode (see figure 6). By scanning the AFM tip across the sample while monitoring the tip deflection, the topographical image of the surface can be constructed. AFM was invented by Binning, Quate and Gerber in 1986, since then it is under constant development. Presently it is a very important and well-established technique in material science. 46,47

AFM has many different measurement modes, exploiting different types of forces between the tip and the surface. Among those, tapping mode and contact mode are

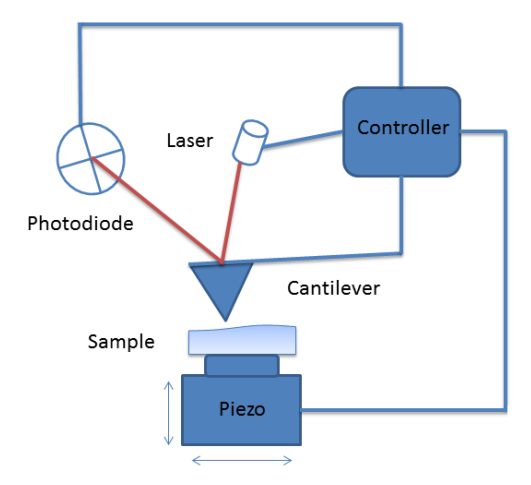


Figure 6: Schematic diagram of Atomic force microscopy. An oscillating tip of nano-meter size mounted onto a cantilever of micrometer size is brought in the vicinity of the sample, the forces between the tip and the sample cause a deflection of cantilever, which is measured by a laser beam reflecting from the back of the tip and leading to a photodiode.

frequently used for most of the surface imaging. AFM has been extensively used in all fields of material science. In particular, developments in the technology have made it feasible to record the morphology of membrane proteins under physiological conditions with very high resolution. 7-12,25-27,29,48-51

1.3.2 Conductive atomic force microscopy (C-AFM)

In the early stages of development AFM was mainly known as an imaging technique, which utilizes forces between the tip and the sample, unlike scanning tunneling microscopy (STM), which exploits the conductive ability of the surface for generating current maps.⁴⁷ The latter technique is confined to materials with appropriate conductivity because its feedback relies on current measurement; it is not suitable for insulating materials. AFM on the other hand relies on atomic forces between the surface and a sharp tip and it provides precise control over surface to tip distance, which makes it a very useful technique to image all kinds of surface without damaging the surface under investigation.

AFM can be modified to make it suitable for measuring the local conductivity of materials. This requires the integration of a conductive probe (a normal AFM cantilever is insulating) and an additional I-V convertor with the scanning system. This experimental setup is called current sensing AFM or conductive AFM (C-AFM). C-AFM thus provides an additional feature for surface analysis, which is based on local current-voltage (I-V) spectroscopy, measuring (tunneling) currents as a function of bias voltage between the underlying surface and the tip.⁵² This technique has been extensively used in material science to investigate charge transport mechanisms of organic and inorganic material down to the molecular level. I-V characteristics of a material are recorded by constructing a tunneling junction. The molecules are sandwiched between the two electrodes, where a conductive AFM tip serves as one electrode and a metal surface is generally used as the other electrode. Subsequently, a potential ramp is applied between the electrodes and the resulting current is measured to obtain an I-V curve, which can be further analyzed to extract relevant information.

Surface-confined biomolecules as well as synthetic molecules have been intimately probed by C-AFM to study electronic properties at the molecular level⁵³⁻⁵⁸. For example, Davis and coworkers employed this technique to characterize molecular junctions of metalloproteins, in particular azurin as a function of compressional

force.^{59,60} The I-V curves obtained at different compressional forces were fitted to the so-called Simmons model to extract junction parameters^{55,58}. The Simmons model establishes the relation between current (I) and voltage (V) for two electrodes separated by a thin insulator, represented as a rectangular potential barrier, which can be expressed as

$$I = \frac{e^2}{2\pi h L^2} \left\{ \left(\varphi - \frac{V}{2} \right) \exp \left[-K \left(\sqrt{\varphi - \frac{V}{2}} \right) \right] - \left(\varphi + \frac{V}{2} \right) \exp \left[-K \left(\sqrt{\varphi + \frac{V}{2}} \right) \right] \right\}$$

where $K = \frac{4\pi L}{h} \sqrt{2me}$ and e is the elementary charge, m is the electron mass, L and φ are representing the barrier width and barrier height, respectively. ⁵⁹⁻⁶¹

We measured I-V characteristics of pigment protein complexes, LH2, RC-LH1 and isolated RCs deposited on gold electrode. 2D crystals of RC-LH1 complexes were adsorbed on a gold electrode and I-V curves were measured as a function of the applied force. Asymmetric I-V curves around V=0 were observed for RC complexes, which appear to function as current rectifiers. In contrast, LH1 and LH2 complexes show a highly symmetric response. The results are discussed and interpreted in terms of the role of the cofactors and their composition in the various complexes.

1.3.3 Langmuir-Blodgett deposition

The Langmuir-Blodgett (LB) technique is a very useful method for transferring mono or multilayers of molecules floating on a water-air interface to a flat, solid substrate with precise control. ⁶² This method relies on the principle of alignment of amphiphilic molecules on the water-air interface. Such molecules contain hydrophobic and hydrophilic domains, which results in a specific orientation of the molecule on the water surface. The surface assembled molecules can then be compressed in a LB trough by movable barriers, up to a desired surface pressure by which a densely packed monolayer can be assembled on the surface.

The technique is named after two scientists Irving Langmuir and Katharine Blodgett. Langmuir received the Nobel prize for chemistry in 1932 for his research on surface chemistry. Katharine Blodgett contributed, together with Langmuir, to refinement of the technique for transferring the floating molecular layer onto solid substrates. The most striking features of this technique are precise control of film thickness, possibility of depositing composite materials and deposition of films on

different substrates without inducing any change in the intrinsic properties or structure of the molecules. This method can be exploited to deposit tailored material according to demands of organic, inorganic and hybrid devices for fundamental studies as well as for practical applications.

Molecular monolayer at the air/water interface

The first step of LB deposition is spreading the desired molecules on the water surface which is termed the sub-phase. The surface active molecules (surfactants) make a uniform monolayer on the air-water interface, keeping their hydrophobic region away from the water surface while the hydrophilic part points to the water sub-phase. Surfactants assemble on the water surface if the attractive forces between the molecules and water are higher than the intermolecular forces. The behavior of surfactants on the air/water interface is dependent on the size and the shape of the hydrophobic region as well as the size of the hydrophilic part of the molecules. Surface functionalization using a variety of organic and inorganic

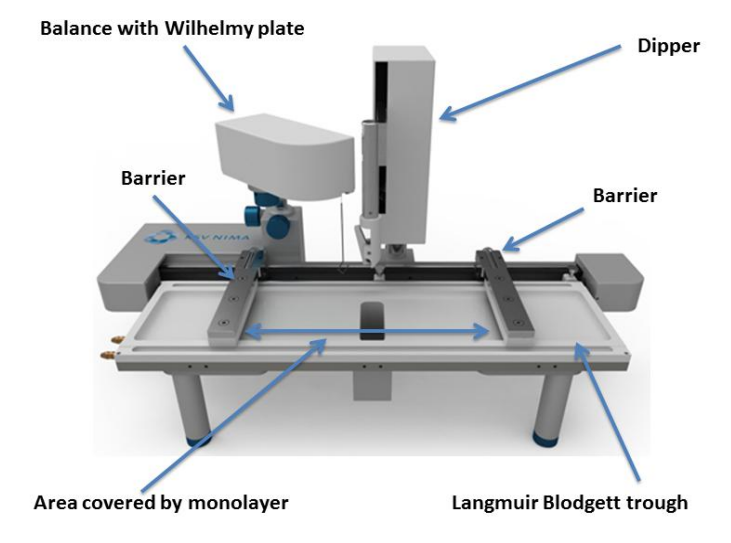


Figure 7: Schematic diagram of Langmuir –Blodgett deposition setup. It comprises of a Teflon trough which contains sub-phase. Desired material is spread on the surface of the sub phase (which is generally ultra-pure water) between the barriers and compressed to make a uniformly distributed monolayer of the molecules. The trough is equipped with a Wilhelmy plate for surface pressure measurement. After achieving the desired surface pressure the substrate is dipped in or pulled out by using the dipper to deposit the monolayer on solid support. Figure is provided by KSV NIMA, Finland.

molecules, including protein complexes, have been studied by transferring LB mono-layers of these compounds to solid supports. We have studied RC-LH1 and RC complexes by depositing LB monolayer of these complexes on a gold surface in a defined orientation.

Surface pressure

The prerequisite for understanding the behavior and organization of molecules in a LB film is to know and measure the forces involved at the air-water interface in the trough. Water in liquid form exerts electrostatic forces on dissolved molecules arising from interactions between permanent dipole moments. However, molecules at the surface experience a different force towards air, which may result in an imbalance of forces leading to the assembly of molecules at the interface until equilibrium is attained.

An important parameter for application of the LB method is the surface tension of the sub-phase, which is denoted by γ , with unit of N/m. The magnitude of γ for ultra-pure water is about 73 mN/m at 20 °C, which is very high compared to other liquids. It is exactly the reason why water is such a good sub-phase for LB deposition. Apart from temperature, the surface tension of water varies with contaminations on the surface; therefore it is very important to thoroughly clean the trough before use. An example of a Langmuir Blodgett trough is shown in figure 7. Usually it is made of teflon to avoid any contamination and leakage of the sub phase. The system is equipped with two movable barriers to compress the monolayer, and a balance to measure the surface pressure. The temperature of the trough can be controlled by circulating water in the channels under the trough.

The intermolecular forces are often not strong enough to keep the molecules together laterally on the water surface without compression of the monolayer. The uncompressed state is similar to a two dimensional gas since, depending on surface coverage, the molecules are free to diffuse on the surface. Under those conditions they do not significantly affect the surface tension of the sub-phase. When the molecules are compressed by moving the barriers, they start exerting repulsive forces on one another, which results in a change of the surface tension. The change in surface pressure can be determined by measuring the difference of surface tension of the pure sub phase (γ) and that of the sub phase when covered with a

layer of surfactant molecules (γ_{\circ}):

$$\Pi = \gamma_{\circ} - \gamma$$

Pressure versus area isotherm

Before deposition of a Langmuir Blodgett film on a solid substrate it is useful to first measure the surface pressure-area (Π -a) isotherm to optimize the packing of the monolayer. The isotherm is generally recorded by compressing the surface assembled molecules at a constant rate by moving barriers of the trough. A schematic diagram of the Π -a isotherm shows three different regions (see figure 8). By compressing the surface assembled molecules, the layer goes through different phases, the first one is analogous to a 2D gas because the molecules are far apart and the molecules are free to diffuse on the surface. The second is comparable to a liquid (less intermolecular distance), and the third one is similar to solid state when the molecules are packed at maximum surface density. Further compressing the film results in collapse of the film and it is no more a monolayer but multilayered stacking of molecules.

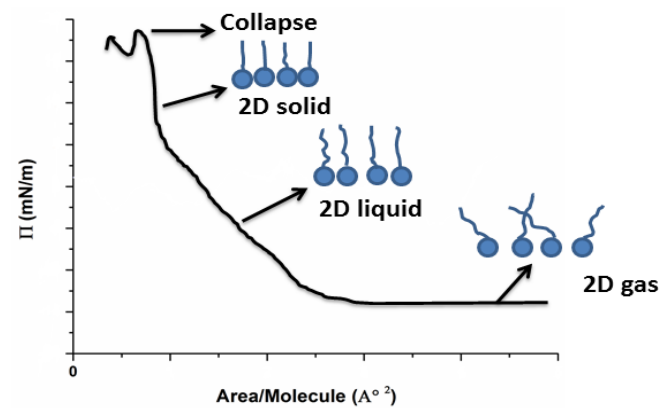


Figure 8: Schematic representation of isotherm of Langmuir Blodgett deposition. The curve shows different phases of the compressed film at air water interface. At lower surface pressure the molecules are in gas phase because of larger distance between them, by increasing the pressure the intermolecular distance decreases, this is called liquid phase. At a certain pressure the molecules are closely packed, this situation is called solid phase. Further increasing the pressure the film is collapsed.

1.4 Photoelectrochemistry

Photocurrent generated by bacterial reaction centers (RCs) can be measured by using a conventional electrochemistry setup. It consists of a potentiostat, three electrodes and a light source to generate charge separation. Three electrodes are inserted in a cell containing a buffer solution. The working electrode is generally made of gold or graphite, the reference electrode is saturated calomel and a piece of platinum wire is used as the counter electrode.

The potential is applied between the working and the reference electrode, while the current is measured between the working and the counter electrode. In our experiments we utilized two types of working electrodes. The first one is a standard gold working electrode (purchased from BAS) with diameter of 3 mm, the other one is prepared by sputtering a thin film of gold on a glass coverslip of 25 mm diameter. LB film of the desired photosynthetic complexes is deposited on gold coated glass cover slip. After LB film deposition the cover slip is incorporated as

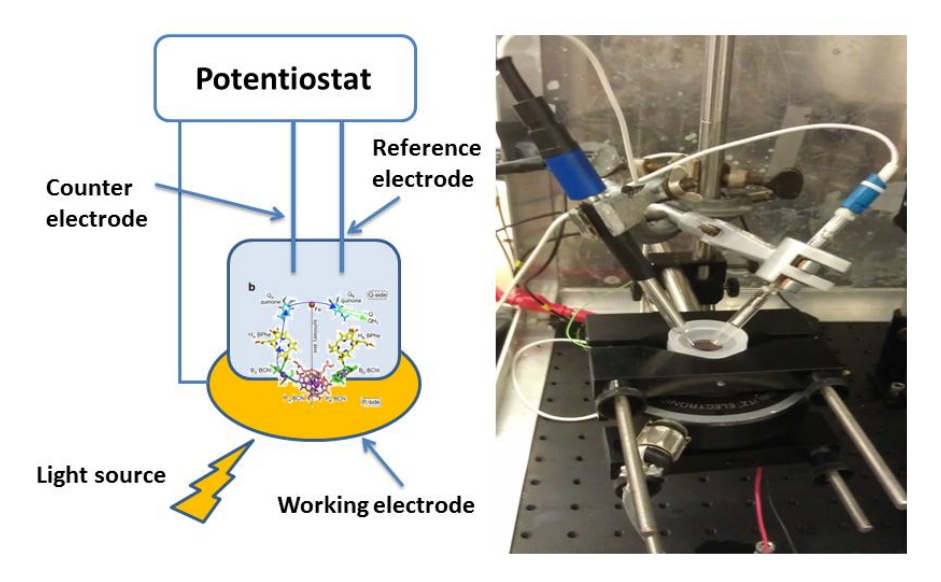


Figure 9: Left hand side is schematic diagram of the electrochemistry setup. Right hand side is the picture of the photocurrent experiments setup. Reference and counter electrode are inserted into a home built cell containing buffer solution (Tris-HCl pH 8), the base of the cell is a gold coated glass cover slip, which also served as working electrode. Light illumination is provided from the bottom of the cell. A computer controlled shutter is placed between the light source and the working electrode.

the base of the home made measuring cell. Reference and counter electrodes are inserted from the top of the cell and illumination is provided from the bottom of the cell, through the semitransparent working electrode.

Two types of light sources are used for the measurements, a white light source equipped with a monochromator for measuring action spectrum, and a light-emitting diode (LED) with central wavelength 880 nm and bandwidth of 50 nm for measuring the photocurrent response. The LED is operated with 800 mA at 7.6 V. The light illumination intensity hitting the surface of the electrode was 46 mW/cm² but after transmission through the cover slip it is reduced by one half, so the net value of light intensity is 23 mW/cm². In the case of measuring action spectra the (net) intensity of the light reaching the working electrode is 2 mW/cm².

A computer controlled shutter is placed between the light source and working electrode to enable the light illumination on/off. Ubiquinone and cytochrome C were used as redox mediators in the solution for photocurrent experiments. Figure 9 shows a schematic representation of the experimental setup, along with a picture of the experimental setup.

Absorbance and transmission spectra

Absorbance spectra of protein complexes in solution were recorded by using a UV spectrometer. The absorbance spectra of LB films deposited on the electrode and adsorbed protein complexes on the surface of the electrode and transmission spectra of gold coated glass cover slips were recorded by utilizing a fiber-coupled spectrometer (QE6500, Ocean Optics Inc., USA). Halogen and deuterium lamps were used as light sources.

References

- 1. Bahatyrova, S.; Frese, R. N.; Siebert, C. A.; Olsen, J. D.; van der Werf, K. O.; van Grondelle, R.; Niederman, R. A.; Bullough, P. A.; Otto, C.; Hunter, C. N. The native architecture of a photosynthetic membrane. *Nature* **2004**, *430* (7003), 1058-1062.
- 2. Bahatyrova, S.; Frese, R. N.; van der Werf, K. O.; Otto, C.; Hunter, C. N.; Olsen, J. D. Flexibility and size heterogeneity of the LH1 light harvesting complex revealed by atomic force microscopy Functional significance for bacterial photosynthesis. *Journal of Biological Chemistry* **2004**, *279* (20), 21327-21333.
- 3. Cogdell, R. J.; Fyfe, P. K.; Barrett, S. J.; Prince, S. M.; Freer, A. A.; Isaacs, N. W.; McGlynn, P.; Hunter, C. N. The purple bacterial photosynthetic unit. *Photosynthesis Research* **1996**, *48* (1-2), 55-63.
- 4. Cogdell, R. J.; Gall, A.; Kohler, J. The architecture and function of the light-harvesting apparatus of purple bacteria: from single molecules to in vivo membranes. *Ouarterly Reviews of Biophysics* **2006**, *39* (3), 227-324.
- 5. Papiz, M. Z.; Prince, S. M.; Hawthornthwaitelawless, A. M.; Mcdermott, G.; Freer, A. A.; Isaacs, N. W.; Cogdell, R. J. A model for the photosynthetic apparatus of purple bacteria. *Trends in Plant Science* **1996**, *I* (6), 198-206.
- 6. van Grondelle, R.; Novoderezhkin, V. I. Energy transfer in photosynthesis: experimental insights and quantitative models. *Physical Chemistry Chemical Physics* **2006**, 8 (7), 793-807.
- 7. Liu, L. N.; Sturgis, J. N.; Scheuring, S. Native architecture of the photosynthetic membrane from Rhodobacter veldkampii. *J. Struct. Biol.* **2011**, *173* (1), 138-145.
- 8. Scheuring, S.; Seguin, J.; Marco, S.; Levy, D.; Robert, B.; Rigaud, J. L. Nanodissection and high-resolution imaging of the Rhodopseudomonas viridis photosynthetic core complex in native membranes by AFM. Atomic force microscopy. *Proc. Natl. Acad. Sci. U. S A* **2003**, *100* (4), 1690-1693.
- 9. Scheuring, S.; Sturgis, J. N.; Prima, V.; Bernadac, A.; Levy, D.; Rigaud, J. L. Watching the photosynthetic apparatus in native membranes. *Proc. Natl. Acad. Sci. U. S A* **2004**, *101* (31), 11293-11297.
- Scheuring, S.; Rigaud, J. L.; Sturgis, J. N. Variable LH2 stoichiometry and core clustering in native membranes of Rhodospirillum photometricum. *EMBO J.* 2004, 23 (21), 4127-4133.
- 11. Scheuring, S.; Goncalves, R. P.; Prima, V.; Sturgis, J. N. The photosynthetic apparatus of Rhodopseudomonas palustris: structures and organization. *J. Mol. Biol.* **2006**, *358* (1), 83-96.
- 12. Scheuring, S.; Boudier, T.; Sturgis, J. N. From high-resolution AFM topographs to atomic models of supramolecular assemblies. *J. Struct. Biol.* **2007**, *159* (2), 268-276.
- 13. Borisov, A. Y.; Godik, V. I. Excitation-Energy Transfer in Photosynthesis. *Biochimica et Biophysica Acta* **1973**, *301* (3-4), 227-248.
- 14. Isaacs, N. W.; Cogdell, R. J.; Freer, A. A.; Prince, S. M. Light-harvesting mechanisms in purple photosynthetic bacteria. *Curr. Opin. Struct. Biol.* **1995**, *5* (6), 794-797.
- Sener, M. K.; Olsen, J. D.; Hunter, C. N.; Schulten, K. Atomic-level structural and functional model of a bacterial photosynthetic membrane vesicle. *Proceedings of the National Academy of Sciences of the United States of America* 2007, 104 (40), 15723-15728.

- 16. Mcdermott, G.; Prince, S. M.; Freer, A. A.; Isaacs, N. W.; Papiz, M. Z.; Hawthornthwaitelawless, A. M.; Cogdell, R. J. The 3-Dimensional Structure of the Light-Harvesting Antenna Complex (Lh-Ii) from Rps-Acidophila, Strain-10050, at 2.5 Angstrom Resolution. *Protein Engineering* **1995**, *8*, 43.
- Mcdermott, G.; Prince, S. M.; Freer, A. A.; Hawthornthwaitelawless, A. M.; Papiz, M. Z.; Cogdell, R. J.; Isaacs, N. W. Crystal-Structure of An Integral Membrane Light-Harvesting Complex from Photosynthetic Bacteria. *Nature* 1995, 374 (6522), 517-521.
- Mcdermott, G.; Prince, S. M.; Freer, A. A.; Hawthornthwaitelawless, A. M.; Papiz, M. Z.; Cogdell, R. J.; Isaacs, N. W. Crystal-Structure of An Integral Membrane Light-Harvesting Complex from Photosynthetic Bacteria. *Nature* 1995, 374 (6522), 517-521.
- 19. Borland, C. F.; Cogdell, R. J.; Land, E. J.; Truscott, T. G. Bacteriochlorophyll Alpha-Triplet State and Its Interactions with Bacterial Carotenoids and Oxygen. *Journal of Photochemistry and Photobiology B-Biology* **1989**, *3* (2), 237-245.
- 20. Cogdell, R. J.; Hipkins, M. F.; Macdonald, W.; Truscott, T. G. Energy-Transfer Between the Carotenoid and the Bacteriochlorophyll Within the B-800-850 Light-Harvesting Pigment-Protein Complex of Rhodopseudomonas-Sphaeroides. *Biochimica et Biophysica Acta* **1981**, *634* (1), 191-202.
- 21. Cogdell, R. J.; Frank, H. A. How carotenoids function in photosynthetic bacteria. *Biochim. Biophys. Acta* **1987**, *895* (2), 63-79.
- 22. Cogdell, R. J.; Howard, T. D.; Bittl, R.; Schlodder, E.; Geisenheimer, I.; Lubitz, W. How carotenoids protect bacterial photosynthesis. *Philos. Trans. R Soc. Lond B Biol. Sci.* **2000**, *355* (1402), 1345-1349.
- 23. Limantara, L.; Fujii, R.; Zhang, J. P.; Kakuno, T.; Hara, H.; Kawamori, A.; Yagura, T.; Cogdell, R. J.; Koyama, Y. Generation of triplet and cation-radical bacteriochlorophyll a in carotenoidless LH1 and LH2 antenna complexes from Rhodobacter sphaeroides. *Biochemistry* **1998**, *37* (50), 17469-17486.
- 24. Hofmann, C.; Aartsma, T. J.; Kohler, J. Energetic disorder and the B850-exciton states of individual light-harvesting 2 complexes from Rhodopseudomonas acidophila. *Chemical Physics Letters* **2004**, *395* (4-6), 373-378.
- 25. Scheuring, S.; Seguin, J.; Marco, S.; Levy, D.; Breyton, C.; Robert, B.; Rigaud, J. L. AFM characterization of tilt and intrinsic flexibility of Rhodobacter sphaeroides light harvesting complex 2 (LH2). *J. Mol. Biol.* **2003**, *325* (3), 569-580.
- Liu, L. N.; Aartsma, T. J.; Frese, R. N. Dimers of light-harvesting complex 2 from Rhodobacter sphaeroides characterized in reconstituted 2D crystals with atomic force microscopy. Febs Journal 2008, 275 (12), 3157-3166.
- 27. Stamouli, A.; Kafi, S.; Klein, D. C. G.; Oosterkamp, T. H.; Frenken, J. W. M.; Cogdell, R. J.; Aartsma, T. J. The ring structure and organization of light harvesting 2 complexes in a reconstituted lipid bilayer, resolved by atomic force microscopy. *Biophysical Journal* **2003**, *84* (4), 2483-2491.
- 28. Olsen, J. D.; Tucker, J. D.; Timney, J. A.; Qian, P.; Vassilev, C.; Hunter, C. N. The Organization of LH2 Complexes in Membranes from Rhodobacter sphaeroides. *Journal of Biological Chemistry* **2008**, 283 (45), 30772-30779.
- 29. Scheuring, S.; Reiss-Husson, F.; Engel, A.; Rigaud, J. L.; Ranck, J. L. High-resolution AFM topographs of Rubrivivax gelatinosus light-harvesting complex LH2. *Embo Journal* **2001**, *20* (12), 3029-3035.

- 30. Sturgis, J. N.; Niedermann, R. A. The effect of different levels of the B800-850 light-harvesting complex on intracytoplasmic membrane development in Rhodobacter sphaeroides. *Arch. Microbiol.* **1996**, *165* (4), 235-242.
- 31. Scheuring, S.; Sturgis, J. N. Chromatic adaptation of photosynthetic membranes. *Science* **2005**, *309* (5733), 484-487.
- 32. Fotiadis, D.; Qian, P.; Philippsen, A.; Bullough, P. A.; Engel, A.; Hunter, C. N. Structural analysis of the reaction center light-harvesting complex I photosynthetic core complex of Rhodospirillum rubrum using atomic force microscopy. *Journal of Biological Chemistry* **2004**, *279* (3), 2063-2068.
- 33. Harrold, J. W.; Woronowicz, K.; Lamptey, J. L.; Baird, J.; Moshar, A.; Vittadello, M.; Falkowski, P.; Niederman, R. A. Functional Interfacing of Rhodospirillum rubrum Chromatophores to a Conducting Support for Capture and Conversion of Solar Energy. *J. Phys. Chem. B* **2013**.
- 34. Roszak, A. W.; Howard, T. D.; Southall, J.; Gardiner, A. T.; Law, C. J.; Isaacs, N. W.; Cogdell, R. J. Crystal structure of the RC-LH1 core complex from Rhodopseudomonas palustris. *Science* **2003**, *302* (5652), 1969-1972.
- 35. Barz, W. P.; Francia, F.; Venturoli, G.; Melandri, B. A.; Vermeglio, A.; Oesterhelt, D. Role of Pufx Protein in Photosynthetic Growth of Rhodobacter-Sphaeroides .1. Pufx Is Required for Efficient Light-Driven Electron-Transfer and Photophosphorylation Under Anaerobic Conditions. *Biochemistry* **1995**, *34* (46), 15235-15247.
- 36. Barz, W. P.; Vermeglio, A.; Francia, F.; Venturoli, G.; Melandri, B. A.; Oesterhelt, D. Role of the Pufx Protein in Photosynthetic Growth of Rhodobacter-Sphaeroides .2. Pufx Is Required for Efficient Ubiquinone Ubiquinol Exchange Between the Reaction-Center Q(B) Site and the Cytochrome Bc(1) Complex. *Biochemistry* **1995**, *34* (46), 15248-15258.
- 37. Bohm, P. S.; Southall, J.; Cogdell, R. J.; Kohler, J. Single-molecule spectroscopy on RC-LH1 complexes of Rhodopseudomonas acidophila strain 10050. *J. Phys. Chem. B* **2013**, *117* (11), 3120-3126.
- 38. Richter, M. F.; Baier, J.; Southall, J.; Cogdell, R. J.; Oellerich, S.; Kohler, J. Refinement of the x-ray structure of the RC LH1 core complex from Rhodopseudomonas palustris by single-molecule spectroscopy. *Proc. Natl. Acad. Sci. U. S A* **2007**, *104* (51), 20280-20284.
- 39. Richter, M. F.; Baier, J.; Prem, T.; Oellerich, S.; Francia, F.; Venturoli, G.; Oesterhelt, D.; Southall, J.; Cogdell, R. J.; Kohler, J. Symmetry matters for the electronic structure of core complexes from Rhodopseudomonas palustris and Rhodobacter sphaeroides PufX-. *Proc. Natl. Acad. Sci. U. S A* **2007**, *104* (16), 6661-6665.
- Sumino, A.; Dewa, T.; Sasaki, N.; Kondo, M.; Nango, M. Electron Conduction and Photocurrent Generation of a Light-Harvesting/Reaction Center Core Complex in Lipid Membrane Environments. *Journal of Physical Chemistry Letters* 2013, 4 (7), 1087-1092.
- 41. Deisenhofer, J.; Epp, O.; Miki, K.; Huber, R.; Michel, H. Structure of the Protein Subunits in the Photosynthetic Reaction Center of Rhodopseudomonas-Viridis at 3A Resolution. *Nature* **1985**, *318* (6047), 618-624.
- 42. Deisenhofer, J.; Michel, H.; Huber, R. The Structural Basis of Photosynthetic Light Reactions in Bacteria. *Trends in Biochemical Sciences* **1985**, *10* (6), 243-248.
- 43. Watson, A. J.; Fyfe, P. K.; Frolov, D.; Wakeham, M. C.; Nabedryk, E.; van Grondelle, R.; Breton, J.; Jones, M. R. Replacement or exclusion of the B-branch bacteriopheophytin in the purple bacterial reaction centre: The H-B cofactor is not

- required for assembly or core function of the Rhodobacter sphaeroides complex. *Biochimica et Biophysica Acta-Bioenergetics* **2005**, *1710* (1), 34-46.
- 44. Ridge, J. P.; van Brederode, M. E.; Goodwin, M. G.; van Grondelle, R.; Jones, M. R. Mutations that modify or exclude binding of the QA ubiquinone and carotenoid in the reaction center from Rhodobacter sphaeroides. *Photosynthesis Research* **1999**, *59* (1), 9-26.
- 45. Rigaud, J. L. Membrane proteins: functional and structural studies using reconstituted proteoliposomes and 2-D crystals. *Brazilian Journal of Medical and Biological Research* **2002**, *35* (7), 753-766.
- 46. Binnig, G.; Quate, C. F.; Gerber, C. Atomic Force Microscope. *Physical Review Letters* **1986**, *56* (9), 930-933.
- 47. Binning, G.; Rohrer, H.; Gerber, C.; Weibel, E. Surface Studies by Scanning Tunneling Microscopy. *Physical Review Letters* **1982**, *49* (1), 57-61.
- 48. Liu, L. N.; Duquesne, K.; Oesterhelt, F.; Sturgis, J. N.; Scheuring, S. Forces guiding assembly of light-harvesting complex 2 in native membranes. *Proc. Natl. Acad. Sci. U. S A* **2011**, *108* (23), 9455-9459.
- 49. Liu, L. N.; Scheuring, S. Investigation of photosynthetic membrane structure using atomic force microscopy. *Trends Plant Sci.* **2013**, *18* (5), 277-286.
- 50. Scheuring, S.; Levy, D.; Rigaud, J. L. Watching the components of photosynthetic bacterial membranes and their in situ organisation by atomic force microscopy. *Biochim. Biophys. Acta* **2005**, *1712* (2), 109-127.
- 51. Scheuring, S. AFM studies of the supramolecular assembly of bacterial photosynthetic core-complexes. *Curr. Opin. Chem. Biol.* **2006**, *10* (5), 387-393.
- 52. Stamouli, A.; Frenken, J. W.; Oosterkamp, T. H.; Cogdell, R. J.; Aartsma, T. J. The electron conduction of photosynthetic protein complexes embedded in a membrane. *FEBS Lett.* **2004**, *560* (1-3), 109-114.
- 53. Berthoumieu, O.; Patil, A. V.; Xi, W.; Aslimovska, L.; Davis, J. J.; Watts, A. Molecular Scale Conductance Photoswitching in Engineered Bacteriorhodopsin. *Nano Letters* **2012**, *12* (2), 899-903.
- 54. Cui, X. D.; Primak, A.; Zarate, X.; Tomfohr, J.; Sankey, O. F.; Moore, A. L.; Moore, T. A.; Gust, D.; Harris, G.; Lindsay, S. M. Reproducible measurement of single-molecule conductivity. *Science* **2001**, *294* (5542), 571-574.
- 55. Davis, J. J.; Wang, N.; Morgan, A.; Zhang, T. T.; Zhao, J. W. Metalloprotein tunnel junctions: compressional modulation of barrier height and transport mechanism. *Faraday Discussions* **2006**, *131*, 167-179.
- 56. Lindsay, S. Single-molecule electronic measurements with metal electrodes. *Journal of Chemical Education* **2005**, 82 (5), 727-733.
- 57. Rawlett, A. M.; Hopson, T. J.; Nagahara, L. A.; Tsui, R. K.; Ramachandran, G. K.; Lindsay, S. M. Electrical measurements of a dithiolated electronic molecule via conducting atomic force microscopy. *Applied Physics Letters* **2002**, *81* (16), 3043-3045.
- 58. Zhao, J. W.; Davis, J. J. Force dependent metalloprotein conductance by conducting atomic force microscopy. *Nanotechnology* **2003**, *14* (9), 1023-1028.
- Zhao, J. W.; Davis, J. J.; Sansom, M. S. P.; Hung, A. Exploring the electronic and mechanical properties of protein using conducting atomic force microscopy. *Journal* of the American Chemical Society 2004, 126 (17), 5601-5609.

- Zhao, J. W.; Davis, J. J. Molecular electron transfer of protein junctions characterised by conducting atomic force microscopy. *Colloids and Surfaces B-Biointerfaces* 2005, 40 (3-4), 189-194.
- 61. Axford, D.; Davis, J. J.; Wang, N.; Wang, D. X.; Zhang, T. T.; Zhao, J. W.; Peters, B. Molecularly resolved protein electromechanical properties. *Journal of Physical Chemistry B* **2007**, *111* (30), 9062-9068.
- 62. Zasadzinski, J. A.; Viswanathan, R.; Madsen, L.; Garnaes, J.; Schwartz, D. K. Langmuir-Blodgett-Films. *Science* **1994**, 263 (5154), 1726-1733.
- 63. Alegria, G.; Dutton, P. L. Langmuir-Blodgett Monolayer Films of Bacterial Photosynthetic Membranes and Isolated Reaction Centers Preparation, Spectrophotometric and Electrochemical Characterization .1. *Biochimica et Biophysica Acta* **1991**, *1057* (2), 239-257.
- 64. Birdi, K. S.; Vu, D. T. Structures of Collapsed Lipid Monolayers Investigated As Langmuir-Blodgett-Films by Atomic-Force Microscopy. *Langmuir* **1994**, *10* (3), 623-625.
- 65. Bryce, M. R.; Petty, M. C. Electrically Conductive Langmuir-Blodgett-Films of Charge-Transfer Materials. *Nature* **1995**, *374* (6525), 771-776.
- 66. Choi, J. W.; Nam, Y. S.; Kong, B. S.; Lee, W. H.; Park, K. M.; Fujihira, M. Bioelectronic device consisting of cytochrome c/poly-L-aspartic acid adsorbed hetero-Langmuir-Blodgett films. *Journal of Biotechnology* **2002**, *94* (3), 225-233.
- 67. Facci, P.; Erokhin, V.; Paddeu, S.; Nicolini, C. Surface pressure induced structural effects in photosynthetic reaction center Langmuir-Blodgett films. *Langmuir* **1998**, *14* (1), 193-198.
- 68. Tredgold, R. H. Langmuir-Blodgett Films Organic Monolayer Imaged. *Nature* **1985**, 313 (6001), 348.
- 69. Yasuda, Y.; Sugino, H.; Toyotama, H.; Hirata, Y.; Hara, M.; Miyake, J. Control of Protein Orientation in Molecular Photoelectric Devices Using Langmuir-Blodgett-Films of Photosynthetic Reaction Centers from Rhodopseudomonas-Viridis. *Bioelectrochemistry and Bioenergetics* **1994**, *34* (2), 135-139.
- 70. Zasadzinski, J. A.; Viswanathan, R.; Madsen, L.; Garnaes, J.; Schwartz, D. K. Langmuir-Blodgett-Films. *Science* **1994**, 263 (5154), 1726-1733.
- 71. Zhao, Y. Y.; Gao, M. L.; Ren, Y. Z.; Dong, Z. J.; Wang, H.; Liu, W.; Li, T. J. Synthesis of Monoesters of Polymaleic Acid and Characterization of Their Langmuir-Blodgett-Films. *Thin Solid Films* **1992**, *210* (1-2), 610-613.

CHAPTER 2

Electron tunneling and electron transfer of 2D crystals of RC-LH1 complexes on a gold electrode.

Abstract:

In photosynthesis the primary reactions involve light absorption, excited state energy transfer and electron transfers. These reactions are carried out by lightharvesting and reaction center protein complexes which can operate near unity quantum efficiency. The photosynthetic purple bacterial reaction center – light harvesting 1 complex (RC-LH1) is a potential building block for the implementation of biological photovoltaic devices and biosolar cells. In order to enhance the performance of such a device several factors need to be optimized: surface coverage, orientation and electron relay-function between protein and surface. Here we report on the functionality of RC-LH1 complexes from the purple bacterium Rhodopseudomonas acidophila interfaced with a bare gold electrode when densely packed within a self-organised lipid membrane structure based on a 2D crystallization protocol. The 2D crystals were probed with conductive atomic force microscopy and photoelectrochemistry to inspect their functionality. Within a range of moderate applied forces we find the reaction center complexes within the crystals to show diode-like behavior, indicative of a uniform orientation. The recorded photocurrents showed a considerably higher contribution of light absorption by the LH1 antenna complex than that by the reaction center. We interpret our data as sustained energy transfers between LH1 complexes in the densely packed configuration of a 2D crystal, successfully competing with direct quenching of excitation energy by the gold electrode.

2.1 Introduction:

Excitonic and photovoltaic components embedded within cell membranes of photosynthetic bacteria are responsible for the primary conversion of solar energy into an electrochemical potential across the membrane. The photosynthetic unit (PSU) in the purple bacterium *Rhodopseudomonas (Rps.) acidophila* consists of light harvesting 1 (LH1), light harvesting 2 (LH2) and reaction center (RC) complexes. These complexes contain bacteriochlorophyll *a* and carotenoid molecules bound to the protein scaffolds, precisely tuned to absorb specific wavelengths of sunlight and storing the energy temporarily as an electronically excited state, which is subsequently funneled to a RC to initiate charge separation.

The advances in atomic force microscopy (AFM) have made it feasible to observe the supramolecular arrangement of photosynthetic proteins in their native environment¹⁻⁶. High resolution imaging of several bacterial photosynthetic membranes has revealed that LH2 and RC-LH1 complexes are closely packed within a membrane environment consisting of 2-dimensional (2D) arrays of RC-LH1 and LH2 complexes with variable composition and arrangement. The intrinsic heterogeneity of the PSU, which might be enhanced by treatment and imaging protocols, makes it difficult to study the functioning of the entire system as a whole. Decades of research focusing on isolated components resulted in a wealth of knowledge on the intrinsic properties of individual photosynthetic complexes^{2,7-24}. However, the native structure and *in vivo* function may be influenced by the inherently close packing of the complexes within the membranes.

2D crystallization is one of the methods to study the effects of close packing within domains of individual components of PSU.^{20,25-31} The method relies on mixing of detergent-solubilized pigment-protein complexes with artificial liposomes, followed by slow removal of the detergent which results in the formation of reconstituted proteolipisomes. Upon surface adsorption these proteoliposomes may rupture to form a flattened lipid bilayer patch on the surface.

This method facilitates the use of scanning probe techniques to study the organization and structure of 2D crystals of protein complexes with sufficient resolution to resolve details of their substructure. In particular, it has allowed the observation of the structural arreangement of photosynthetic pigment-protein complexes down to the submolecular level.³² Such studies were performed on LH2, LH1 and RC complexes from various bacterial species while embedded in surfaceadsorbed lipid bilayers^{8,15,17,28,29,32-35}. Because of the close packing of the proteoliposomes, even adopting in many cases an ordered 2D crystalline arrangement, they provide an environment which mimics the native state of these complexes. One has to be careful, however, because the self-organization of protein complexes in 2D crystals may result in an up-down packing configuration²⁰, in contrast to the situation *in vivo* where each component of the PSU has the same orientation. This may complicate the study of bacterial photosynthetic complexes in a reconstituted lipid bilayer from a functional point of view. Nevertheless, in other cases the protein-complexes pack in a well-defined, one side up configuration. 29,35 Energy transfer in more or less crystalline 2Daggregates with both LH2 and RC-LH1 has been observed, confirming the close packing of these complexes in the artificial lipid bilayer. It has been shown that it is possible to construct hybrid 2D crystals containing both LH2 and RC-LH1 by reconstitution in one artificial lipid bilayer in which their function of light absorption, energy transfer and charge separation is recovered. Remarkably, the energy transfer between LH2 and RC-LH1 complexes from two different species has also been observed, which makes this technique very promising for applications targeting enhanced solar energy absorption in bio-hybrid devices.^{22,36} Because of the intrinsic high quantum efficiency, the bacterial PSU has drawn much attention for utilization in photovoltaic applications, either by using the isolated pigment-protein complexes as building blocks or at the conceptual level by mimicking their structure and functionality. ³⁷⁻⁴⁰ For such purposes the individual components of PSU need to be immobilized on a solid support for their characterization while keeping them functionally and structurally intact. Several strategies have been developed to attach the pigment protein complexes to conducting electrodes. Metal electrodes modified with self-assembled monolayers (SAMs) of organic molecules, genetically modified protein complexes and porous or gel materials are commonly used methods to immobilize the protein complexes in a defined orientation. Such immobilization techniques have resulted in photocurrents of the order of microamperes from surface-assembled photosynthetic components, indicative of a successful, functional connection of RCs and RC-LH1 complexes to a metal electrode 11,40-45.

Understanding the relationship between the electronic properties and the structure of photosynthetic protein complexes is very important for any application of these complexes, e.g. for their integration in a photovoltaic device. Scanning tunneling microscopy (STM) can be used to study the electronic properties of molecules immobilized on conducting surfaces. However, low conductivity and heterogeneity of the biological materials can complicate the interpretation of the STM topographs. For such applications conductive atomic force microscopy (C-AFM) can is preferred because it offers more control over experimental parameters; this technique is well known in material science and it has been used to study electronic properties of heterogeneous systems. The capability of C-AFM for large area topography imaging, combined with current-voltage (I-V) spectroscopy, provides the possibility of studying local electrical properties of organic materials under well-defined conditions. C-AFM has been utilized to characterize a wide range of materials including metals, semiconductors, graphene, carbon nanotubes, molecular

mono-layers, polymer blends and soft materials. ^{11,14,16,29,46-59} Force feedback of AFM provides precise control on tip-sample interaction, which is very useful for local I-V spectroscopy of soft materials. Also organic materials, including membrane proteins, have been extensively studied by using this technique. ^{14,29,35,50,51,59} Stamouli et al., for example, have reported I-V curves of LH2 complexes embedded in a lipid bilayer, demonstrating the role of the LH2 cofactors in electron tunneling over a distance of about 5-6 nm, the thickness of the LH2-containing lipid patch on a gold electrode ²⁹.

Previous experiment on the I-V spectroscopy of RCs and LH1-RC complexes involved their deposition on electrodes which were modified with self-assembled monolayers of particular organic molecules ^{16,35,60}. In particular, Sumino et al. have reported electron tunneling characteristics of RC-LH1 complexes from *Rps. palustris* in 2D crystalline form. ³⁵ Asymmetric current–voltage curves were recorded by using C-AFM, indicative of unidirectional electron transfer across RC-LH1 complexes in the lipid bilayer. In addition, they have recorded high-resolution AFM images of 2D crystals of RC-LH1 complexes indicating preferential orientation of the complexes in a lipid bilayer. This system was capable of generating a photocurrent with a magnitude of 15 nA/cm² when the 2D crystals of RC-LH1 were adsorbed on an indium tin oxide (ITO) electrode. The electrode was pre-modified with a SAM of 3-aminopropyltriethoxysilane.

Isolated RC-LH1 complexes from another purple bacterial species, *Rps. acidophila*, when adsorbed directly onto a bare gold electrode, appear to have superior protein-metal connectivity as indicated by the highest photocurrent of protein monolayers to date $(25 \, \mu \text{A/cm}^2 \text{ under high light})^{35,61}$.

Here we report a more detailed study of RC-LH1 complexes from *Rps. acidophila* embedded in reconstituted lipid bilayers in terms of functionality and its performance on bare gold electrodes by using conductive AFM and photoelectrochemistry. The results are compared to those obtained for 2D crystals of LH2 complexes. In contrast to LH2, the distinct characteristics of cofactors present in LH1 and the RC lead to hybrid I-V curves, which contain the signature of both types of pigment-protein complexes and their cofactors. The 2D crystals of RC-LH1 complex adsorbed on a bare gold electrode produced substantial photocurrents with a magnitude of 780 nA/cm², which confirms that the functional integrity of

these crystals on the gold electrode is preserved. The action spectra of 2D crystals as a function of incident light intensity show that RC-LH1 complexes show a larger photocurrent response than when they are adsorbed on the gold electrode from detergent solution. The data suggest that transfer of excitation from LH1 to the RC is more efficient in 2D crystal-form than in RC-LH1 complexes adsorbed from solution.

2.2 Materials and methods

Materials:

L- α -phosphatidylcholine (egg PC), cytochrome (cyt) c from horse heart, n-octyl- β -D-glucopyranoside (OTG) and water soluble ubiquinone-0 (Q-0) were purchased from Sigma and used without further purification. SM-2 biobeads were purchased from Bio-Rad Laboratories. RC-LH1 from *Rps. acidophila* was purified and isolated as described elsewhere 62 .

Preparation of 2D crystals

The lipid solution was prepared by dissolving 20 mg egg PC in 1 ml of chloroform, after which the solution was dried under a flow of nitrogen to get a nice, even film on the wall of the glass container. The lipids were solubilized in a solution of 49 mg OTG in 8 ml of buffer (10 mM Tris-HCl, pH 8, also containing 1mM EDTA and 400 mM NaCl) which was added to the container. Its content was sonicated three times with a tip sonicator, after which a transparent solution was obtained without any foaming. This lipid solution was stored at -20 °C for later use.

For the preparation of 2D-crystals of RC-LH1, the lipid solution (2.5 mg/mL) was mixed with detergent solubilized RC-LH1 complexes (10 mg/mL) to make a total volume of 75 μ L in an Eppendorf tube. Different lipid to protein ratios (LPR) were tested, and it was found that a LPR of 0.5 gives an optimum yield of 2D crystals. The mixture was kept on a magnetic stirrer, and detergent was removed gradually by stepwise addition of biobeads. The biobeads were washed beforehand in methanol and subsequently dispersed in buffer (10 mM Tris-HCl, 1 mM EDTA, 400 mM NaCl, pH 8). An aliquot containing 5 mg of biobeads was added to the Eppendorf tube with the RC-LH1 solution. This step was repeated two times with one hour intervals between additions; subsequently the biobeads were separated from the solution and the latter was stored at 4 $^{\circ}$ C for further measurements.

Absorption spectra of the sample were measured after the crystallization process to verify that the RC-LH1 system was still intact.

Gold film preparation:

Glass cover slips with a diameter of 25 mm were purchased from Menzel-Gläser and cleaned before use in various steps. They were first sonicated for one hour in methanol, then washed with milli-Q water and finally dried under a flow of nitrogen. Subsequently, prior to gold deposition, the cover slips were ozone-cleaned for one hour by using a UV-ozone photoreactor (UVP PR-100).

Gold was sputtered on the clean glass cover slips or freshly cleaved mica by utilizing a magnetron sputtering setup (ATC 1800-F, AJA Corporation)⁶³. A thin layer of 1 to 2 nm thick molybdenum-germanium (MoGe) was deposited as an adhesion layer; subsequently a 12 nm thick, semi-transparent gold layer was sputtered on top of it. The deposition rate for MoGe was 1.32 nm/min, under 10 mTorr argon pressure, whereas the gold was sputtered at a deposition rate of 9.06 nm/min in the same argon environment but with the addition of 1% oxygen. Gold coated glass cover slips were stored in a desiccator and used within one week.

AFM Measurements

Samples for AFM imaging were prepared by putting 50 μ l of adsorption buffer (10 mM Tris-HCl, 150 mM KCl, 25 mM MgCl₂) on a freshly sputtered gold electrode, subsequently 2 μ l of the RC-LH1 proteoliposome solution was added. After incubation for one hour the electrode was rinsed with recording buffer (10mM Tris-HCl, 150 mM KCl, pH 7.5), followed by a rinse with distilled water, in order to remove weakly bound crystal patches and salt residues. These steps were all performed at 4 $^{\circ}$ C. The electrode was then dried under a gentle stream of nitrogen gas. For imaging we used a commercial AFM instrument (Nano scope III; Digital Instruments, Santa Barbara, CA, USA) operated in tapping mode in ambient conditions. The cantilever had a spring constant of 2 N/m and a resonance frequency of 75 kHz.

Conductive AFM (C-AFM)

Conductive AFM was used to study I-V spectroscopy of 2D crystals of RC-LH1. A combination of tapping and contact mode was used for these measurements. A junction was formed by the gold-coated AFM tip and conductive substrate with the 2D crystals of the RC-LH1 complex in between. These tips were prepared by

coating a standard silicon nitride cantilevers with a spring constant of 2 N/m and a resonant frequency of 75 kHz with layer of gold or platinum with a thickness of a few nanometers. The radius of curvature of the tip, after sputtering the conductive layer, was about 15 nm as checked with a scanning electron microscope (SEM). The conductive layer of gold or platinum was deposited on the AFM cantilevers using a magnetron sputtering system (ATC 1800-F, AJA Corporation).

A freshly sputtered gold film on mica was used as substrate for C-AFM measurements. Tapping mode AFM was used to locate a patch of RC-LH1, after which the instrument was switched to contact mode: the oscillation of the cantilever was stopped, a voltage ramp was applied between the tip and the substrate, and the resulting current was measured. Current measurements were limited to the range of 0 to ± 10 nA by the current-voltage converter which was mounted close to the probe tip.

Photocurrent Measurement

Photocurrents were measured by using a conventional electrochemistry setup equipped with a light source for excitation of the sample. The experimental setup was configured with a working, a reference and a counter electrode, each of which was connected to a potentiostat to control the potential between the working and the reference electrode. The reference electrode (Ag/AgCl, saturated KCl) and counter electrode (platinum wire) were inserted into a home built measuring cell with a volume of 7 mL. A gold coated glass slide was used as the working electrode. Illumination was provided from below, through the bottom of the measuring cell. The light source consisted of a high power light emitting diode (LED) purchased from Roithner Laser Technik with central wavelength of 880 nm and bandwidth of 50 nm. The action spectra were taken with a scanning monochromator (bandwidth 40 nm) with a white light source (a halogen/tungsten lamp) at the input slit. A computer controlled shutter was introduced between the light source and the measuring cell to switch the excitation light on or off.

Photocurrents were typically measured at an open circuit potential of -0.1 V vs. the standard calomel reference electrode (SCE). The measuring buffer (Tris-HCl, pH 8) was bubbled with nitrogen and the photocurrent measurements were performed at room temperature. The intensity of the light reaching the sample at the surface of

the working electrode was 2.5 mW/cm² when the LED was used for excitation, whereas that of the monochromator output was 2.4 mW/cm².

Measurement of action spectra

The working electrode was a commercial gold electrode which was functionalized by incubation with a solution of RC-LH1 crystals for one hour at 4 °C. The electrode with adsorbed RC-LH1 crystals was inserted into the measuring cell containing 7 mL of buffer which also contained 100 μ M ubiquinone-0 (Q-0) and 20 μ M of cytochrome (cyt) c. The light intensity could be adjusted by using a filter in the light path. The maximum light intensity at the surface of the working electrode was 2.4 mW/cm². Photocurrents were measured at different wavelengths starting from 400 nm and ending at 950 nm in steps of 5 nm. The light illumination was switched on and off at intervals of 10 seconds to measure current and background signals, respectively. The photocurrent as a function of the wavelength of excitation (in the range of 400-950nm) was normalized to the light intensity at the output of the monochromator.

2.3 Results

2D crystals of RC-LH1 complexes from *Rps. acidophila* were prepared as described in Materials and Methods. The crystals were subsequently transferred onto a freshly prepared, gold sputtered glass slide and probed structurally and functionally. Figure 1 shows the topography of these 2D crystals for the case of RC-LH1 complexes, adsorbed on a gold electrode as visualized by tapping mode AFM under ambient conditions. The observed patches have varying sizes ranging from tens of nanometers to several micrometers. An enlarged image of adsorbed 2D crystals of RC-LH1 is shown in figure 2(left panel). From the height profile, shown in Figure 2(right panel), we find that the height of the 2D crystals of RC-LH1 on the surface is about 7 nm. We obtained similar results for 2D crystals of LH2, but in this case the height was about 5.5 nm, significantly lower than for RC-LH1. The results are in agreement with earlier reports²⁹.

Current *versus* voltage (I-V) curves were recorded by first locating RC-LH1- or LH2-containing lipid bilayer patches on the surface of the electrode by using tapping mode AFM. For these measurements we used conductive tips which were obtained by coating standard AFM cantilevers with a thin layer of gold or

platinum. After mapping the surface, the scanning probe tip was placed at a specific patch, and the system was switched from tapping mode to contact mode. A potential ramp was then applied between the tip and the gold surface and the resulting tunneling current was measured. The applied force was precisely controlled and held constant during such a measurement. The current measurements were limited by the external current-to-voltage convertor to the range -10 to +10 nA.

2.3.1 2D-crystals of LH2

We will first present the results of IV spectroscopy on 2D crystals of LH2. Results of such measurement were reported before by Stamouli et al., but in that case they were performed without force feedback.²⁹ Therefore there was some uncertainty about the question to what extent the results were affected by possible deformation of the protein-lipid layer underneath the tip. We thus repeated the IV measurements while varying the force applied by the tip in small increments from 0 to 14 nN. The results are shown in Figure 2. The IV curves are highly symmetric, and the magnitude of the tunneling current increases with the applied pressure. At a force of 14 nN the current shows a step-wise increase at V = 0, indicating direct contact between the tip and the underlying gold electrode. By measuring the slope

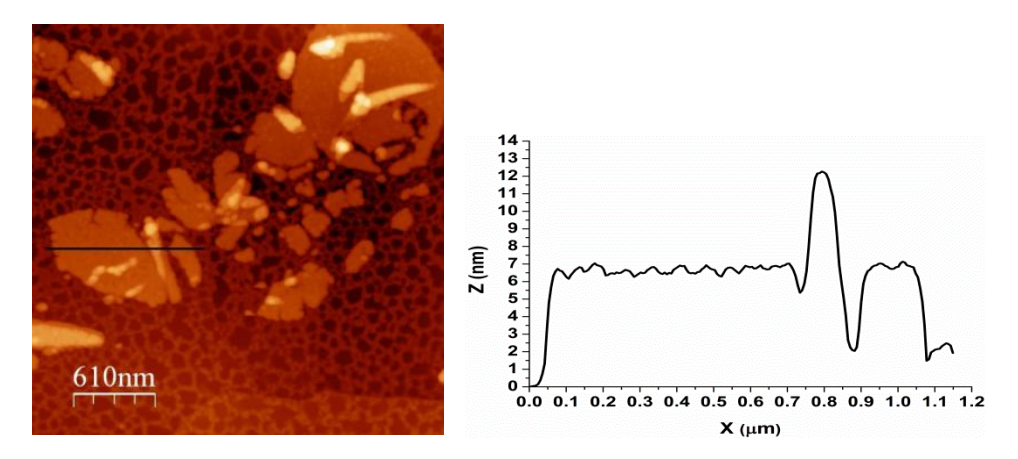


Figure 1: Typical Atomic force microscopy (AFM) image with height profile of 2D-crystals of RC-LH1 complexes adsorbed on a thin (10 nm) gold layer. The mage was recorded by using AFM in tapping mode in air under ambient temperature. The panel on the right shows the height profile along the line in the image.

of the curves around V = 0 we can determine the effective resistance in this range. The values are given in Table 1. The resistance values decrease by about two orders of magnitude when the force is increased from 2 to 13 nN.

We note that the shape of the I-V-curves for any given pressure is quite reproducible when we use fresh AFM tips, although the measured current may vary in amplitude by up to 20%. The tips became easily contaminated and/or damaged, however, and were replaced frequently to obtain consistent results. The gold-coated tips had typically a radius of curvature of about 15 nm, as verified by scanning electron microscopy. They were not sharp enough to resolve structural details of the 2D-crystalline LH2-patches that we reported earlier.²⁹ In fact, the amplitude and shape of the measured I-V curves were not very sensitive to the actual location of the probing tip within a single LH2- patch. This is not very

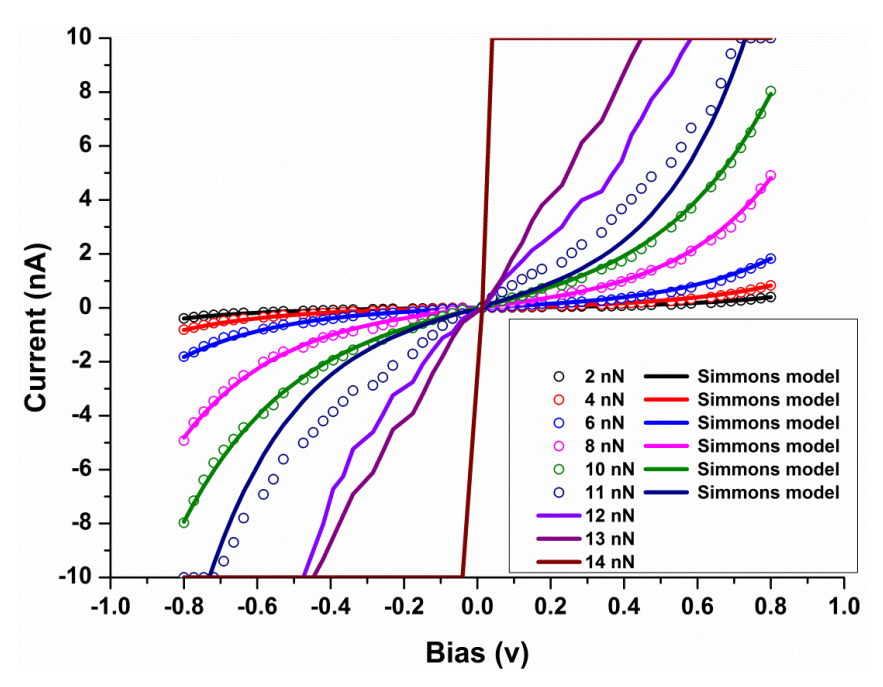


Figure 2: IV spectroscopy of LH2 complexes embedded in a lipid bilayer as a function of loading force. The tunneling junction is formed by sandwiching the 2D crystal of a LH2 complex between the conductive AFM tip and a gold electrode. In the force range of 2-11 nN the experimental data are plotted as open circles, while the solid lines are fits of the experimental data to the Simmons equation. The curves at forces of 12-14 nN were not fitted: the solid lines in these cases represent the experimental data.

surprising because the diameter of the tip end is somewhat larger than that of an LH2-ring. Also between patches there was little variation in the current response.

The traces in figure 2 have clearly the signature of electron tunneling across a barrier. An approximation for the barrier height and thickness can be obtained from a fit of the I-V curves to the so-called Simmons equation: ⁶⁴

$$I = \frac{e^2}{2\pi h L^2} \left\{ \left(\varphi - \frac{V}{2} \right) \exp \left[-K \left(\sqrt{\varphi - \frac{V}{2}} \right) \right] - \left(\varphi + \frac{V}{2} \right) \exp \left[-K \left(\sqrt{\varphi + \frac{V}{2}} \right) \right] \right\},$$

Where $K = (4\pi L/h)\sqrt{2me}$. The barrier height φ and thickness L are treated as adjustable parameters. This equation is based on a simplified form of the free electron model, using the Wentzel-Kramers-Brillouin approximation to obtain the tunnel probability.

Loading force (nN)	Resistance (GΩ)	L (nm)
2	6.25	1.41
4	3.04	1.36
6	1.26	1.26
8	0.45	1.22
10	0.25	1.16
11	0.11	1.12
12	0.06	
13	0.05	

Table 1:

The center column shows the resistance values as a function of the loading force, calculated from the slope of the IV curves in the range between ± 0.2 V. The column to the right shows the values of the (effective) barrier width, L, as determined by a fit of the Simmons model with a fixed value for the barrier height of $\varphi = 1.08$ eV.

The data in the lower force range (2-11 nN) can be very well fitted by the Simmons equation. Remarkably, good fits are obtained in all cases using the same value for the barrier height, $\varphi = 1.08$ eV: the change of the tunneling current seems to reflect primarily a variation of the barrier width. The quality of the fits does not significantly improve when both parameters, φ and L, are made adjustable. The values for L that were obtained from the fit are shown in the right-hand column of Table 1. At an applied force of 11 nN the fit to the Simmons equation starts to break down, and the I-V relationship shows a more "ohmic" character. This is particularly evident for the I-V curve at 13 nN. At a force of 14 nN a stepwise

change of the current is seen at V = 0, indicating direct contact between the tip and the supporting gold-electrode. We conclude that at this force the tip has perforated the protein-lipid layer. It appears that this perforation step occurs over the relative small force range of 11-14 nN, while the change of the barrier width from 2 to 11 nN is rather small.

Certainly at low force we thus observe tunneling over the full 5.5 nm height of the 2D-LH2 patch on the gold surface, although the barrier width as determined from the fit to the Simmons equation is significantly smaller. Electron tunneling over such a large distance is actually quite remarkable. In fact, we do not observe a tunneling current when we perform similar measurements on a lipid bilayer with a thickness of about 5 nm. Indeed, the tunneling rates drop of sharply over distances that exceed 1.5-2 nm in self-assembled layers of lipids, (thiol)alkanes and proteins. This suggests that electron tunneling across the 2D LH2 crystals is assisted by the cofactors of the LH2 protein complex. The cofactors of LH2 consist of BChl a and carotenoid molecules. Especially the carotenoid molecules appear to be effective conduits for electron tunneling since they are conjugated (i.e., π -electrons are essentially delocalized) over the full length of the molecule, and span the largest part of the height of the 2D-crystals. We will discuss the ramifications of this conclusion in more detail in the discussion section.

2.3.2 2D-crystals of RC-LH1

If the cofactor composition is a determining element for the probability of electron tunneling in 2D-assemblies of protein complexes we suspect that results of I-V spectroscopy will be different for complexes with another composition than that of LH2. To verify this conjecture we investigated the RC-LH1 complex using similar methods as described above. (See Chapter 1 of this thesis for details about the LH2 and RC-LH1 cofactor arrangements.)

It was shown by Fotiadis et al. (2003) that detergent-solubilized RC-LH1 complexes (from *Rhodospirillum rubrum*), when dialysed in the presence of lipids, can be readily assembled into 2D crystals with uniform orientation.⁶⁸ They showed that these 2D crystals did adsorb on mica, and could be imaged in high resolution with AFM. The RC-LH1 complexes were arranged in an orthorombic form with prominent protrusions that correspond to the H-subunit of the reaction center. A small minority of the complexes was oppositely oriented.

We adopted the same strategy to obtain 2D crystals of RC-LH1 complexes from *Rps. acidophila* in order to perform I-V spectroscopy on these samples when adsorbed on a gold surface. However, rather than dialysis, we applied the method that was developed by Rigaud et al., using biobeads to remove the detergent from the solution. This method is quicker and simpler, and provides good results. The 2D crystals that we obtained did adsorb on a thin gold electrode and formed (mostly) single-layer patches with a typical size of the order of about 1 μ m² (see figure 1). The height of these patches is about 6.5 nm, somewhat higher than in the case of LH2.

After removal of excess material and washing with buffer solution and deionized water the sample was dried (but not dehydrated) in a gentle flow of nitrogen. I-V spectroscopy was performed on the RC-LH1 patches as described in the previous section. At applied forces below 2 nN we observe negligible current at negative potentials, while the current gradually increases at positive potentials. A typical I-V curve at 1 nN is shown by the black curve in Figure 3A. At a force of 3 nN the curve looks very different, although it is still asymmetric: at a positive bias voltage the current is higher than at the same negative voltage. A larger family of curves is shown in Figure 3B in the force range of 2-13 nN. The amplitude of the current

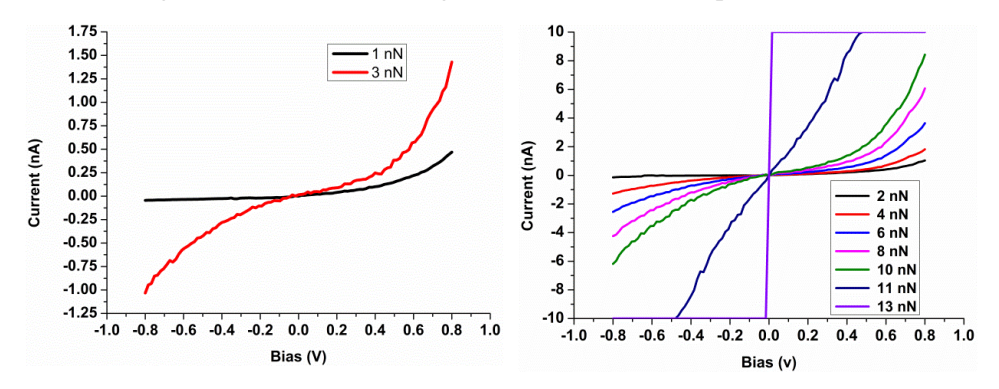


Figure 3. Comparison of IV curves measured by conductive AFM of RC-LH1 complexes embedded in a lipid bilayer as a function of applied force.

- (A) IV curves at an applied force of 1 nN (black) and of 3 nN red). IV curves are recorded at different applied forces, at lower force (Black curve) the behavior of IV curve is completely different compared to the response at relatively higher forces (red curve).
- **(B)** IV curves at applied force of 2 nN (black), 4 nN (red), 6 nN (blue), 8 nN (pink), 10 nN (green), 11 nN (dark blue) and 13 nN (purple).

gradually increases with the applied force, but the asymmetry between the positive and negative voltage ranges remains. This asymmetry is in stark contrast with the results that we obtained in the case of LH2.

In some ways the LH1- and LH2-rings of Rps. acidophila are similar: they are composed of heterodimeric, membrane-spanning subunits, each containing a carotenoid molecule and BCl a pigments, the latter being arranged on the periplasmic side of the complexes in the case of LH1. The carotenoid molecule spans in both case a large part of the height of the ring. The LH1 and LH2 complexes differ in the number of subunits in the ring, and in the number of BChl a molecules per subunit, three in the case of LH2 and two for LH1. We may assume that the similarity in architecture is reflected in the electron tunneling characteristics as measured by conductive AFM. In particular, we surmise that the contribution of the LH1 complex to the I-V curves as a function of bias voltage is symmetric around V = 0, as it is in LH2. In that case we expect that the asymmetry of the I-V-curves of RC-LH1 complexes arises from the contribution of the reaction center that is contained within the LH1-ring. This is corroborated by the fact that an asymmetric I-V-response was reported earlier for the case of lipidembedded RCs from Rb. sphaeroides R26 adsorbed on highly ordered pyrolythic graphite (HOPG).

Assuming that the part of the I-V curves at negative bias voltages is dominated by the contribution from the LH1 complex, we fitted this part with the Simmons equation. We applied a similar procedure as for the case of LH2, keeping the barrier height fixed and varying only the barrier width. We also allowed for a small, but constant contribution from the RC component at negative potentials. Following this procedure, we could extrapolate the LH1 contribution to the I-V response in the positive bias region. The difference between the Simmons fit and the measured I-V curve then reflects the contribution from the RC. The results are shown in figure 4 for the set of curves ranging from 4 to 10 nN. The contributions of both, the LH1 and the RC complexes, increase with applied force. At forces above 10 nN the I-V curves show an increasing ohmic behavior, until the proteolipid layer breaks down at about 14 nN, similar as in the case of LH2.

The magnitude of the tunneling current in the case of RC-LH1 complexes has a similar range as in the case of LH2. The measurements show that relatively facile

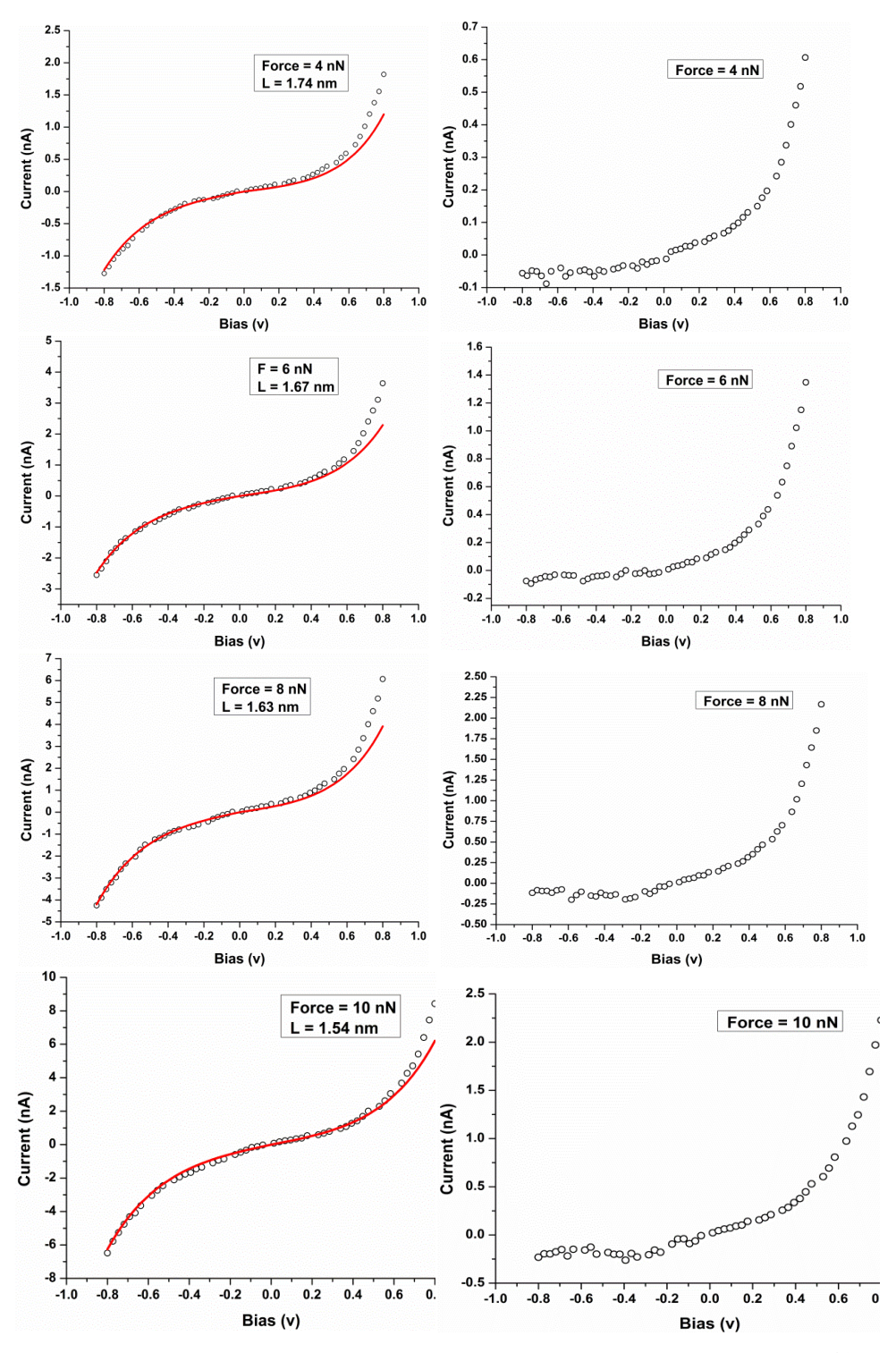
electron tunneling can be achieved over distances as large as 5-7 nm when photosynthetic pigment-protein complexes are sandwiched between a gold-coated tip and a flat gold-surface. Before we discuss these results in more detail we will describe results of light-induced electron transfer from the flat gold electrode to the adsorbed RC-LH1 complex. These experiments shed light on the orientation of the 2D crystals and the mechanism of this electron transfer step.

2.3.3 Light-induced electron transfer

The conductive AFM measurements show that electrons can be exchanged between the RC-LH1 complexes and bare gold electrodes. The key question is whether this exchange can also be driven by light. Optical excitation leads to charge separation in the RC, leaving a "hole" behind at the primary donor. Can this hole be filled by electron transfer from the electrode? We thus investigated the efficacy of the gold-adsorbed 2D crystals for the conversion of light energy to a charge transfer reaction, using spectroelectrochemistry. For this purpose a gold-coated microscope cover slip was incubated with a buffer solution of 2D crystals of RC-LH1 for one hour at 4 °C. The functionalized electrode was then rinsed with buffer solution to remove non-adsorbed RC-LH1 complexes, and then inserted in an electrochemical cell. This cell was equipped with a reference and a counter electrode, while the gold-coated microscope cover slip was configured as the working electrode. The cell was filled with buffer solution to which Q-0 and cyt c were added to serve as mediators.

Figure 4: The left-hand panels show fits of the IV data (circles) from 2D crystals of RC-LH1 complexes with the Simmons model (red curve), as a function of the applied force. In all cases we used a barrier height of $\varphi = 1.24$ eV, and only the part of the curve in the negative bias region was fitted. The barrier width, L, was adjusted for the best result, together with a small offset to account for the RC contribution at negative potentials.

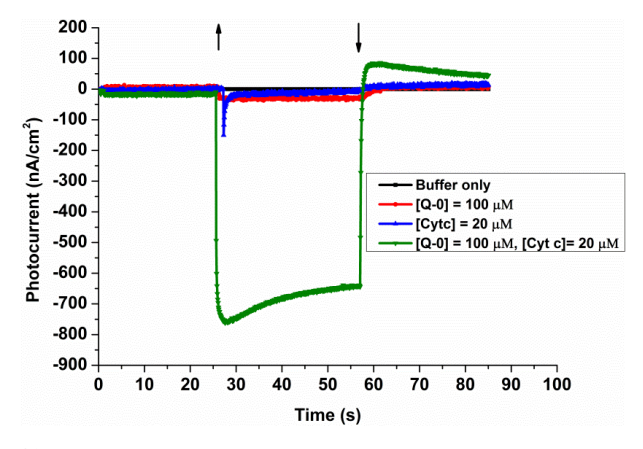
The right hand panels show the difference between the fitted curve and the experimental data, thus resolving the contribution of the RC complex to the IV response.



To verify that the photocurrent is associated with the RC-LH1 complex we measured the action spectra of photocurrent generation at different light intensities. The sample was excited with light from a scanning monochromator which filtered the light from a tungsten-halogen light source. A typical result is shown in Figure 6A for 2D RC-LH1 crystals adsorbed on the gold electrode. The action spectrum closely follows the absorption spectrum in the near infrared of RC-LH1 complexes in solution, with a maximum of 15 nA at 880 nm at a light intensity of 0.4 mW/cm², which is equivalent to 150 nA/cm² (black curve). Figure 6C (red data points) shows the dependence of the photocurrent response of the RC-LH1 crystals at 880 nm as a function of excitation intensity which was varied from 0.175 to 2.4 mW/cm². The shape of the action spectrum is more or less the same at all excitation intensities, but the ratio of the amplitudes at 880 and 800 nm changes as indicated in Fig. 6C (black data points).

At 880 nm absorption by the RC-LH1 complex is dominated by the LH1 antenna, whereas at 800 nm only the accessory bacteriochlorophylls, B_A and B_B , in the RC are excited. We assume that excitation of B_A and B_B elicits the typical RC response, *i.e.*, energy transfer to the special pair and subsequent charge separation. The data in Figure 6C indicate that the photocurrent response seems to saturate at higher excitation intensities.

Very similar results were obtained when detergent solubilized RC-LH1 complexes were adsorbed on the gold electrode. The working electrode was incubated with a solution of RC-LH1 for one hour, subsequently washed with the buffer to get rid of loosely bound and dissolved RC-LH1 complexes, and finally imounted in the



Photocurrent of 2D crystals of RC-LH1 deposited on a bare gold electrode, at a potential of -100 mV.

Figure 5

The mediator composition is indicated in the figure legend.

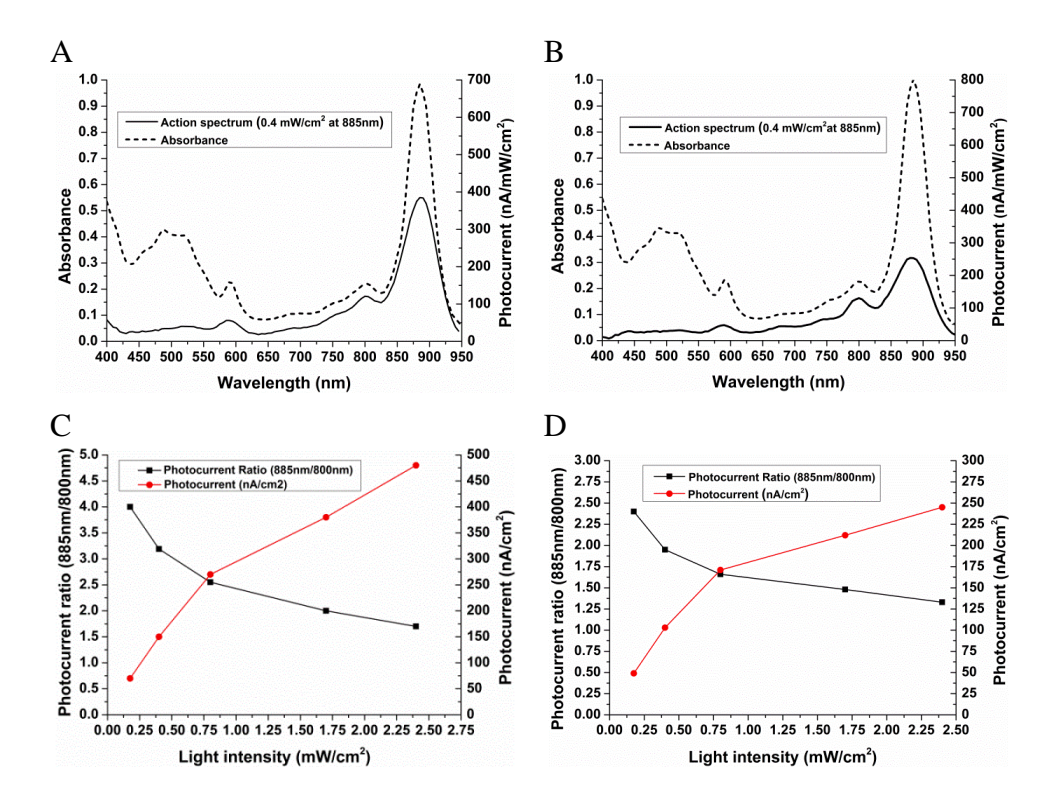


Figure 6

- (A) Action spectrum (solid line) of 2D crystals of RC-LH1 adsorbed on a gold electrode, and the absorption spectrum of RC-LH1 complexes in solution (dashed line). The action spectrum was recorded at a potential of -100 mV and by illumination at 800 nm with a light intensity of 0.4 mW/cm2. The absorbance spectrum is displaced upward by 0.05 units for clarity.
- (B) Action spectrum (solid line) of detergent-solubilized RC-LH1 complexes adsorbed on a gold electrode, and the absorption spectrum of RC-LH1 complexes in solution (dashed line). Conditions were the same as in (A). Also here the absorption spectrum is displaced upward.
- (C) Intensity dependence (red dots) of the 800 nm band and amplitude ratio (black dots) of the 800 and 880 nm bands in the action spectrum of gold-adsorbed 2D RC-LH1 crystals.
- (D) Intensity dependence (red dots) of the 800 nm band and amplitude ratio (black dots) of the 880 and 800 nm bands in the action spectrum of gold-adsorbed RC-LH1 complexes from detergent solution.

measuring cell which was filled with the measuring buffer solution. Magis et al. have shown that a high surface coverage can be obtained⁶¹.

A typical action spectrum is shown in Figure 6B (solid line) together with the absorption spectrum of RC-LH1 in solution. Figure 6D show a similar intensity dependence of the 880 and 800 nm bands as in the case of adsorbed 2D crystals.

2.4 Discussion

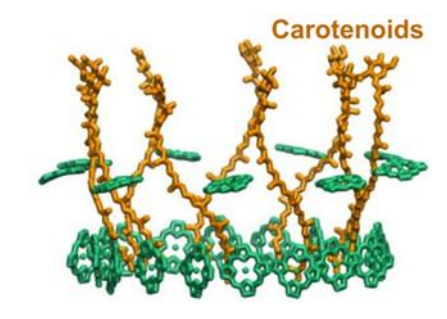
The topography of the 2D crystals of LH2 and RC-LH1 were recorded by using AFM in tapping mode. The height of RC-LH1 complexes embedded in lipid bilayers is rather homogeneous and amounts to about 6.5 nm which is consistent with a uniform monolayer of RC-LH1 complexes. The height of the RC-LH1 patches is somewhat higher than that of LH2 (~5 nm) which is largely due to the protruding H-subunit of the RC-complex.⁶⁸ The 2D crystals have a flake-like appearance, adsorb flat on a gold surface, and their thickness confirms that they consist of a single layer of densely packed pigment-protein complexes. Because of their size they are easily identified when adsorbed on the surface, and the dense, uniform packing makes them very suitable for C-AFM measurements since positioning of the tip is not very critical. The metal-coated tip, used for C-AFM measurements, was not sharp enough to resolve the individual complexes and their ordering in the 2D-crystals, but separate AFM measurements with sharp tips (data not shown) revealed that the crystals have a similar high level of ordering as that reported by others on similar samples. ^{19,20,26,28,68}

Normally, electron tunneling over a distance of 5-7 nm has a low to zero probability. Estimates of the electron tunneling rates can be based on the relationship between conductance (G) and molecular length (L) given by $G = A\exp(-\beta L)$, where A is a constant and β a decay constant which depends on molecular properties and structure. For alkanes and polypeptide β range from ~0.7 to $1 \text{ Å}^{-1,70}$ while for conjugated molecules, in particular carotenoids, a value of $0.22 \pm 0.04 \text{ Å}^{-1}$ has been reported Electron transfer within a protein medium appears to be limited to distances less than 1.4 nm. Of course, in a real C-AFM or STM experiment the tunneling current may depend on the contact area between the nanotip and the underlying electrode since multiple contacts may form with increasing tip size. With the type of tips that we used we did not observe any

tunneling current by C-AFM if the tip was positioned on a lipid bilayer. Obviously, with a tip radius of 15 nm there are probably multiple contacts in this case, but, nevertheless, the large decay constant strongly limits the tunneling probability.

It is somewhat surprising then that a significant tunneling current is observed in the case of 2D LH2-crystals. The I-V curve is highly symmetric, and the excellent fit to the Simmons equation suggests that the nanotip and the flat gold surface with the LH2 complex in between form a true tunneling junction. It is concluded that the tunneling current must be related to the properties of the co-factors in LH2. Their

arrangement is schematically shown in Figure 7, a side view of the LH2 complex with the periplasmic side at the bottom. The green ring-like structures represent the BChls, the extended yellow molecules the carotenoids. The plane of the B800 rings (about half way between top and bottom) is about 2.2 nm from the cytoplasmic surface, too large to contribute to electron



about 2.2 nm from the cytoplasmic surface, **Figure 7**too large to contribute to electron Arrangement of LH2 cofactors
tunneling, as already was pointed out by Stamouli et al.²⁹ A similar argument

applies to the B850 ring at the periplasmic side, although these molecules lie close (~0.8 nm) to the periplasmic face.

The most likely candidate to facilitate electron tunneling across the LH2 layer is

the carotenoid molecule. In the case of LH2 from *Rps. acidophila*, this molecule is rhodopsin glucoside, a carotenoid with 11 conjugated double bonds in a back bone of 30 carbon atoms, with a glucose moiety at one end. Their orientation in the LH2 complex is particularly favorable since they span almost the full height of the complex. The β -constant of such highly conjugated molecules is much smaller than that of a saturated carbon chain, indicating that they are relatively efficient charge carriers. For a carotenoid polyene with 11 double bonds He et al.(2005) have reported that the conductance $G = 0.11 \pm 0.7$ nS in the low bias regime, based on break-junction type measurements⁷¹. This is lower than the values that we obtain, which range from 0.16 to 20 nS, depending on the contact force. The differences between the measurements are two-fold. First, break junctions have a low contact barrier for electron tunneling and the measured conductance is therefore presumably more representative of the intrinsic property of the molecule.

Secondly, the larger contact area and the number of carotenoid molecules per LH2 complex imply that the tunneling currents from the present measurements likely contain contributions from multiple carotenoid molecules, certainly at higher force. We conclude that the increase of the conductance with increasing force is due to the increased number of carotenoid molecules that contribute to electron tunneling, and to a lowering of the contact resistance. The latter conjecture is based on the assumption that the LH2 complexes underneath the tip become (partially) compressed. This is corroborated by the reduction of the barrier width at increasing contact force. In fact, the barrier width is much smaller than the height of the LH2 crystal, which might well indicate that the electron tunneling is dominated by the contact resistance.

The directional character of the light-induced and of the bias voltage-induced electron transfer suggests that in both cases the electrons follow the same path. The C-AFM measurements indicate that the RC-LH1 crystals are predominantly oriented with the periplasmic side to the flat gold surface, with the H-subunit protruding out towards the C-AFM tip. The same orientation was observed by Fotiadis et al. (2004) in high resolution AFM images of 2D-crystals of *Rhodospirillum rubrum* adsorbed on a mica surface⁶⁸.

At higher applied forces (above 2 nN) the I-V curves of RC-LH1 complexes are deviating from diode like behavior, that is, current is also recorded for negative potentials. The analysis in figure 4 suggests that a symmetric contribution is superimposed on the RC-associated tunneling contribution. Such symmetric I-V curves may be typical for LH1 and LH2 which both contain complex-spanning carotenoids molecules. The long polyene chains of the carotenoids can conduct charge in both directions. Taking into account the symmetric I-V curves of LH2 and our measurements of asymmetric behavior of RC-LH1, we conclude that the I-V curves of RC-LH1 are a combination of two types of curves: symmetric I-V curves arising from tunneling via the LH1 ring and the rectifying behavior coming from the RC.

The possibility of direct integration of 2D crystals with an electrode may also represent a means of increasing the efficiency of photocurrent generation by the high packing density, improved electrode contact and favorable orientation. Therefore, we studied photocurrent generation 2D crystals of RC-LH1 complexes

adsorbed on a bare gold electrode. Detergent-solubilized RC-LH1 complexes and chromatophores have previously been deposited on bare gold electrode and it was shown that their functional and structural integrity was retained^{61,72}. The results reported in this chapter support this finding.

Adsorbed 2D crystals on bare gold produced substantial photocurrents. Despite low surface coverage and a relatively low concentration of mediators, a photocurrent of 780 nA/cm² was recorded by illumination with a light intensity of 2.5 mW/cm². This can be compared with recent data for 2D crystals of RC-LH1 from another photosynthetic bacterial species, Rps. palustris.35 In that work a photocurrent of 15 nA/cm² was reported at light illumination intensity of 0.4 mW/cm², 50 times less than reported here.³⁵ Apart from the light intensity and surface coverage, the observed difference can be attributed to a number of other factors. Firstly we have used bare gold electrode to deposit 2D crystals of RC-LH1 rather than a (3-aminopropyl)triethoxysilane (APS)-modified ITO-coated surface: the absence of the insulating layer between the electrode and RC-LH1 complex may provide a closer proximity of the RC-LH1 complex to the electrode, which increases the electron tunneling rate. Secondly we have used RC-LH1 complex from Rps. acidophila; this particular RC-LH1 complex has a tetrahedral cytochrome c associated with its periplasmic side by which the performance of this type of RC-LH1 is better than the other species in terms of photocurrent generation, especially when cyt c is used as a mediator in addition to Q-0. The presence of cyt c seems to improve the electron exchange between the working electrode and the special pair.

We find that the contribution of light absorption by LH1 (at 880 nm) to the photocurrent action spectra, relative to that by the RC (at 803 nm) depends on the light intensity. The relative LH1 contribution decreases with increasing light intensity. This confirms an earlier report of this effect. Presumably there is a rate limiting step in the electron transfer from the working electrode and the counter electrode via the mediators and the RC-LH1 complex.

Interestingly, the RC-LH1 complexes embedded in the 2D-crystals reported here have a much higher contribution in photocurrent per unit power at 880 nm compared to a layer of gold-adsorbed RC-LH1 complexes from detergent solution. A possible reason for this higher contribution may be enhanced energy transfers

between closely packed RC-LH1 complexes in 2D crystals and a more uniform orientation. Relative to adsorbed isolated RC-LH1 complexes, energy transfer may compete more effectively with quenching when RC-LH1 complexes are closely packed together. Also, the native like environment provided by lipid bilayer may optimize absorption and energy transfer process which may lead to enhanced performance of the pigment protein complexes.

RC-LH1 complexes embedded in lipid bilayer could be further explored in terms of their functionality incorporating in different types of lipids and using various lipids to protein ratios. 2D crystallization of pigment protein complexes may provide a useful platform for applications that require a uniformly oriented monolayer of photosynthetic protein complexes in a native like environment.

2.5 Conclusion:

Membrane protein complexes embedded in lipid bilayers with defined orientation and closely packed assembly provide an excellent platform to study individual components of the PSU in terms of the relation between structure and electronic properties. We have been able to probe and distinguish the role of the cofactors in RC-LH1 complex by utilizing C-AFM as a function of the contact force. The 2D crystalline packing of RC-LH1 complex improves the efficiency of photocurrent generation, compared to detergent solubilized RC-LH1 complexes. The RC-LH1 complexes in 2D-crystalline form can be adsorbed on bare, unmodified gold electrodes while keeping their functional integrity to produce substantial photocurrents.

References

- 1. Bahatyrova, S.; Frese, R. N.; Siebert, C. A.; Olsen, J. D.; Van Der Werf, K. O.; van, G. R.; Niederman, R. A.; Bullough, P. A.; Otto, C.; Hunter, C. N. The native architecture of a photosynthetic membrane. *Nature* **2004**, *430* (7003), 1058-1062.
- 2. Kirchhoff, H.; Lenhert, S.; Buchel, C.; Chi, L.; Nield, J. Probing the organization of photosystem II in photosynthetic membranes by atomic force microscopy. *Biochemistry* **2008**, *47* (1), 431-440.
- 3. Scheuring, S.; Sturgis, J. N.; Prima, V.; Bernadac, A.; Levy, D.; Rigaud, J. L. Watching the photosynthetic apparatus in native membranes. *Proc. Natl. Acad. Sci. U. S A* **2004**, *101* (31), 11293-11297.
- 4. Scheuring, S.; Goncalves, R. P.; Prima, V.; Sturgis, J. N. The photosynthetic apparatus of Rhodopseudomonas palustris: structures and organization. *J. Mol. Biol.* **2006**, *358* (1), 83-96.
- 5. Sturgis, J. N.; Tucker, J. D.; Olsen, J. D.; Hunter, C. N.; Niederman, R. A. Atomic Force Microscopy Studies of Native Photosynthetic Membranes. *Biochemistry* **2009**, 48 (17), 3679-3698.
- 6. Sznee, K.; Dekker, J. P.; Dame, R. T.; van Roon, H.; Wuite, G. J. L.; Frese, R. N. Jumping Mode Atomic Force Microscopy on Grana Membranes from Spinach. *Journal of Biological Chemistry* **2011**, 286 (45), 39164-39171.
- 7. Fotiadis, D.; Muller, D. J.; Tsiotis, G.; Hasler, L.; Tittmann, P.; Mini, T.; Jeno, P.; Gross, H.; Engel, A. Surface analysis of the photosystem I complex by electron and atomic force microscopy. *Journal of Molecular Biology* **1998**, *283* (1), 83-94.
- 8. Goncalves, R. P.; Busselez, J.; Levy, D.; Seguin, J.; Scheuring, S. Membrane insertion of Rhodopseudomonas acidophila light harvesting complex 2 investigated by high resolution AFM. *Journal of Structural Biology* **2005**, *149* (1), 79-86.
- 9. Hofmann, C.; Francia, F.; Venturoli, G.; Oesterhelt, D.; Kohler, J. Energy transfer in a single self-aggregated photosynthetic unit. *Febs Letters* **2003**, *546* (2-3), 345-348.
- Ketelaars, M.; Hofmann, C.; Kohler, J.; Howard, T. D.; Cogdell, R. J.; Schmidt, J.; Aartsma, T. J. Spectroscopy on individual light-harvesting 1 complexes of Rhodopseudomonas acidophila. *Biophys. J.* 2002, 83 (3), 1701-1715.
- Kondo, M.; Iida, K.; Dewa, T.; Tanaka, H.; Ogawa, T.; Nagashima, S.; Nagashima, K. V.; Shimada, K.; Hashimoto, H.; Gardiner, A. T.; Cogdell, R. J.; Nango, M. Photocurrent and electronic activities of oriented-His-tagged photosynthetic light-harvesting/reaction center core complexes assembled onto a gold electrode. *Biomacromolecules.* 2012, 13 (2), 432-438.
- Kunz, R.; Timpmann, K.; Southall, J.; Cogdell, R. J.; Freiberg, A.; Kohler, J. Exciton Self Trapping in Photosynthetic Pigment-Protein Complexes Studied by Single-Molecule Spectroscopy. *Journal of Physical Chemistry B* 2012, 116 (36), 11017-11023.
- Magis, G. J.; Olsen, J. D.; Reynolds, N. P.; Leggett, G. J.; Hunter, C. N.; Aartsma, T. J.; Frese, R. N. Use of engineered unique cysteine residues to facilitate oriented coupling of proteins directly to a gold substrate. *Photochem. Photobiol.* 2011, 87 (5), 1050-1057.
- Mikayama, T.; Iida, K.; Suemori, Y.; Dewa, T.; Miyashita, T.; Nango, M.; Gardiner, A. T.; Cogdell, R. J. The electronic behavior of a photosynthetic reaction center monitored by conductive atomic force microscopy. *J. Nanosci. Nanotechnol.* 2009, 9 (1), 97-107.

- 15. Pflock, T.; Dezi, M.; Venturoli, G.; Cogdell, R. J.; Kohler, J.; Oellerich, S. Comparison of the fluorescence kinetics of detergent-solubilized and membrane-reconstituted LH2 complexes from Rps. acidophila and Rb. sphaeroides. *Photosynth. Res.* **2008**, 95 (2-3), 291-298.
- 16. Reiss, B. D.; Hanson, D. K.; Firestone, M. A. Evaluation of the photosynthetic reaction center protein for potential use as a bioelectronic circuit element. *Biotechnology Progress* **2007**, *23* (4), 985-989.
- 17. Richter, M. F.; Baier, J.; Cogdell, R. J.; Kohler, J.; Oellerich, S. Single-molecule spectroscopic characterization of light-harvesting 2 complexes reconstituted into model membranes. *Biophysical Journal* **2007**, *93* (1), 183-191.
- Rutkauskas, D.; Novoderezkhin, V.; Cogdell, R. J.; van Grondelle, R. Fluorescence spectral fluctuations of single LH2 complexes from Rhodopseudomonas acidophila strain 10050. *Biochemistry* 2004, 43 (15), 4431-4438.
- 19. Scheuring, S.; Reiss-Husson, F.; Engel, A.; Rigaud, J. L.; Ranck, J. L. High-resolution AFM topographs of Rubrivivax gelatinosus light-harvesting complex LH2. *Embo Journal* **2001**, *20* (12), 3029-3035.
- Scheuring, S.; Seguin, J.; Marco, S.; Levy, D.; Breyton, C.; Robert, B.; Rigaud, J. L. AFM characterization of tilt and intrinsic flexibility of Rhodobacter sphaeroides light harvesting complex 2 (LH2). *Journal of Molecular Biology* 2003, 325 (3), 569-580.
- 21. Tubasum, S.; Cogdell, R. J.; Scheblykin, I. G.; Pullerits, T. Excitation-Emission Polarization Spectroscopy of Single Light Harvesting Complexes. *Journal of Physical Chemistry B* **2011**, *115* (17), 4963-4970.
- 22. Uchiyama, D.; Oikawa, H.; Otomo, K.; Nango, M.; Dewa, T.; Fujiyoshi, S.; Matsushita, M. Reconstitution of bacterial photosynthetic unit in a lipid bilayer studied by single-molecule spectroscopy at 5 K. *Physical Chemistry Chemical Physics* **2011**, *13* (24), 11615-11619.
- 23. van Oijen, A. M.; Ketelaars, M.; Kohler, J.; Aartsma, T. J.; Schmidt, J. Unraveling the electronic structure of individual photosynthetic pigment-protein complexes. *Science* **1999**, 285 (5426), 400-402.
- Zaitsev, S. Y.; Kalabina, N. A.; Zubov, V. P.; Chumanov, G.; Gaul, D.; Cotton, T. M. Monolayer Characteristics of Bacterial Photosynthetic Reaction Centers. *Colloids and Surfaces A-Physicochemical and Engineering Aspects* 1993, 78, 211-219.
- 25. Ghosh, R.; Hoenger, A.; Hardmeyer, A.; Mihailescu, D.; Bachofen, R.; Engel, A.; Rosenbusch, J. P. 2-Dimensional Crystallization of the Light-Harvesting Complex from Rhodospirillum-Rubrum. *Journal of Molecular Biology* **1993**, *231* (2), 501-504.
- 26. Liu, L. N.; Aartsma, T. J.; Frese, R. N. Dimers of light-harvesting complex 2 from Rhodobacter sphaeroides characterized in reconstituted 2D crystals with atomic force microscopy. *FEBS J.* **2008**, *275* (12), 3157-3166.
- 27. Rigaud, J. L. Membrane proteins: functional and structural studies using reconstituted proteoliposomes and 2-D crystals. *Brazilian Journal of Medical and Biological Research* **2002**, *35* (7), 753-766.
- Stamouli, A.; Kafi, S.; Klein, D. C.; Oosterkamp, T. H.; Frenken, J. W.; Cogdell, R. J.; Aartsma, T. J. The ring structure and organization of light harvesting 2 complexes in a reconstituted lipid bilayer, resolved by atomic force microscopy. *Biophys. J.* 2003, 84 (4), 2483-2491.

- 29. Stamouli, A.; Frenken, J. W.; Oosterkamp, T. H.; Cogdell, R. J.; Aartsma, T. J. The electron conduction of photosynthetic protein complexes embedded in a membrane. *FEBS Lett.* **2004,** *560* (1-3), 109-114.
- 30. Werten, P. J. L.; Remigy, H. W.; de Groot, B. L.; Fotiadis, D.; Philippsen, A.; Stahlberg, H.; Grubmuller, H.; Engel, A. Progress in the analysis of membrane protein structure and function. *Febs Letters* **2002**, *529* (1), 65-72.
- Xu, W.; Zhang, X.; Lou, S. Q.; Wang, K. B.; Huang, Y. G.; Kuang, T. Y. Two-dimensional crystallization and preliminary structure analysis of LHC-II from cucumber and spinach. Science in China Series C-Life Sciences 1998, 41 (3), 265-271.
- 32. Milhiet, P. E.; Gubellini, F.; Berquand, A.; Dosset, P.; Rigaud, J. L.; Le Grimellec, C.; Levy, D. High-resolution AFM of membrane proteins directly incorporated at high density in planar lipid bilayer. *Biophysical Journal* **2006**, *91* (9), 3268-3275.
- 33. Dewa, T.; Sumino, A.; Watanabe, N.; Noji, T.; Nango, M. Energy transfer and clustering of photosynthetic light-harvesting complexes in reconstituted lipid membranes. *Chemical Physics* **2013**, *419*, 200-204.
- 34. Sumino, A.; Dewa, T.; Kondo, M.; Morii, T.; Hashimoto, H.; Gardiner, A. T.; Cogdell, R. J.; Nango, M. Selective Assembly of Photosynthetic Antenna Proteins into a Domain-Structured Lipid Bilayer for the Construction of Artificial Photosynthetic Antenna Systems: Structural Analysis of the Assembly Using Surface Plasmon Resonance and Atomic Force Microscopy. *Langmuir* 2011, 27 (3), 1092-1099.
- Sumino, A.; Dewa, T.; Sasaki, N.; Kondo, M.; Nango, M. Electron Conduction and Photocurrent Generation of a Light-Harvesting/Reaction Center Core Complex in Lipid Membrane Environments. *Journal of Physical Chemistry Letters* 2013, 4 (7), 1087-1092.
- 36. Fujii, R.; Shimonaka, S.; Uchida, N.; Gardiner, A. T.; Cogdell, R. J.; Sugisaki, M.; Hashimoto, H. Construction of hybrid photosynthetic units using peripheral and core antennae from two different species of photosynthetic bacteria: detection of the energy transfer from bacteriochlorophyll a in LH2 to bacteriochlorophyll b in LH1. *Photosynth. Res.* **2008**, *95* (2-3), 327-337.
- 37. Amao, Y.; Kuroki, A. Photosynthesis Organ Grana from Spinach Adsorbed Nanocrystalline TiO2 Electrode for Photovoltaic Conversion Device. *Electrochemistry* **2009**, *77* (10), 862-864.
- 38. Blankenship, R. E.; Tiede, D. M.; Barber, J.; Brudvig, G. W.; Fleming, G.; Ghirardi, M.; Gunner, M. R.; Junge, W.; Kramer, D. M.; Melis, A.; Moore, T. A.; Moser, C. C.; Nocera, D. G.; Nozik, A. J.; Ort, D. R.; Parson, W. W.; Prince, R. C.; Sayre, R. T. Comparing Photosynthetic and Photovoltaic Efficiencies and Recognizing the Potential for Improvement. *Science* **2011**, *332* (6031), 805-809.
- 39. Cogdell, R. J.; Lindsay, J. G. Can photosynthesis provide a 'biological blueprint' for the design of novel solar cells? *Trends in Biotechnology* **1998**, *16* (12), 521-527.
- Das, R.; Kiley, P. J.; Segal, M.; Norville, J.; Yu, A. A.; Wang, L. Y.; Trammell, S. A.; Reddick, L. E.; Kumar, R.; Stellacci, F.; Lebedev, N.; Schnur, J.; Bruce, B. D.; Zhang, S. G.; Baldo, M. Integration of photosynthetic protein molecular complexes in solidstate electronic devices. *Nano Letters* 2004, 4 (6), 1079-1083.
- 41. Lu, Y.; Xu, J.; Liu, Y.; Liu, B.; Xu, C.; Zhao, D.; Kong, J. Manipulated photocurrent generation from pigment-exchanged photosynthetic proteins adsorbed to nanostructured WO3-TiO2 electrodes. *Chem. Commun. (Camb.)* **2006,** (7), 785-787.

- 42. Lu, Y. D.; Liu, Y.; Xu, J. J.; Xu, C. H.; Liu, B. H.; Kong, J. L. Bio-nanocomposite photoelectrode composed of the bacteria photosynthetic reaction center entrapped on a nanocrystalline TiO2 matrix. *Sensors* **2005**, *5* (4-5), 258-265.
- 43. Lukashev, E. P.; Nadtochenko, V. A.; Permenova, E. P.; Sarkisov, O. M.; Rubin, A. B. Electron phototransfer between photosynthetic reaction centers of the bacteria Rhodobacter sphaeroides and semiconductor mesoporous TiO2 films. *Doklady Biochemistry and Biophysics* **2007**, *415* (1), 211-216.
- 44. Mahmoudzadeh, A.; Saer, R.; Jun, D.; Mirvakili, S. M.; Takshi, A.; Iranpour, B.; Ouellet, E.; Lagally, E. T.; Madden, J. D. W.; Beatty, J. T. Photocurrent generation by direct electron transfer using photosynthetic reaction centres. *Smart Materials & Structures* **2011**, *20* (9).
- 45. Mershin, A.; Matsumoto, K.; Kaiser, L.; Yu, D.; Vaughn, M.; Nazeeruddin, M. K.; Bruce, B. D.; Graetzel, M.; Zhang, S. Self-assembled photosystem-I biophotovoltaics on nanostructured TiO(2) and ZnO. *Sci. Rep.* **2012**, *2*, 234.
- 46. Alvarez, J.; Ngo, I.; Gueunier-Farret, M. E.; Kleider, J. P.; Yu, L.; Cabarrocas, P. R.; Perraud, S.; Rouviere, E.; Celle, C.; Mouchet, C.; Simonato, J. P. Conductive-probe atomic force microscopy characterization of silicon nanowire. *Nanoscale. Res. Lett.* **2011**, *6* (1), 110.
- 47. Atanassov, A.; Hendler, Z.; Berkovich, I.; Ashkenasy, G.; Ashkenasy, N. Force modulated conductance of artificial coiled-coil protein monolayers. *Biopolymers* **2013**, *100* (1), 93-99.
- 48. Balke, N.; Tselev, A.; Arruda, T. M.; Jesse, S.; Chu, Y. H.; Kalinin, S. V. Probing local electromechanical effects in highly conductive electrolytes. *ACS Nano* **2012**, *6* (11), 10139-10146.
- 49. Casuso, I.; Fumagalli, L.; Samitier, J.; Padros, E.; Reggiani, L.; Akimov, V.; Gomila, G. Electron transport through supported biomembranes at the nanoscale by conductive atomic force microscopy. *Nanotechnology* **2007**, *18* (46).
- 50. Davis, J. J.; Wang, N.; Morgan, A.; Zhang, T.; Zhao, J. Metalloprotein tunnel junctions: compressional modulation of barrier height and transport mechanism. *Faraday Discuss.* **2006**, *131*, 167-179.
- 51. Frederix, P. L. T. M.; Bosshart, P. D.; Akiyama, T.; Chami, M.; Gullo, M. R.; Blackstock, J. J.; Dooleweerdt, K.; de Rooij, N. F.; Staufer, U.; Engel, A. Conductive supports for combined AFM-SECM on biological membranes. *Nanotechnology* **2008**, *19* (38).
- 52. Kim, C. M.; Bechhoefer, J. Conductive probe AFM study of Pt-thiol and Au-thiol contacts in metal-molecule-metal systems. *J. Chem. Phys.* **2013**, *138* (1), 014707.
- 53. Lee, D.; Yang, S. M.; Yoon, J. G.; Noh, T. W. Flexoelectric rectification of charge transport in strain-graded dielectrics. *Nano Lett.* **2012**, *12* (12), 6436-6440.
- MacDonald, G. A.; Veneman, P. A.; Placencia, D.; Armstrong, N. R. Electrical property heterogeneity at transparent conductive oxide/organic semiconductor interfaces: mapping contact ohmicity using conducting-tip atomic force microscopy. *ACS Nano* 2012, 6 (11), 9623-9636.
- 55. Rakshit, T.; Mukhopadhyay, R. Solid-state electron transport in Mn-, Co-, holo-, and Cu-ferritins: force-induced modulation is inversely linked to the protein conductivity. *J. Colloid Interface Sci.* **2012**, *388* (1), 282-292.

- 56. Wang, W. H.; Dong, R. X.; Yan, X. L.; Yang, B. Memristive characteristics in semiconductor/metal contacts tested by conductive atomic force microscopy. *Journal of Physics D-Applied Physics* **2011**, *44* (47).
- 57. Wanger, G.; Gorby, Y.; El-Naggar, M. Y.; Yuzvinsky, T. D.; Schaudinn, C.; Gorur, A.; Sedghizadeh, P. P. Electrically conductive bacterial nanowires in bisphosphonate-related osteonecrosis of the jaw biofilms. *Oral Surg. Oral Med. Oral Pathol. Oral Radiol.* 2013, 115 (1), 71-78.
- 58. Xu, D. G.; Watt, G. D.; Harb, J. N.; Davis, R. C. Electrical conductivity of ferritin proteins by conductive AFM. *Nano Letters* **2005**, *5* (4), 571-577.
- Zhao, J.; Davis, J. J. Molecular electron transfer of protein junctions characterised by conducting atomic force microscopy. *Colloids Surf. B Biointerfaces.* 2005, 40 (3-4), 189-194.
- 60. Trammell, S. A.; Wang, L. Y.; Zullo, J. M.; Shashidhar, R.; Lebedev, N. Orientated binding of photosynthetic reaction centers on gold using Ni-NTA self-assembled monolayers. *Biosensors & Bioelectronics* **2004**, *19* (12), 1649-1655.
- 61. den Hollander, M. J.; Magis, J. G.; Fuchsenberger, P.; Aartsma, T. J.; Jones, M. R.; Frese, R. N. Enhanced photocurrent generation by photosynthetic bacterial reaction centers through molecular relays, light-harvesting complexes, and direct protein-gold interactions. *Langmuir* **2011**, *27* (16), 10282-10294.
- 62. Tredgold, R. H. Langmuir-Blodgett Films Organic Monolayer Imaged. *Nature* **1985**, 313 (6001), 348.
- 63. van Baarle, G. J. C.; Troianovski, A. M.; Nishizaki, T.; Kes, P. H.; Aarts, J. Imaging of vortex configurations in thin films by scanning-tunneling microscopy. *Applied Physics Letters* **2003**, 82 (7), 1081-1083.
- 64. Zhao, J. W.; Davis, J. J.; Sansom, M. S. P.; Hung, A. Exploring the electronic and mechanical properties of protein using conducting atomic force microscopy. *Journal of the American Chemical Society* **2004**, *126* (17), 5601-5609.
- Page, C. C.; Moser, C. C.; Chen, X. X.; Dutton, P. L. Natural engineering principles of electron tunnelling in biological oxidation-reduction. *Nature* 1999, 402 (6757), 47-52.
- Mcdermott, G.; Prince, S. M.; Freer, A. A.; Hawthornthwaitelawless, A. M.; Papiz, M. Z.; Cogdell, R. J.; Isaacs, N. W. Crystal-Structure of An Integral Membrane Light-Harvesting Complex from Photosynthetic Bacteria. *Nature* 1995, 374 (6522), 517-521.
- 67. Mcdermott, G.; Prince, S. M.; Freer, A. A.; Isaacs, N. W.; Papiz, M. Z.; Hawthornthwaitelawless, A. M.; Cogdell, R. J. The 3-Dimensional Structure of the Light-Harvesting Antenna Complex (Lh-Ii) from Rps-Acidophila, Strain-10050, at 2.5 Angstrom Resolution. *Protein Engineering* **1995**, *8*, 43.
- 68. Fotiadis, D.; Qian, P.; Philippsen, A.; Bullough, P. A.; Engel, A.; Hunter, C. N. Structural analysis of the reaction center light-harvesting complex I photosynthetic core complex of Rhodospirillum rubrum using atomic force microscopy. *Journal of Biological Chemistry* **2004**, *279* (3), 2063-2068.
- 69. Rigaud, J. L.; Mosser, G.; Lacapere, J. J.; Olofsson, A.; Levy, D.; Ranck, J. L. Biobeads: An efficient strategy for two-dimensional crystallization of membrane proteins. *Journal of Structural Biology* **1997**, *118* (3), 226-235.
- 70. Tao, N. J. Electron transport in molecular junctions. *Nature Nanotechnology* **2006,** *1* (3), 173-181.

- 71. He, J.; Chen, F.; Li, J.; Sankey, O. F.; Terazono, Y.; Herrero, C.; Gust, D.; Moore, T. A.; Moore, A. L.; Lindsay, S. M. Electronic decay constant of carotenoid polyenes from single-molecule measurements. *Journal of the American Chemical Society* **2005**, *127* (5), 1384-1385.
- 72. Magis, G. J.; den Hollander, M. J.; Onderwaater, W. G.; Olsen, J. D.; Hunter, C. N.; Aartsma, T. J.; Frese, R. N. Light harvesting, energy transfer and electron cycling of a native photosynthetic membrane adsorbed onto a gold surface. *Biochim. Biophys. Acta* **2010**, *1798* (3), 637-645.

CHAPTER 3

Photosynthetic protein complexes as bio-photovoltaic building blocks with a high internal quantum efficiency

Abstract

Photosynthetic compounds have been a paradigm for biosolar cells and biosensors and for application in photovoltaic and photocatalytic devices. However, the interconnection of proteins and protein complexes with electrodes, in terms of electronic contact, structure, alignment and orientation, remains a challenge. Here we report on a deposition method that relies on the self organizing properties of these biological protein complexes to produce a densely packed and uniformly oriented monolayer by using Langmuir-Blodgett technology. The monolayer was deposited onto a gold electrode with defined orientation and produces the highest light induced photocurrents per protein complex to date, $45~\mu\text{A/cm}^2$ (with illumination power of $23~\text{mW/cm}^2$ at 880~nm) under ambient conditions. Our work shows for the first time that a significant portion of the intrinsic quantum efficiency of primary photosynthesis can be retained in a functional device outside the biological cell, leading to an internal quantum efficiency of 32% for light-induced electron transfer from the electrode to the photosynthetic protein complex.

3.1- Introduction

The design characteristics of photosynthesis are paradigm in solar cell research primarily because of the high, near unity quantum efficiency of the light driven steps in this process.¹ The primary photo-conversion reactions involve light absorption, energy transfer and charge transfer. The process relies on the interplay between various types of light-harvesting protein complexes, structurally welldefined polymers with embedded light-absorbing chromophores held in exact geometries. Besides mimicking individual aspects of photosynthesis there is a growing interest for the direct application of the protein complexes in biosolar cells and biosensors. ²⁻¹² However, the interconnection of proteins and protein complexes with electrodes, in terms of electronic contact, structure, alignment and orientation, remains a challenge. Several immobilization techniques have been examined in the past, which mostly involved bio-films formed by self-assembly on the surface of electrodes by incubation in a solution of photosynthetic complexes. 13-19 Even though photosynthetic proteins readily adsorb on the electrode, these techniques often produce monolayers with a non-uniform protein orientation. In order to control the orientation of the complexes on the electrodes, much research has been aimed at the development of genetically engineered complexes that bind specifically to an electrode that has been pre-modified with a suitable monolayer of linker molecules.^{5,20-26} A drawback of this method is the decrease in electron transfer (ET) efficiency due to the increased tunneling distance introduced by the thickness of the monolayer of linker molecules. A variety of photosynthetic proteins have been explored within the context of bio-hybrid devices, with emphasis on photosystem I (PSI), photosystem II (PSII), and reaction center (RC) complexes from different photosynthetic organisms. 4-6,9,10,12,13,18-20,24,27-36 As far as we know the quantum efficiency of any photosynthesis based biohybrid device reported has always been extremely low, with one moderate exception of 12% reported by Das et al. albeit upon illumination by monochromatic laser light of 10W/cm², the equivalent of more than 100 suns.⁵

Here we report on the Langmuir-Blodgett method that relies on the self-organizing properties of photosynthetic protein complexes to produce a uniformly oriented, densely packed monolayer of photosynthetic proteins. This method stands out by its simplicity, and by depositing Langmuir-Blodgett films directly onto a bare gold

electrode we produce record photocurrents with an internal quantum efficiency of 32%, under illumination by a light emitting diode with intensity of 23 mW/cm².

The Langmuir-Blodgett (LB) technique (see Figure 1) has been widely used for the deposition of mono- or multilayers of amphiphilic molecules on to solid substrates. 37-47 This method relies on the fact that when spread on a water surface, amphiphilic molecules take on a particular orientation with their hydrophilic side facing the water and their hydrophobic side facing upward (see Figure 1). The end result is a highly oriented monolayer of the sample at the air-water interface. This monolayer can then be deposited onto a particular substrate by vertically dipping the substrate into the water sub-phase. By reversing the dipping procedure, from the water phase into air, the orientation of the protein complexes is expected to be reversed as well. In this study, we employ isolated bacterial reaction center-light harvesting 1 (RC-LH1) complexes from the photosynthetic purple bacterium Rhodopseudomonas (Rps.) acidophila. The cylindrical wall of the RC-LH1 complex is strongly hydrophobic which explains its propensity for self-assembly in 2D arrays and its affinity for lipid bylayers. The two end-surfaces are more hydrophilic, but the difference between them may be sufficient to induce a preferred orientation upon the assembly of a LB layer. In the case of Rb. sphaeroides, for example, RCs in LB films are oriented with their H-subunit towards the water phase. 48 RCs from Rps. viridis, however, have the opposite

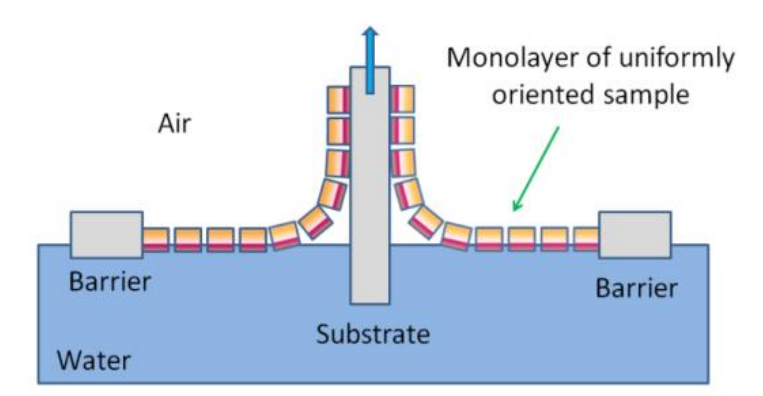


Figure 1. Schematic representation of the Langmuir-Blodgett deposition method. A sample containing amphiphilic molecules form a uniformly oriented monolayer on the water-air interface, with its hydrophilic side (purple) facing the water and its hydrophobic side (yellow) pointing upwards. The sample retains its orientation as it is being deposited on the substrate.

orientation because of the more hydrophilic cytochrome subunit at the periplasmic side of the complex. 48

The LH1 complex is a cylindrically shaped protein complex with a diameter of approximately 11 nm that contains 48 light absorbing pigments, including 32 bacteriochlorophylls and 16 carotenoid molecules. Light is absorbed by these pigments and excitations are transferred among the complexes until they are trapped by the reaction center which is surrounded by the LH1 proteins. The reaction center consists of several pigments and once an excitation is trapped, charge is transferred along a well-defined branch of redox-active cofactors in the RC, *i.e.* from a special bacteriochlorophyll *a* dimer to a pair of ubiquinone acceptors (Q_A and Q_B) via an intermediary bacteriochlorophyll *a* and a bacteriopheophytin molecule.

In nature this RC-LH1 complex is embedded in a lipid bilayer in a uniform orientation often mixed with additional light harvesting 2 (LH2) complexes. In several purple bacterial, photosynthetic species domains are formed of clusters of RC-LH1 complexes with varying size and order. likely assisted by the hydrophobic character of the outer walls of the cylindrical protein structure. This particular feature also drives the formation of RC-LH1 complexes to orient in two dimensional arrays on the water-air interface of a Langmuir–Blodgett (LB) trough. In order to make surface-adhered protein complexes viable for technological applications, some basic issues need to be addressed. Two of the main concerns are the preservation of the functional integrity of the proteins once they are adhered on conducting surfaces, and the efficiency of electron transfer between the protein and the electrode.

3.2 Materials and Methods

Langmuir Blodgett film deposition

The LB films were deposited on a gold sputtered glass slide by vertically dipping it into the sub-phase (forward dipping) or pulling it out (reverse dipping). The sub-phase of the LB trough consisted of milli-Q water. Before dipping, a solution of isolated RC-LH1 complexes was spread over the water surface and compressed to a surface pressure of 50 mN/m. In order to avoid structural deformation and achieve higher surface coverage, the surface pressure was kept constant at 50

mN/m during the LB deposition.⁴² In forward dipping mode, the gold coated glass slide was vertically dipped with a velocity of 1 mm/min and then removed at the highest available speed in order to avoid any deposition during the extraction. In reverse dipping the gold coated slide was dipped into the sub-phase before spreading the RC-LH1 complexes on the water surface. After compression of the LB-film the slide was pulled out slowly at a constant surface pressure of 50 mN/m to deposit the complexes with their hydrophilic side facing the electrode.

3.2.1 Photocurrent measurements

After the LB deposition step, the slide was incorporated into a measuring cell containing 2 ml of Tris buffer solution (pH 8). Light induced current measure-

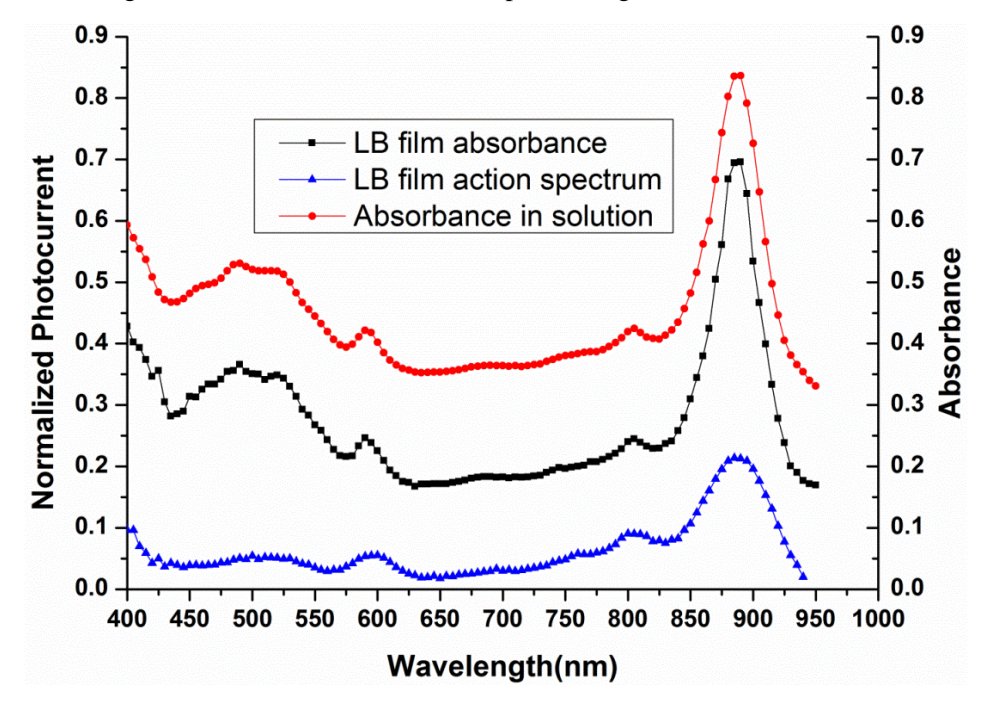


Figure 2. Action spectrum (blue triangles) and absorption spectra (black squares, forward dipped) of isolated RC-LH1 complexes deposited by the Langmuir-Blogdett method on a bare gold electrode. The action spectrum is obtained by measuring the photocurrent as a function of wavelengths, and is normalized for the intensity of light illumination. Absorption of isolated RC-LH1 complexes in buffer solution (red circles, Tris-HCl pH8) is shown for comparison. The absorption spectra are vertically displaced for better viewing. The vertical right-hand scale applies to the absorption spectrum; the LB-absorption spectrum is stretched vertically by a factor of 70.

ments were carried out using a potentiostat employing a conventional three-electrode setup, with the gold layer acting as the working electrode, a saturated calomel electrode as reference and a platinum wire serving as the counter electrode. The sample was illuminated from below, through the gold layer which was 12 nm thick with an optical transmission of 51 % at 880 nm, see Figure S1 in Supplementary Information (SI-3). The light source was a light emitting diode (LED) centered at $\lambda = 880$ nm, with a bandwidth of 50 nm, providing a light intensity of 23 mW/cm² at the surface of the working electrode of the electrochemical cell.

For measuring the action spectrum the excitation wavelength was scanned by passing white light (from a tungsten/halogen lamp) through a monochromator with a bandwidth of 40 nm. In this case, the light intensity at the surface of the electrode was 2 mW/cm² at $\lambda=880$ nm. More details of experimental conditions and procedures are available in Supporting Information. The Tris-buffered electrolyte contained ubiquinone-0 (Q-0) and horse heart cytochrome (cyt\) c as redox mediators which are responsible for electron transport from the Q_B site to the counter electrode and to assist the reduction of the special pair of the RC at the gold electrode.

3.3 Results and discussion

First of all we note that the absorption spectrum of the LB-deposited layer on the gold electrode is virtually identical to that of RC-LH1 complexes in solution (Figure 2, see also SI-3, Figure S3). The absorption spectra are sensitive to pigment-pigment interactions within the complex, and therefore it may be concluded that the structure of the complexes is not significantly affected by monolayer formation and deposition. This is confirmed by the fact that the shape of the light-induced current action spectrum is similar to the absorption spectrum of RC-LH1 complexes (Figure 2, triangles), indicating that light-induced charge separation is still fully operational, consistent with previous studies of surface-assembled RCs and chromatophores. The action spectrum also shows that the RC-LH1 complexes are the source of the generated photocurrents. It is evident from the action spectrum that pigments absorbing below 550 nm show a diminished contribution to photocurrent generation. Carotenoid molecules absorb in this region and they transfer the excitation to the RC less efficiently. From the

absorption spectrum of the LB-deposited RC-LH1 monolayers (see figure 2, and SI-3, Figure S3) we determined the surface coverage in the forward as well as the reverse dipped case. Forward dipped LB films have 5.6×10^{11} protein complexes per cm² whereas reverse dipped film contains 5.4×10^{11} complexes per cm². Adsorption of RC-LH1 complexes by incubating the gold surface for one hour in the dark at 4 °C with a solution of detergent solubilized RC-LH1 complexes (Tris buffer, pH 8) resulted in coverage of 6×10^{11} molecules per cm².

We measured the light-induced current response of the LB-deposited monolayers of RC-LH1 complexes on the gold electrode under various conditions. Ubiquinone-0 (Q-0) or a mixture of Q-0 and cytochrome (cyt) c were used as redox mediator. The magnitude of the photocurrents was influenced by the concentration of mediators, the applied potential, and the intensity of the light source. Figure 3 (black trace) shows that by omitting both mediators from the measuring solution no

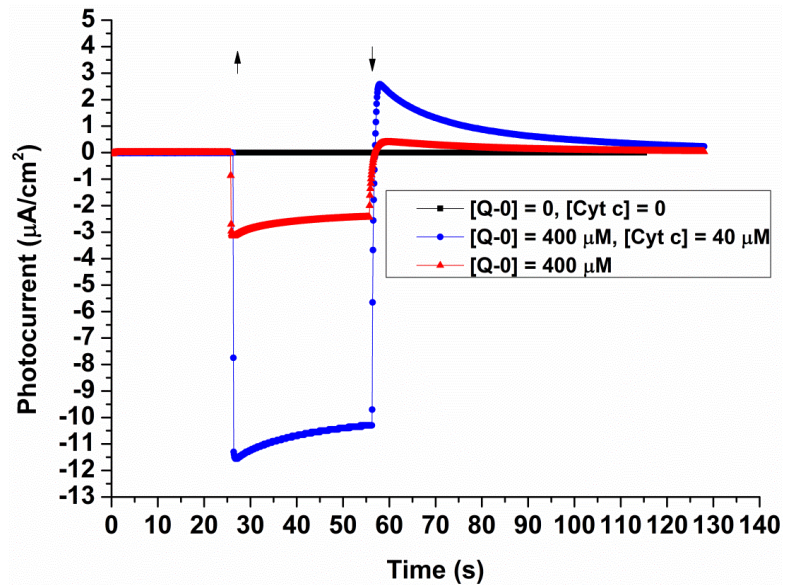


Figure 3. Photocurrents obtained from forward dipped Langmuir-Blodgett films with different redox mediator composition of the electrolyte. **Black squares**: When no redox mediators are present no current is observed. **Red triangles**: photocurrent of forward dipped LB film containing RC-LH1 using 400 μ M of quinones (Q₀) as the only as redox mediator. **Blue circles**: photocurrent with both Q₀ (400 μ M) and cyt c (40 μ M). The arrows indicate when the light was switched on (upward arrow) and off (downward arrow). The applied potential is -100 mV (vs. SCE) in all cases and the light source is an 880 nm LED with 23 mW/cm² of illumination power. Tris-HCl (pH 8) is used as measuring buffer.

photocurrent is produced. The trace formed by the red triangles in Figure 3 is the response when only Q-0 is present as mediator at a potential of -100 mV (vs. SCE). This is well above the reduction potential of the quinone/semiquinone half reaction not only of the RC-embedded Q_A molecule, but also of the small Q-10 pool of 4-9 molecules that may be retained within the RC-LH1 complex, assuming that these values are similar for Rhodobacter (Rb.) sphaeroides and Rps. acidophila. 50 Note that the Q_A reduction potential in Rps. acidophila is about 100 mV more negative than in the purple bacterium Rb. sphaeroides since it consists of menaquinone (MK-10) rather than ubiquinone (O-10).⁵¹ The light-induced current response shows that electron exchange occurs between the O-10 molecules in the RC-LH1 complexes and the Q-0 pool in solution. It is likely that electron transfer occurs directly from Q_A to Q-0 since Q-0 molecules can bind at the Q_B site of the RC, particularly at higher Q-0 concentrations, although we have to take into account that the binding constant for Q-0 is significantly lower than for Q-10, at least in the case of Rb. sphaeroides.⁵² The current response with only O-0 as mediator saturates, with a peak value of about 12 µA/cm², at a Q-0 concentration of about 3 mM (see SI-3, Fig. S4) which is comparable to that observed for the turn-over rate of O-0 by isolated reaction centers in solution. ⁵³

The current response in the presence of only Q-0 (Fig. 3) shows a transient component with a relative amplitude which increases with the Q-0 concentration (see SI-3, Figure S4). This feature can be attributed to the storage and equilibration of charge in the Q-0 pool in solution. The reverse current peak that is observed when the light is switched off is consistent with this interpretation, presumably resulting from charge recombination. The amplitude of the reverse current peak also increases with increasing concentration, following the storage capacity of the solution. It is reminiscent of the alternating current response of RC-LH1 complexes from *Rb. sphaeroides* in a photoelectrochemical cell upon illumination with N,N,N',N'-tetramethyl-p-phenylenediamine as mediator, reported by Tan and coworkers.¹⁰

The experiments provide evidence for direct electron transfer from the gold electrode to the special pair in the RC complex at negative potentials. The results also show that Q-0 is an effective mediator for light-induced current generation by RC-LH1 complexes that are directly immobilized on a gold electrode in an electrochemical cell. Nevertheless, earlier experiments have indicated that

photocurrent generation can be enhanced by the addition of cyt c to the solution. ^{13,22} Indeed, if cyt c is added as an extra mediator a significant increase of the photocurrent is observed (Figure 3, blue circles).

When the conditions are optimized in terms of mediator concentrations and applied potential, we obtain the results shown in Figure 4. Here we compare the photocurrent response of the LB film in forward and reverse dipped samples with that obtained by adsorption of RC-LH1 from solution. The latter was carried out by incubating the gold electrode with a solution of isolated RC-LH1 complexes for 1 hour in the dark at 4 °C. The electrode was then rinsed with buffer to remove unattached complexes.

The current reponse shown in Figure 4 is in stark contrast with that observed at positive potentials (see SI-3, Figure S6). In that case the photocurrent is dominated

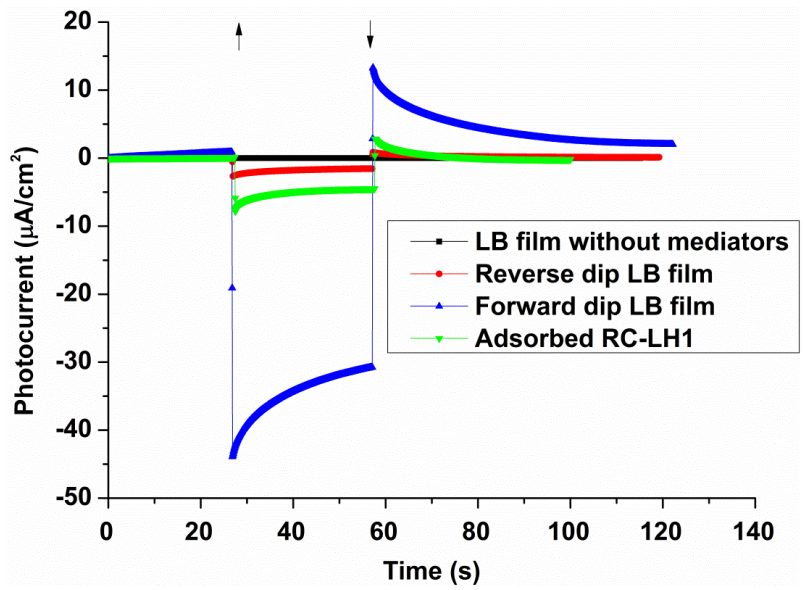


Figure 4. Photocurrent produced with different methods. Photocurrents were obtained from forward dipped LB deposition (blue triangles), reverse dipped LB film (red circles) and adsorbed (incubated for one hour on the electrode and then rinsed, green triangles) RC-LH1 complexes on gold electrode. The arrows indicate when the light is switched on (arrow pointing upwards) and when the light is switched off (arrow pointing downwards). The applied potential is $-175\,$ mV (vs. SCE) in all cases and the light source is an 880 nm LED with 23 mW/cm² of illumination power. Q-0 (1600 μ M) and cyt c (320 μ M) were used as charge carriers in the buffer solution.

by a fast transient response with a sign which is opposite to that of the signal in Figure 4. This can be attributed to the lower driving force for electron transfer from the electrode to the RC, and the loss of reducing capacity of the cyt c mediator. The fast transient response is likely due to the reduction of the quinones in the surface-assembled RCs.

At negative potentials, a major difference in photocurrent response can be observed for forward dipping compared to reverse dipping and simple incubation (cf. Figure 4). A maximum current density of 45 μ A/cm² was recorded for the forward dipped case, 3 μ A/cm² for the reverse dipped sample, and 8 μ A/cm² for adsorbed RC-LH1. The concentration of Q-0 and cyt c used in all three cases was 1600 μ M and 320 μ M, respectively, and the applied potential was -175 mV at which the response was maximal (see SI-3, Figure S6). The light intensity at the gold surface was 23 mW/cm² in all three experiments, corrected for absorption by the gold layer.

The forward dipped LB film generated a peak photocurrent density of $45 \,\mu\text{A/cm}^2$ under light illumination of $23 \,\text{mW/cm}^2$ (at $\lambda = 880 \,\text{nm}$) using Q-0 and cyt c as redox mediators. This compares very favorably with results obtained previously using RC-LH1 from *Rps. acidophila*, where maximally $25 \,\mu\text{A/cm}^2$ could be obtained but at twenty times higher intensity of light illumination. The results presented here thus show the largest photocurrent per photosynthetic complex reported to date. Recently, Mershin and co-workers reported a photocurrent of $362 \,\mu\text{A/cm}^2$ under AM1.5 solar irradiation, obtained by a photovoltaic device with photosystem 1 complexes interconnected to TiO2. This very high photocurrent could be obtained by three dimensional structuring of the electrode which enhanced the effective surface area by a factor of $200.^{54}$ If a similar enhancement factor would apply to the case of RC-LH1 complexes we would obtain a peak current of the order of milliamperes per cm².

Previous reports on comparison of ET efficiency for two different orientations of RCs have shown more efficient electron transfer for RC with the electron donor side facing the electrode compared to the opposite orientation. The large difference in photocurrent response of the forward and reverse dipped LB films suggests that we have different orientations of RC-LH1 complexes in these cases. In forward dipping we seem to have primary electron donor side close to the electrode whereas reverse dipping results in the opposite orientation. Comparison

with simple incubation supports our earlier conclusion that RC-LH1 complexes upon adsorption have a preferred orientation, with the primary donor of the RC facing the gold. The photo-current density for forward dipped LB films is much larger than that of solution-adsorbed RC-LH1 complexes though, which can be attributed to a significant fraction with unfavorable RC-LH1 orientation when adsorbed from solution, compared to the more uniformly oriented monolayers obtained by LB deposition.

Finally, the internal quantum efficiency is calculated by taking the ratio of the number of electrons generated per second to the number of photons absorbed per second. The number of electrons produced on our electrode is calculated from the maximum measured photocurrent density of $45~\mu\text{A/cm}^2$ which is equivalent to $5.7 \text{x} 10^{14}$ electrons per second. The number of photons absorbed on our electrode per second is estimated from the measured absorbance of the LB film and our light illumination intensity. We measured the absorbance of our LB film monolayer to be 0.0038, which leads to $1.8 \text{x} 10^{15}$ photons being absorbed per second. This result in a quantum efficiency of 32 %. (see SI-3 for detailed calculations).

3.4 Conclusion

We have used the Langmuir-Blodgett technique to deposit isolated bacterial RC-LH1 complexes on a bare gold electrode and showed that this method retains the functionality of the proteins, allows the control of the orientation of the protein, and increases the photocurrent output making it a promising method for fabrication of biosensors and biosolar cells. The highest photocurrent observed was 45 μ A/cm2 with an internal quantum efficiency of up to 32% under 23 mW/cm2 (at $\lambda = 880$ nm) light illumination intensity. This photocurrent is the highest of any single-layered photosynthetic protein complex to date, without any modifications to the proteins or substrate, and under ambient conditions.

References

- Blankenship, R. E.; Tiede, D. M.; Barber, J.; Brudvig, G. W.; Fleming, G.; Ghirardi, M.; Gunner, M. R.; Junge, W.; Kramer, D. M.; Melis, A.; Moore, T. A.; Moser, C. C.; Nocera, D. G.; Nozik, A. J.; Ort, D. R.; Parson, W. W.; Prince, R. C.; Sayre, R. T. Comparing Photosynthetic and Photovoltaic Efficiencies and Recognizing the Potential for Improvement. *Science* 2011, 332 (6031), 805-809.
- 2. Amao, Y.; Kuroki, A. Photosynthesis Organ Grana from Spinach Adsorbed Nanocrystalline TiO2 Electrode for Photovoltaic Conversion Device. *Electrochemistry* **2009**, 77 (10), 862-864.

- 3. Badura, A.; Guschin, D.; Kothe, T.; Kopczak, M. J.; Schuhmann, W.; Rogner, M. Photocurrent generation by photosystem 1 integrated in crosslinked redox hydrogels. *Energy & Environmental Science* **2011**, *4* (7), 2435-2440.
- 4. Ciesielski, P. N.; Hijazi, F. M.; Scott, A. M.; Faulkner, C. J.; Beard, L.; Emmett, K.; Rosenthal, S. J.; Cliffel, D.; Kane, J. G. Photosystem I based biohybrid photoelectrochemical cells. *Bioresour. Technol.* **2010**, *101* (9), 3047-3053.
- Das, R.; Kiley, P. J.; Segal, M.; Norville, J.; Yu, A. A.; Wang, L. Y.; Trammell, S. A.; Reddick, L. E.; Kumar, R.; Stellacci, F.; Lebedev, N.; Schnur, J.; Bruce, B. D.; Zhang, S. G.; Baldo, M. Integration of photosynthetic protein molecular complexes in solidstate electronic devices. *Nano Letters* 2004, 4 (6), 1079-1083.
- 6. Frolov, L.; Rosenwaks, Y.; Carmeli, C.; Carmeli, I. Fabrication of a photoelectronic device by direct chemical binding of the photosynthetic reaction center protein to metal surfaces. *Advanced Materials* **2005**, *17* (20), 2434-+.
- 7. Giardi, M. T.; Pace, E. Photosynthetic proteins for technological applications. *Trends in Biotechnology* **2005**, *23* (5), 257-263.
- 8. Lebedev, N.; Trammell, S. A.; Tsoi, S.; Spano, A.; Kim, J. H.; Xu, J.; Twigg, M. E.; Schnur, J. M. Increasing efficiency of photoelectronic conversion by encapsulation of photosynthetic reaction center proteins in arrayed carbon nanotube electrode. *Langmuir* **2008**, *24* (16), 8871-8876.
- 9. Takshi, A.; Madden, J. D. W.; Mahmoudzadeh, A.; Saer, R.; Beatty, J. T. A Photovoltaic Device Using an Electrolyte Containing Photosynthetic Reaction Centers. *Energies* **2010**, *3* (11), 1721-1727.
- 10. Tan, S. C.; Crouch, L. I.; Jones, M. R.; Welland, M. Generation of alternating current in response to discontinuous illumination by photoelectrochemical cells based on photosynthetic proteins. *Angew. Chem. Int. Ed Engl.* **2012**, *51* (27), 6667-6671.
- 11. Tan, S. C.; Crouch, L. I.; Mahajan, S.; Jones, M. R.; Welland, M. E. Increasing the open-circuit voltage of photoprotein-based photoelectrochemical cells by manipulation of the vacuum potential of the electrolytes. *ACS Nano* **2012**, *6* (10), 9103-9109.
- 12. Yehezkeli, O.; Tel-Vered, R.; Wasserman, J.; Trifonov, A.; Michaeli, D.; Nechushtai, R.; Willner, I. Integrated photosystem II-based photo-bioelectrochemical cells. *Nat. Commun.* **2012**, *3*, 742.
- 13. den Hollander, M. J.; Magis, J. G.; Fuchsenberger, P.; Aartsma, T. J.; Jones, M. R.; Frese, R. N. Enhanced photocurrent generation by photosynthetic bacterial reaction centers through molecular relays, light-harvesting complexes, and direct protein-gold interactions. *Langmuir* **2011**, *27* (16), 10282-10294.
- 14. Kato, M.; Cardona, T.; Rutherford, A. W.; Reisner, E. Photoelectrochemical water oxidation with photosystem II integrated in a mesoporous indium-tin oxide electrode. *J. Am. Chem. Soc.* **2012**, *134* (20), 8332-8335.
- 15. Magis, G. J.; den Hollander, M. J.; Onderwaater, W. G.; Olsen, J. D.; Hunter, C. N.; Aartsma, T. J.; Frese, R. N. Light harvesting, energy transfer and electron cycling of a native photosynthetic membrane adsorbed onto a gold surface. *Biochim. Biophys. Acta* **2010**, *1798* (3), 637-645.

- 16. Mershin, A.; Matsumoto, K.; Kaiser, L.; Yu, D.; Vaughn, M.; Nazeeruddin, M. K.; Bruce, B. D.; Graetzel, M.; Zhang, S. Self-assembled photosystem-I biophotovoltaics on nanostructured TiO(2) and ZnO. *Sci. Rep.* **2012**, *2*, 234.
- 17. Nakamura, C.; Hasegawa, M.; Yasuda, Y.; Miyake, J. Self-assembling photosynthetic reaction centers on electrodes for current generation. *Applied Biochemistry and Biotechnology* **2000**, *84-6*, 401-408.
- Yaghoubi, H.; Li, Z.; Jun, D.; Saer, R.; Slota, J. E.; Beerbom, M.; Schlaf, R.; Madden, J. D.; Beatty, J. T.; Takshi, A. The Role of Gold-Adsorbed Photosynthetic Reaction Centers and Redox Mediators in the Charge Transfer and Photocurrent Generation in a Bio-Photoelectrochemical Cell. *Journal of Physical Chemistry C* 2012, 116 (47), 24868-24877.
- 19. Zhao, J. Q.; Liu, B. H.; Zou, Y. L.; Xu, C. H.; Kong, J. L. Photoelectric conversion of photosynthetic reaction center in multilayered films fabricated by layer-by-layer assembly. *Electrochimica Acta* **2002**, *47* (12), 2013-2017.
- Kondo, M.; Nakamura, Y.; Fujii, K.; Nagata, M.; Suemori, Y.; Dewa, T.; Iida, K.; Gardiner, A. T.; Cogdell, R. J.; Nango, M. Self-assembled monolayer of light-harvesting core complexes from photosynthetic bacteria on a gold electrode modified with alkanethiols. *Biomacromolecules.* 2007, 8 (8), 2457-2463.
- Kondo, M.; Iida, K.; Dewa, T.; Tanaka, H.; Ogawa, T.; Nagashima, S.; Nagashima, K. V.; Shimada, K.; Hashimoto, H.; Gardiner, A. T.; Cogdell, R. J.; Nango, M. Photocurrent and electronic activities of oriented-His-tagged photosynthetic light-harvesting/reaction center core complexes assembled onto a gold electrode. *Biomacromolecules.* 2012, 13 (2), 432-438.
- 22. Lebedev, N.; Trammell, S. A.; Spano, A.; Lukashev, E.; Griva, I.; Schnur, J. Conductive wiring of immobilized photosynthetic reaction center to electrode by cytochrome C. *J. Am. Chem. Soc.* **2006**, *128* (37), 12044-12045.
- 23. Manocchi, A. K.; Baker, D. R.; Pendley, S. S.; Nguyen, K.; Hurley, M. M.; Bruce, B. D.; Sumner, J. J.; Lundgren, C. A. Photocurrent generation from surface assembled photosystem I on alkanethiol modified electrodes. *Langmuir* **2013**, *29* (7), 2412-2419.
- 24. Reiss, B. D.; Hanson, D. K.; Firestone, M. A. Evaluation of the photosynthetic reaction center protein for potential use as a bioelectronic circuit element. *Biotechnology Progress* **2007**, *23* (4), 985-989.
- 25. Trammell, S. A.; Spano, A.; Price, R.; Lebedev, N. Effect of protein orientation on electron transfer between photosynthetic reaction centers and carbon electrodes. *Biosens. Bioelectron.* **2006**, *21* (7), 1023-1028.
- 26. Trammell, S. A.; Griva, I.; Spano, A.; Tsoi, S.; Tender, L. M.; Schnur, J.; Lebedev, N. Effects of distance and driving force on photoinduced electron transfer between photosynthetic reaction centers and gold electrodes. *Journal of Physical Chemistry C* **2007**, *111* (45), 17122-17130.
- Ciesielski, P. N.; Scott, A. M.; Faulkner, C. J.; Berron, B. J.; Cliffel, D. E.; Jennings, G. K. Functionalized nanoporous gold leaf electrode films for the immobilization of photosystem I. ACS Nano 2008, 2 (12), 2465-2472.
- 28. Faulkner, C. J.; Lees, S.; Ciesielski, P. N.; Cliffel, D. E.; Jennings, G. K. Rapid assembly of photosystem I monolayers on gold electrodes. *Langmuir* **2008**, 24 (16), 8409-8412.

- 29. Gunther, D.; LeBlanc, G.; Prasai, D.; Zhang, J. R.; Cliffel, D. E.; Bolotin, K. I.; Jennings, G. K. Photosystem I on graphene as a highly transparent, photoactive electrode. *Langmuir* **2013**, 29 (13), 4177-4180.
- Lu, Y.; Xu, J.; Liu, Y.; Liu, B.; Xu, C.; Zhao, D.; Kong, J. Manipulated photocurrent generation from pigment-exchanged photosynthetic proteins adsorbed to nanostructured WO3-TiO2 electrodes. *Chem. Commun. (Camb.)* 2006, (7), 785-787.
- Lu, Y. D.; Liu, Y.; Xu, J. J.; Xu, C. H.; Liu, B. H.; Kong, J. L. Bio-nanocomposite photoelectrode composed of the bacteria photosynthetic reaction center entrapped on a nanocrystalline TiO2 matrix. Sensors 2005, 5 (4-5), 258-265.
- 32. Lukashev, E. P.; Nadtochenko, V. A.; Permenova, E. P.; Sarkisov, O. M.; Rubin, A. B. Electron phototransfer between photosynthetic reaction centers of the bacteria Rhodobacter sphaeroides and semiconductor mesoporous TiO2 films. *Doklady Biochemistry and Biophysics* **2007**, *415* (1), 211-216.
- 33. Mahmoudzadeh, A.; Saer, R.; Jun, D.; Mirvakili, S. M.; Takshi, A.; Iranpour, B.; Ouellet, E.; Lagally, E. T.; Madden, J. D. W.; Beatty, J. T. Photocurrent generation by direct electron transfer using photosynthetic reaction centres. *Smart Materials & Structures* **2011**, *20* (9).
- Matsumoto, K.; Nomura, K.; Tohnai, Y.; Fujioka, S.; Wada, M.; Erabi, T. Immobilization of photosynthetic reaction center complexes onto a hydroquinonethiol-modified gold electrode. *Bulletin of the Chemical Society of Japan* 1999, 72 (10), 2169-2175.
- Nikandrov, V. V.; Borisova, Y. V.; Bocharov, E. A.; Usachev, M. A.; Nizova, G. V.; Nadtochenko, V. A.; Lukashev, E. P.; Trubitsin, B. V.; Tikhonov, A. N.; Kurashov, V. N.; Mamedov, M. D.; Semenov, A. Y. Photochemical properties of photosystem 1 immobilized in a mesoporous semiconductor matrix. *High Energy Chemistry* 2012, 46 (3), 200-205.
- 36. Terasaki, N.; Iwai, M.; Yamamoto, N.; Hiraga, T.; Yamada, S.; Inoue, Y. Photocurrent generation properties of Histag-photosystem II immobilized on nanostructured gold electrode. *Thin Solid Films* **2008**, *516* (9), 2553-2557.
- 37. Atkins, K. J.; Honeybourne, C. L. Langmuir-Blodgett-Films of New Amphiphilic Electrooptically Active Charge-Transfer Dyes. *Journal of Physics-Condensed Matter* **1991**, *3*, S319-S327.
- 38. Bernard, J.; Talon, H.; Orrit, M.; Mobius, D.; Personov, R. I. Stark-Effect in Hole-Burning Spectra of Dye-Doped Langmuir-Blodgett-Films. *Thin Solid Films* **1992**, *217* (1-2), 178-186.
- 39. Byrd, H.; Pike, J. K.; Talham, D. R. Inorganic Monolayers Formed at An Organic Template A Langmuir-Blodgett Route to Monolayer and Multilayer Films of Zirconium Octadecylphosphonate. *Chemistry of Materials* **1993**, *5* (5), 709-715.
- 40. Chakraborty, S.; Bhattacharjee, D.; Hussain, S. A. Formation of nanoscale aggregates of a coumarin derivative in Langmuir-Blodgett film. *Applied Physics A-Materials Science & Processing* **2013**, *111* (4), 1037-1043.
- 41. Choi, J. W.; Nam, Y. S.; Kong, B. S.; Lee, W. H.; Park, K. M.; Fujihira, M. Bioelectronic device consisting of cytochrome c/poly-L-aspartic acid adsorbed hetero-Langmuir-Blodgett films. *Journal of Biotechnology* **2002**, *94* (3), 225-233.

- 42. Facci, P.; Erokhin, V.; Paddeu, S.; Nicolini, C. Surface pressure induced structural effects in photosynthetic reaction center Langmuir-Blodgett films. *Langmuir* **1998**, *14* (1), 193-198.
- Fukuda, K.; Shibasaki, Y.; Nakahara, H.; Tagaki, W.; Takahashi, H.; Tamura, S.; Kawabata, Y. Photopolymerization of A Omega-Tricosenoyl Derivative of Beta-Cyclodextrin in Langmuir-Blodgett-Films. *Thin Solid Films* 1992, 210 (1-2), 387-389.
- 44. Yasuda, Y.; Hirata, Y.; Sugino, H.; Kumei, M.; Hara, M.; Miyake, J.; Fujihira, M. Langmuir-Blodgett-Films of Reaction Centers of Rhodopseudomonas-Viridis Photoelectric Characteristics. *Thin Solid Films* **1992**, *210* (1-2), 733-735.
- Yoshida, J.; Saruwatari, K.; Kameda, J.; Sato, H.; Yamagishi, A.; Sun, L. S.; Corriea, M.; Villemure, G. Electron transfer through clay monolayer films fabricated by the Langmuir-Blodgett technique. *Langmuir* 2006, 22 (23), 9591-9597.
- 46. Zarbakhsh, A.; Campana, M.; Mills, D.; Webster, J. R. Structural studies of aliphatic substituted phthalocyanine-lipid multilayers. *Langmuir* **2010**, *26* (19), 15383-15387.
- 47. Zasadzinski, J. A.; Viswanathan, R.; Madsen, L.; Garnaes, J.; Schwartz, D. K. Langmuir-Blodgett-Films. *Science* **1994**, 263 (5154), 1726-1733.
- 48. Zaitsev, S. Y.; Kalabina, N. A.; Zubov, V. P.; Lukashev, E. P.; Kononenko, A. A.; Uphaus, R. A. Monolayers of Photosynthetic Reaction Centers of Green and Purple Bacteria. *Thin Solid Films* **1992**, *210* (1-2), 723-725.
- 49. Alegria, G.; Dutton, P. L. Langmuir-Blodgett Monolayer Films of Bacterial Photosynthetic Membranes and Isolated Reaction Centers Preparation, Spectrophotometric and Electrochemical Characterization .1. *Biochimica et Biophysica Acta* **1991**, *1057* (2), 239-257.
- Comayras, F.; Jungas, C.; Lavergne, J. Functional consequences of the organization of the photosynthetic apparatus in Rhodobacter sphaeroides. I. Quinone domains and excitation transfer in chromatophores and reaction center.antenna complexes. *J. Biol. Chem.* 2005, 280 (12), 11203-11213.
- 51. Hiraishi, A.; Hoshino, Y.; Kitamura, H. Isoprenoid Quinone Composition in the Classification of Rhodospirillaceae. *Journal of General and Applied Microbiology* **1984**, *30* (3), 197-210.
- 52. Diner, B. A.; Schenck, C. C.; Devitry, C. Effect of Inhibitors, Redox State and Isoprenoid Chain-Length on the Affinity of Ubiquinone for the Secondary Acceptor Binding-Site in the Reaction Centers of Photosynthetic Bacteria. *Biochimica et Biophysica Acta* **1984**, 766 (1), 9-20.
- 53. Gerencser, L.; Maroti, P. Turnover of ubiquinone-0 at the acceptor side of photosynthetic reaction center. *European Biophysics Journal with Biophysics Letters* **2008**, *37* (7), 1195-1205.
- 54. Mershin, A.; Matsumoto, K.; Kaiser, L.; Yu, D.; Vaughn, M.; Nazeeruddin, M. K.; Bruce, B. D.; Graetzel, M.; Zhang, S. Self-assembled photosystem-I biophotovoltaics on nanostructured TiO(2) and ZnO. *Sci. Rep.* **2012**, *2*, 234.

Chapter 3: Supporting Information

SI-3.1 Materials and Methods

RC-LH1 Isolation

RC-LH1 complexes from *Rps. acidophila* were isolated by using the protocol from Law et al. (1999) and suspended in buffer with 10 mM Tris (pH 8), supplemented with 0.1% Lauryldimethylamine-N-oxide(LDAO) and 1 mM EDTA(Law et al. 1999)

Gold Working Electrodes:

The working electrodes were prepared by sputtering gold on clean glass cover slips (Van Baarle et al.2003). The glass cover slips (25 mm diameter, 0.13-0.16 mm thickness) were purchased from Menzel-Gläser and cleaned prior to sputtering using various steps. First, the cover slips were sonicated for one hour in methanol, washed with milli-Q water, and dried under the nitrogen flow. The glass cover slips were then ozone-cleaned by using a UVP PR-100, UV-ozone Photoreactor, for one hour. Gold was deposited on the clean glass cover slips by using a magnetron sputtering system (ATC 1800-F, AJA Corporation). A thin layer (1-2 nm thick) of molybdenum-germanium (MoGe) was deposited first in order to serve as an

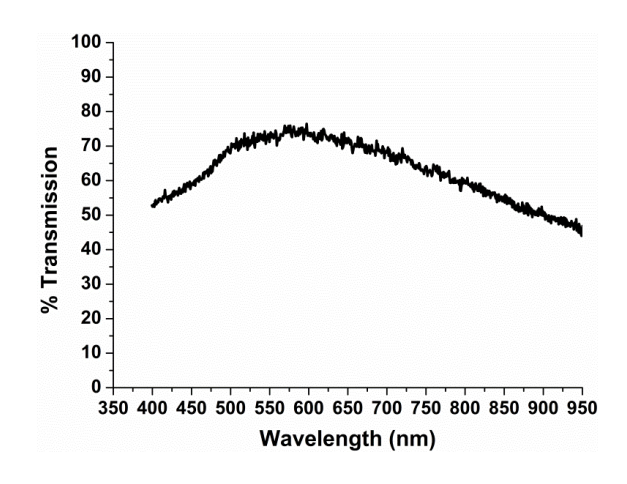


Figure S1.

Optical transmission spectrum of a 12 nm thick gold layer deposited on a microscope glass cover slip. The spectrum was measured with a fiber-coupled spectrometer (QE6500, Ocean Optics Inc., USA). adhesion layer between the gold and the glass surface. A homogeneous, 12 nm thick layer of gold was then sputtered on top of it. MoGe was sputtered at the rate of 1.32 nm/min in a 10 mTorr argon environment, whereas for the gold the sputtering rate was 9.06 nm/min in an argon atmosphere mixed with 1% and oxygen at a total pressure of 10 mTorr. Gold coated glass cover slips were then stored in a desiccator (at most for a few days) until they were used. This gold deposition protocol results in very flat, homogeneous gold layers with a root-mean-square roughness of 2-3 Å and a uniform thickness across the full surface of the cover slip. These properties were very reproducible, and are directly associated with the presence of the MoGe wetting layer. Figure S1 shows the transmission spectrum of such a cover slip when coated with a gold layer of 12 nm thick.

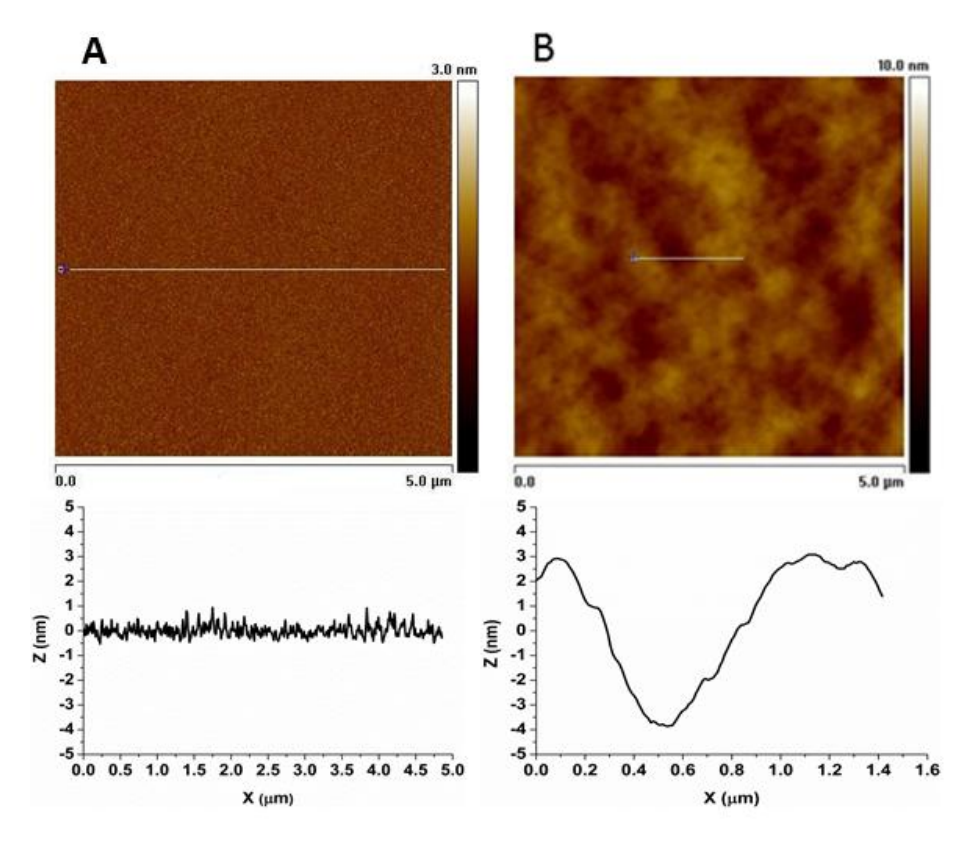


Figure S2. *Top*: Tapping mode AFM image of freshly sputtered gold electrode (left) and Langmuir Blodgett film (right) deposited on gold electrode, imaging was performed under ambient conditions. *Bottom:* Height profiles of the AFM images along the lines in the corresponding top pnales.

Langmuir Blodgett Deposition

A KSV Nima trough (KSV instruments Co., Helsinki, Finland) was used to deposit Langmuir-Blodgett films of isolated RC-LH1 complexes on the gold electrodes. The sub-phase of the LB trough initially contained only milli-Q water. A solution of isolated RC-LH1 complexes (1 mg/ml concentration) was then spread over the water surface and the air-water interface was allowed to settle for 15 minutes. After subsequently compressing the surface layer to a surface pressure of 50 mN/m, the gold coated glass cover slip was vertically dipped into the trough at a velocity of 1 mm/min while maintaining a constant surface pressure of 50 mN/m during the LB deposition. After dipping the slide completely into the water sub-phase, the slide was pulled out at the highest available speed to avoid any deposition during the extraction. For reverse dipping, the gold coated glass cover slip was first dipped into the sub-phase before spreading the RC-LH1 solution on the surface of the milliQ water. After 15 min the slide was vertically extracted with a velocity of 1 mm/min while keeping the surface pressure constant at 50 mN/m.

Atomic Force Microscopy

The topography of the Langmuir-Blodgett film of RC-LH1 complexes on the gold electrode was observed by imaging in tapping mode and in air using a commercial atomic force microscope, equiped with an E-Scanner (AFM, Nanoscope IIIa, Veeco, USA). A typical image is shown in Figure S2. Standard Si-nitride probes with a resonance frequency of 75 kHz and a spring constant of 2.8 Nm⁻¹ were used for imaging. Topography of the freshly sputtered bare gold electrode (S2 A) and gold electrode after Langmuir-Blodgett film deposition (S2 B) is shown in figure S2.

Surface coverage of RC-LH1 on gold electrode by absorption spectra

The surface coverage of RC-LH1 was calculated from the absorption spectra of Langmuir Blodgett films deposited in forward dip, reverse dip, and of adsorbed RC-LH1 complexes from the solution. The absorption spectra were recorded by using a fiber-coupled spectrometer (QE 6500, Ocean Optics Inc.), equipped with a halogen light source. The spectra are shown in Figure S3. The spectra were corrected for reflection and absorption by the gold layer by using a bare gold-coated cover slip from the same coating run as a reference.

The absorption spectra were utilized to calculate the surface coverage. The measured absorbance for the forward dipped LB film at 885 nm was 0.00375 (this is half of the measured absorbance of 0.0075 because we have LB film on both sides of the slide) the numbers of RC-LH1 complexes per cm² for forward dipped LB film are calculated to be 5.6×10^{11} , for reverse dipping the number of complexes is 5.4×10^{11} , whereas the sample with adsorbed RC-LH1 has 6×10^{11} molecules per cm²

Photocurrent Measurement

Light induced current measurements were carried out using a potentiostat (Autolab PGSTAT 128N) in the conventional 3 three-electrode setup, with the gold coated glass cover slip acting as the working electrode, a standard calomel electrode as the reference, and a platinum wire serving as the counter electrode. The reference electrode and the counter electrode were inserted from the top into a home built

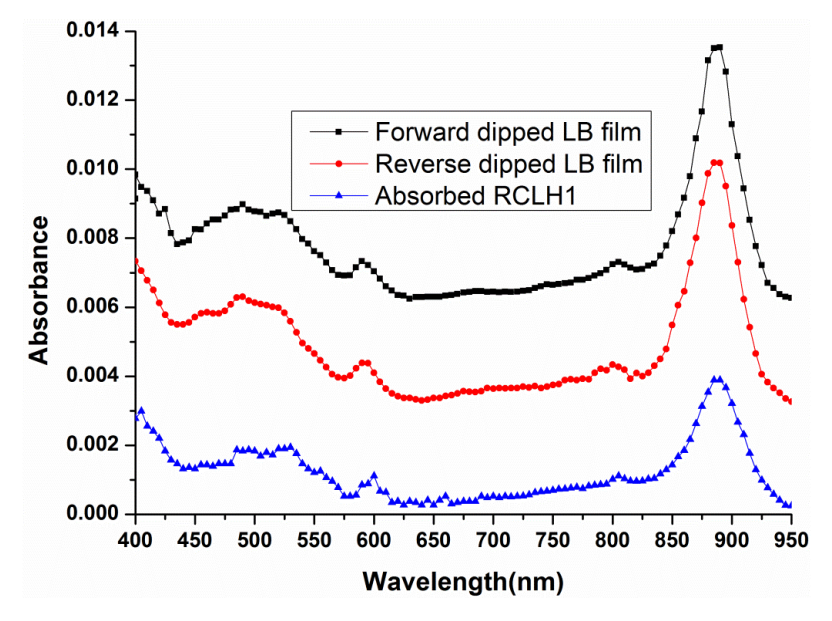


Figure S3: Absorption spectra of Langmuir Blodgett (LB) films of RC-LH1 complexes (red dots: reverse dipped, black dots: forward dipped), and of adsorbed RC-LH1 complexes (blue triangles) on gold electrodes. The sample with adsorbed RC-LH1 complexes was prepared by incubating the gold-coated glass slide with a solution of isolated RC-LH1 complexes (1 mg/ml) for one hour at 4°C and rinsing it afterward with buffer solution (Tris HCl, pH 8). The absorption spectra if the LB-films are vertically displaced by steps of 0.003 absorbance units for better viewing.

electrochemical cell. The gold coated glass cover slip was incorporated as the base of the cell and functioned as the working electrode with an active diameter of 16 mm. A high power light emitting diode (LED) purchased from Roithner LaserTechnik was used as our light source. This LED (LED880-66-60) has a central wavelength of 880 nm and a 50 nm bandwidth (FWHM). The LED was operated with 800 mA at 7.6 V, resulting in a light intensity of 23 mW/cm² at the surface of the gold electrode in the electrochemical cell, corrected for transmission of the gold layer. In the case of the action spectra, the illumination was provided by passing white light from a halogen/tungsten lamp through a scanning monochromator with a bandwidth of 40 nm. In this case, the power of the light source reaching the cell was 2 mW/cm² at 880 nm.

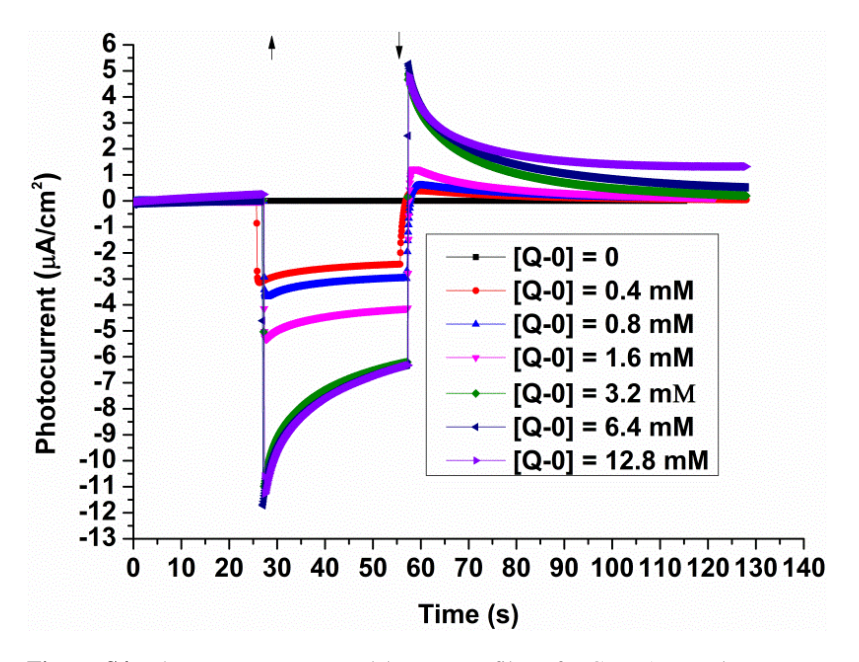


Figure S4: Photocurrent generated by an LB film of RC-LH1 complexes as a function of quinone (Q-0) concentration. The photocurrent was measured with a three-electrode electrochemical cell equipped with a potentiostat and a light source. The cell was iluminated from below with an intensity of 23 mW/cm² at 880 nm (bandwidth 50 nm). The upward arrow (\uparrow) in the figure indicates the moment that the light was turned on whereas the downward arrow (\downarrow) is the moment that the light was turned off. The magnitude of photocurrent increased with increasing the concentration of Q-0. The highest peak-current of 12 μ A/cm² was reached at 3.2 mM of Q-0 as mediator; no further increase was observed at higher concentrations.

A computer controlled shutter was placed between the light source and the measuring cell to switch the light illumination on/off. The redox mediators used in the measuring solution were cytochrome c from equine heart and 2,3-dimethoxy-5-methyl-p-benzoquinone (ubiquinone-0, Q-0), both purchased from Sigma. The photocurrent response with only Q-0 as mediator is shown in Figure S4 as a function of mediator concentration.

At positive potentials the photocurrent response is very different, as shown in Figure S5. The light-induced current is dominated by a fast transient response when the light is switched on. This likely due to the reduction of the quinones contained in the RCs which will be re-oxidized via the Q-0 pool in solution and the working electrode.

Variation of Photocurrent with applied Potential

The light-induced current response of the RC-LH1 monolayer/gold electrode was measured as a function of applied potential. The highest photocurrent was

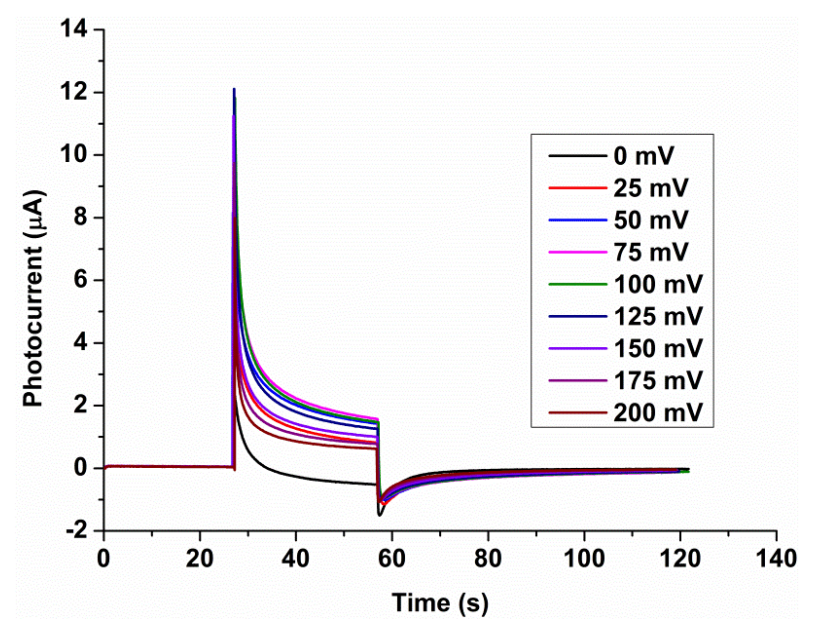


Figure S5: Photocurrent from a forward dipped LB film of RC-LH1 complexes deposited on a bare gold surface at different positive applied potentials in the presence of Q-0 (1600 μ M) and cyt c (320 μ M) as mediators. Applied potentials ranged from between 0 to 200 mV in steps of 25 mV (vs SCE). The upward (\uparrow) and downward arrow (\downarrow) indicate the moment that light illumination was turned on and off, respectively.

recorded at -175 mV for a forward dipped LB-deposited RC-LH1 layer, see figure S6.

Quantum Efficiency (QE) calculations

The quantum efficiency is estimated by taking the ratio of the number of electrons produced per second (N_e) to the number of absorbed photons per second (N_{ap}) (Ciesielski et al. 2010).

$$Q_E = N_e/N_{ap}$$

In order to determine how many photons are absorbed, we need to know the photon flux of the light source which consists of a light-emitting diode (LED), centered at $\lambda=880$ nm with a power density of 23 mW/cm^2 at the sample (corrected for transmission of the gold layer). Taking into account the effective area of 2.01 cm^2 of the working electrode we obtain for the incident number of photons per second at the sample:

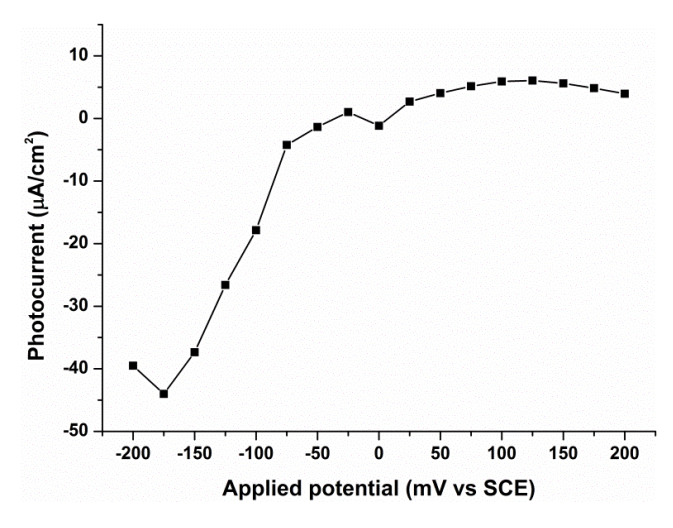


Figure S6: Variation of the peak values of the photocurrent from a LB-deposited RC-LH1 layer (forward dipped) with applied potential. The photocurrent was measured in an electrochemical cell equipped with a potentiostat. The layer was deposited on the working electrode which was incorporated into the measuring cell filled with buffer solution (Tris HCl, pH 8) containing Q-0 (1600 μ M) and cytochrome c (320 μ M) as redox mediators. The intensity of light illumination is 23 mW/cm². The photocurrent was recorded at different potentials in steps of 25mV

$$\phi_e = 2.05 \times 10^{17} \text{ photons/s}$$

The number of photons that are actually being absorbed are given by

$$N_{ap} = \phi_e \times (1 - T),$$

where T is the transmittance. From the measured absorbance, A = 0.00375, we calculate that T = 0.9914, and thus we have

$$N_{ap} = 1.76 \times 10^{15}$$
 photons/s

The peak photocurrent was 45 μ A/cm² which corresponds to

$$N_e = 5.647 \times 10^{14}$$
 electrons/s,

Adjusting this value for the effective area of the working electrode, and substituting the numbers in the equation for Q_E , we obtain $Q_E = 32 \%$

References

- 1. Law, C.J. 1999. PhD thesis, University of Glasgow, United Kingdom.
- Van Baarle, G. J. C., Troianovski, A. M., Nishizaki, T., Kes, P. H. and Aarts, J. Appl. Phys. Lett. 2003, 82, 1081
- 3. Ciesielski, P.N., Faulkner, C. J., Irwin, M. T., Gregory, J. M., Tolk, N. H., Cliffel, D. E. and Jennings, G. K. **2010.** *Adv. Funct.Mater.* **20**, 4048

CHAPTER 4

Role of co-factors in electron tunneling in bacterial RCs on a bare gold electrode

Abstract

In this chapter we examine the role of cofactors in electron tunneling in bacterial reaction center (RC) complexes between a gold surface and a conductive nanotip. In particular, we have studied an antenna-deficient strain of the photosynthetic bacterium Rhodobacter sphaeroides and two mutants, known as AM260W and AM149W, in terms of photo-activity and current-voltage characteristics by utilizing photoelectrochemistry and conductive atomic force microscopy (C-AFM). Using the Langmuir-Blodgett method to assemble monolayers of RC-membrane fragment we can obtain a dense packing, while the layer can be easily transferred to a gold electrode. These layers show a high degree of orientation, with the periplasmic side of the RC complexes facing the gold surface. Direct electron transfer from the gold surface to the special pair was observed, with a strongly asymmetric current response as function of the bias voltage. Electron tunneling by C-AFM is completely blocked in quinone-depleted reaction centers, while absence of the bacteriopheophytin in the so-called inactive branch has no effect. We conclude that electron tunneling as measured by C-AFM occurs exclusively along the A-branch of the reaction center.

4.1 Introduction

Photosynthesis is generally considered as the process used by plants and algae to sustain their metabolism and growth by utilizing solar energy. However, it is also found in a variety of bacterial systems, and the study of photosynthetic bacteria has provided a large part of our current understanding of light capture and energy transduction in photosynthesis. At the core of the photosynthetic reaction is the reaction center (RC) complex. It is a membrane bound pigment-protein complex where the primary reactions of photosynthesis take place. Solar energy absorbed by the antenna complexes is funneled to the RCs to initiate the charge separation leading to the generation of a transmembrane potential which is utilized to drive a series of reactions that are of physiological importance for the organism.

The bacterial RC is the simplest model system to study the basics of charge separation and energy conversion mechanisms in photosynthesis. A bacterial RC complex typically comprises three types of polypeptides, L, M and H, which together bind ten cofactors: four bacteriochlorophyll a molecules (a dimer P, plus two accessory bacteriochlorophyll molecules, B_A and B_B), two bacteriopheophytines (H_A and H_B), two ubiquinones (H_A and H_B), two ubiquinone

The dimer of bacteriochlorophyll a, often termed the special pair, is located close to the periplasmic side of the membrane, whereas the non-heme iron is located close to the cytoplasmic side. The other cofactors are arranged in more or less symmetrical branches, A and B (hence the subscripts to denote the various cofactors). Despite the symmetry, these branches are found to be strongly asymmetric in terms of their functionality: the electron transfer path way is reported to be exclusively along the A-branch. 1,2

The role of these cofactors is to initiate photosynthetic energy transduction by electron transfer across the membrane. Light-induced electron transfer from the special pair (or primary donor) P to Q_B is the key step of energy transduction. This electron transfer occurs in three steps involving subsequently the B_A , H_A and Q_A cofactors, with the first steps happening on a picosecond time scale.

Although the bacterial RC has been extensively studied its functional asymmetry is still poorly understood. There are some studies showing the possibility of electron

transfer along the B-branch by introducing special mutations close to the primary donor site. $^{6-13}$ Up to 35-45% B-branch electron transfer is reported by using a quadruple mutant called LDHW, in which the reduction of H_B is observed but the formation of $P^+Q_B^-$ is not significant. Apparently there is no functional role of the B branch of cofactors, although it is structurally very similar to the so-called active branch.

A key-aspect of the function of the reaction center is the tight packing of the cofactors. Indeed, it is this particular feature that accounts for the efficiency and quantum yield of light-induced, primary charge separation. The RC can be viewed as a natural, nanoscale device with characteristics that are very much sought after in molecular electronics. From this point of view it is of interest to examine the coupling of reaction center complexes with conductive metal contacts. A key question here is the possibility of electron exchange with electronic circuit elements, and in particular how the system responds to the injection of electrons from a connected electrode. To address this question we have investigated the properties of photosynthetic RCs by conductive atomic force microscopy (C-AFM), where membrane-embedded RCs were adsorbed on a flat gold electrode, and probed by a gold-coated AFM tip approaching from the opposite side. C-AFM is a very important technique to study electronic properties of materials down to the molecular level. It has been previously utilized to study organic molecules including photosynthetic pigment-protein complexes¹⁴⁻²⁰.

For this work we have used chromatophores from a RC-only mutant from *Rhodobacter (Rb.) sphaeroides*. Further details were obtained by examining the AM149W and AM260W variants, two well-known mutants of this antennadeficient strain of *Rb. sphaeroides*. Mutation of residue Ala 149 to Trp in the M-subunit of the RC (AM149W) results in the formation of RC complexes without H_B. The other mutant, AM260W, is the result of an Ala 260 to Trp mutation; this mutant RC lacks the Q_A cofactor. These two mutants have been previously studied by utilizing x-ray crystallography^{21,24}, EPR^{6,13} and other spectroscopic techniques. The second of the result of the r

Apart from C-AFM we have also employed photoelectrochemisty techniques to measure the photoactivity of these complexes and the consequences of the removal of the cofactors. By measuring photocurrent generation by membrane-embedded, native RCs and of the AM149W and AM260W mutants, along with current-voltage spectroscopy of these complexes, the role of the co-factors in trans-membrane electron transfer can be evaluated.

Our results indicate that membranes containing RCs attached to bare gold electrode are photoactive and support substantial photocurrents in both directions that is from RCs to electrode and *vice versa* depending on the orientation of the RCs and the polarity of applied electric potentials. Q_A is shown to have a very important role in the electronic communication between the electrodes across the membranes, whereas a missing H_B cofactor does not have any effect on the performance of the mutant RC in comparison with the native complex. The current-voltage spectroscopy measurements support the findings of photocurrent experiments. Our results show that electron injection from the electrode gives rise to charge transfer exclusively along the A branch of the RC, similar to the process that results from optical excitation of the primary donor.

4.2 Materials and methods

RCs containing membranes and mutants

Antenna deficient membranes and mutants AM260W and AM149W were prepared and cultured according to previously described protocols. These mutations were applied to the *Rb. sphaeroides* deletion strain DD13, utilizing a quick-change mutagenesis kit (from Stratagene). The antenna-deficient strains of *Rb. sphaeroides* was grown under semi-aerobic conditions in the dark. Harvested cells were resuspended in 10 mM Tris buffer (pH 8) and broken by using a French press (Arminco). Membranes were purified by ultracentrifugation at 4 °C and 27,000 rpm in a TY45 rotor for 4 hours using a sucrose step gradient (15-40%). Membranes were concentrated by ultracentrifugation and stored at -20 °C. 22,24,25

Working electrode preparation

Working electrodes for photocurrent measurements were prepared by sputtering a gold film on glass cover slips. Before gold deposition, the glass cover slips were cleaned by sonication in methanol for one hour, subsequently rinsed with milli-Q water and then dried in a stream of nitrogen gas. Before gold deposition, the cleaned cover slips were placed in an ozone cleaner (UVP PR-100, UV-ozone Photoreactor) for one hour.

Gold deposition

A thin layer of gold was sputtered on clean glass cover slips by utilizing a magnetron sputtering system (ATC 1800-F from AJA Corporation).²⁷ In order to improve the adhesion between the glass surface and the gold layer, a thin layer (1-2 nm) of molybdenum-germanium (MoGe) was sputtered first on the glass surface. The gold film of 12 nm thickness was then sputtered on top of it. The sputtering rate for MoGe was 1.32 nm/min in a 10 mTorr Argon environment, whereas the gold was deposited at a rate of 9.06 nm/min in a mixure of 10 mTorr Argon and 1 mTorr oxygen. The gold layers we thus obtained were flat (about 2-3 Å root-mean-square roughnes), homogenous and conductive over the full area of the coating. Gold-coated glass cover slips were stored in a desiccator, and used within one week after preparation.

Langmuir Blodgett deposition

The Langmuir Blodgett (LB) technique was used for deposition of RC-only membrane fragments for IV spectroscopy. The solution of membrane fragments (1 mg/mL) was spread on the surface of water in a LB trough, and after equilibration the surface assembled, RC-containing membranes were compressed to a surface pressure of 35 mN/m. A gold-coated glass cover slip with a diameter of 25 mm was vertically dipped into the sub phase at a speed of 1mm/min. The surface pressure was kept constant during this procedure.

Adsorption of RC-membranes on gold electrode from solution

As an alternative to LB deposition, RC-containing membranes were adsorbed on a gold surface by incubating the gold-coated glass cover slips into the solution of RC-membranes for one hour at 4 °C. The gold surface was then rinsed with buffer (Tris-HCl pH 8) to remove the loosely and non-bound membrane fragments.

Photocurrent measurement

Photocurrents generated by bacterial RCs were measured by using a conventional three-electrode setup. The reference electrode (saturated calomel electrode) and counter electrode (platinum wire) were inserted into a homemade measuring cell containing Tris buffer (pH 8) as measuring solution. A gold-sputtered glass slide (25 mm diameter) was incorporated as the base of the cell, and served as the working electrode. Illumination was provided by a light emitting diode (LED) with a central wavelength of 880 nm and a bandwidth of 50 nm. A computer controlled

shutter was placed between the light source and measuring cell to turn the light illumination on or off. The LED was operated at 800 mA and 7.6 V. The intensity of light reaching the surface of the working electrode was 23 mW/cm². In order to record action spectra, a white light source equipped with a monochromator was used as the light source. The light intensity at the surface of the working electrode in this case was 2 mW/cm^2 at 880 nm. The wavelength of the light was increased in steps of 5 nm and light illumination was turned on for 10 seconds at every wavelength. Ubiquinone-0 and cytochrome c were used as redox mediators in the solution for charge transportation to the counter electrode.

Absorption spectra of RC-membranes adsorbed on a gold electrode

In order to estimate the surface coverage of mutants of RC-membranes, we measured the absorption spectra of the RC-membrane/gold-coated cover slips. The spectra were recorded by using a fiber-coupled spectrometer (Ocean Optics, HUV4000) equipped with a CCD array detector, and with halogen and deuterium lamps as light sources.

Atomic force Microscopy (AFM)

The topography of membrane-embedded bacterial RCs deposited on a gold electrode was checked by using AFM (Nanoscope IIIa, Veeco, USA) in tapping mode under ambient conditions. Standard silicon nitride cantilevers with resonant frequency of 75 kHz and force constant of 2 N/m were used for imaging.

Conductive atomic force Microscopy (C-AFM)

Current-voltage characteristics of surface-adsorbed RC membrane fragments were measured by C-AFM. The junction was fabricated by sandwiching the RC complexes between the C-AFM tip and the gold surface. Unlike normal AFM, a conductive probe is required for I-V spectroscopy. Therefore, standard silicon nitride probes were coated with a thin layer of platinum by using a magnetron sputtering system (ATC 1800-F from AJA Corporation). The radius of curvature of the probe after sputtering was about 15 nm (checked by scanning electron microscopy). Tapping mode AFM imaging was used to locate the RC complexes, after which the tip was positioned on top of it with control of the applied force. A voltage ramp was applied between the tip and substrate and the resulting current was measured. The current-to-voltage converter, mounted very close to the C-AFM tip, limited the current measurements to values of less than ± 10 nA.

4.3 Results

It was shown by Magis et al. that membrane fragments isolated form *Rb. sphaeroides* can be adsorbed on a bare gold surface while retaining their functional properties. Moreover, they absorbed strong enough that the fragments were not removed by gentle rinsing and drying. We followed similar procedures to adsorb RC-only membrane fragments from wild-type and mutants of *Rb. sphaeroides* on a semi-transparent, bare gold surface. For this purpose, gold-coated cover slips were incubated for one hour at 4 °C with a solution of the RC-only membrane fragments (see materials and methods). After rinsing with buffer solution, we measured the absorption spectra of the adsorbed layers, which are shown in figure 1. From the extinction coefficient at 803 nm (288 mM $^{-1}$ cm $^{-1}$). We calculate that the surface is covered by about 2.7×10^{12} RC-complexes per cm 2 . Based on the dimensions of the RC complex 29 , we estimate that this corresponds to about 60-70% of a full mono-layer if we assume a close packing.

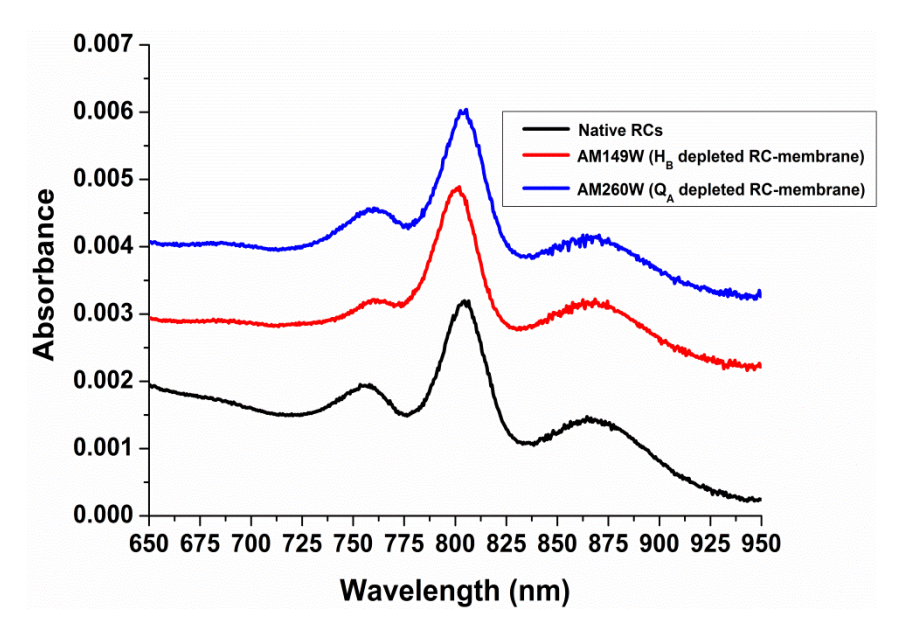


Figure 1. Absorption spectra of layers of membranes fragments containing either native RCs of *Rb. sphaeroides*, or variant RCs with missing cofactors. The absorption spectra were recorded after incubating the gold-coated cover slip for one hour with chromatophores and subsequent rinsing with buffer (Tris pH 8) to remove loosely or non-bound material. Black curve: Membranes containing native RCs; red curve: with H_B -depleted RCs; blue curve: with Q_A -depleted RCs.

The absorption spectra show that the native RCs fragments, the AM149W and the AM260W variants adsorb equally well on the gold surface. The lower amplitude of the 760 nm band in the absorption spectrum of the AM149W variant confirms the depletion of the H_B cofactor. Below we will first discuss the results that were obtained with membrane fragments containing native RCs, after which we turn to data of the RC variants from the AM149W and AM260W mutants of *Rb*. *sphaeroides*.

4.3.1 Monolayers of membrane fragments containing native RCs

For photocurrent measurements the RC-functionalized gold-coated cover slip was incorporated in an electrochemical cell. This cell was configured in a conventional three-electrode configuration with the gold-coated cover slip as the working electrode at the base. The reference (saturated calomel) and counter (platinum wire) electrodes were inserted in the buffer solution (Tris pH 8) that filled the cell. This buffer solution also contained mediators, in particular ubiquinone-0 (Q-0) and

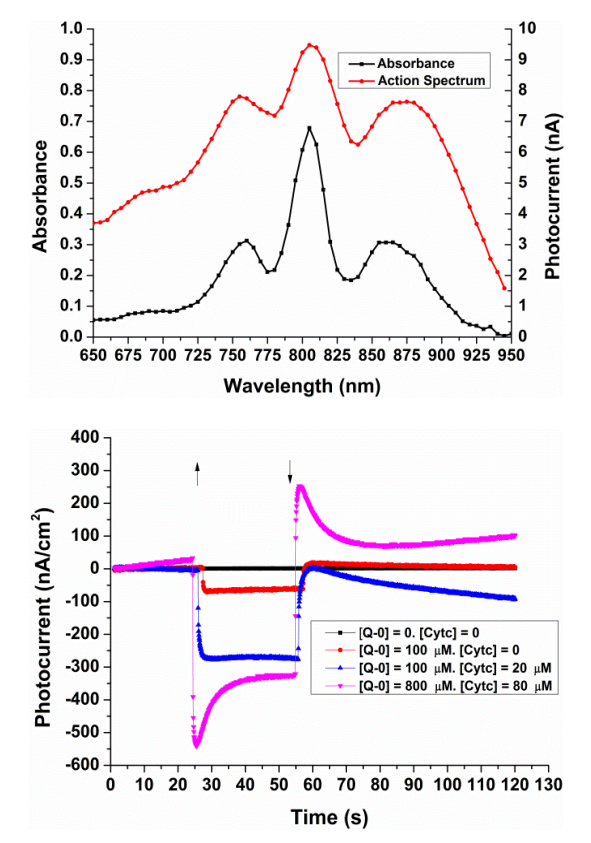


Figure 2

- (A) Absorbance spectrum (black curve) and action spectrum (red curve) of native RCs adsorbed on bare gold electrode. The wavelength of the light was increased in steps of 5nm by using a monochromator, and the photocurrent was recorded at each wavelength by turning the light illumination on for 10 seconds.
- **(B)** Photocurrents generated by native RC-containing membranes different mediator concentrations. Without mediators no photocurrent was recorded (black squares), with 100 µM of Q-0 a small photocurrent was observed (red squares) which increased with the addition of 20 µM of cyt c (blue triangles). The highest photocurrent (peak value) recorded at 800 µM of Q-0 and 80 μ M of cyt c.

cytochrome (cyt) c. The electrodes were connected to a potentiostat, and the sample could be illuminated from the bottom of the cell, through the gold layer.

In order to verify that the source of the photocurrent is the charge separation in the RC we recorded the action spectrum, i.e., the photocurrent as a function of the excitation wavelength in the presence of Q-0 and cyt c. The mediators assist in shuttling electrons from the Q_B site to the counter electrode and from the working electrode to the special pair, respectively. The results for native RCs in figure 2a show that the action spectrum (red curve) follows the absorption spectrum (black curve). The action spectrum is broadened by the 40 nm bandwidth of excitation, which is about an order of magnitude larger than that of the absorption spectrum.

The effect of the mediators is apparent from figure 2B. Here we show the photocurrent response of native RC-containing membrane fragments as a function of time when the light (from a light-emitting diode operating at 850 nm) is switched on for a time interval of a few tens of seconds. The measurements were performed at an applied potential of -100 mV vs SCE. We did not observe any photocurrent in the absence of both mediators (Fig. 2B, black data points). When only Q-0 is present in the measuring solution a photocurrent of about 50 nA/cm² is recorded (red data points). The photocurrent increases substantially, to 350 nA/cm², when the measuring solution is supplemented with 20 μ M of cyt c. The photocurrent depends on the concentration of mediators. The highest photocurrent, a peak value of 550 nA/cm², was obtained when the measuring solution contained 800 μ M of Q-0 and 80 μ M of cyt c. At these high concentrations the photocurrent response shows a transient component.

Figure 3A shows the photocurrent response as a function of applied potential in the range of -175 to +175 mV in steps of 25 mV in the presence of, both, Q-0 (800 μ M) and cyt c (80 μ M) as mediators in the solution. The magnitude of the photocurrent increases sharply with increasingly negative potentials. The highest photocurrent is recorded at -125 mV vs SCE. At positive potentials the photocurrent has the opposite direction of that at negative potentials, although much lower in amplitude. This is likely due to a distribution of opposite orientations of the RC-membrane fragments on the gold surface. The difference in amplitude may be indicative of preferred orientations, but the effectivity of the mediators may also vary from one orientation to the other.

The RC-generated photocurrents are also dependent on the intensity of light illumination. The intensity dependence is shown in figure 3B. The photocurrent was found to be linear over the range of intensities that was available.

Although the adsorbed RC-containing membrane fragments on a gold surface appears to form a rather dense layer, the orientation of the fragments cannot be easily controlled or ascertained. It is known that Langmuir Blodgett (LB) techniques can be used to form mono-layers of RC complexes and of RC-containing membrane fragments at the air-water interface. This method offers more control over experimental parameters than adsorption from solution. For this reason we explored the use of LB techniques to transfer mono-layers of RC-membrane fragments to a gold-coated glass slide. A solution of membranes fragments (1 mg/mL) was spread on the water sub-phase in a LB trough. After equilibration, the surface assembled membranes were compressed by the barriers of the LB trough up to a surface pressure of 35 mN/m. This surface pressure was

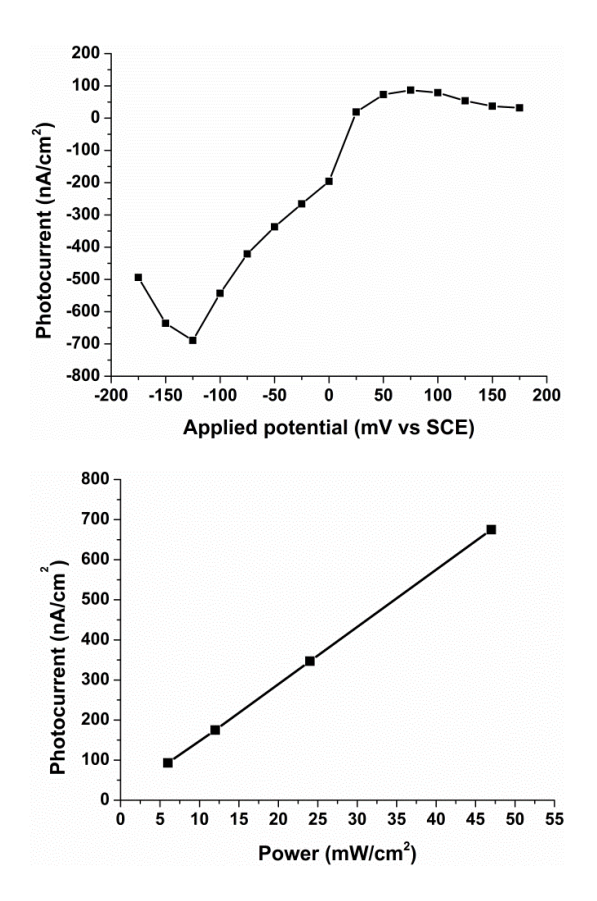


Figure 3

- (A) The photocurrent response of RC-containing membrane fragments adsorbed on a bare gold electrode at different applied potentials. The measuring solution 800 μ M of Q-0 and 80 μ M of cyt c as charge carriers. The potential was varied from -175 mV to +175 mV (vs. SCE) in steps of 25 mV.
- (B) Photocurrent response of RC-containing membrane fragments adsorbed on a bare gold electrode as a function of light intensity at a potential of -125 mV (vs SCE). The measuring solution also contained 800 μ M of Q-0 and 80 μ M of cyt c as redox mediators.

chosen to avoid any structural deformation induced by the deposition process. A gold coated glass slide was dipped in at a speed of 1 mm/min, keeping the surface pressure constant; the slide was then pulled out at the highest available speed to avoid any deposition during this step.

Figure 4A shows the characteristic compression curve of RC-membrane fragments spread on the water surface in the LB trough. Upon compression of the surface-assembled membrane fragments, the surface pressure rises gradually with an increasing slope. After transfer of the monolayer to a gold-coated cover slip we measured the surface topography by atomic force microscopy (AFM) in tapping

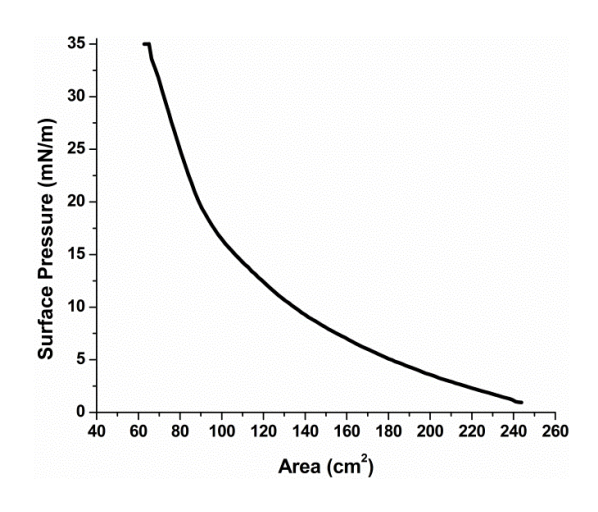
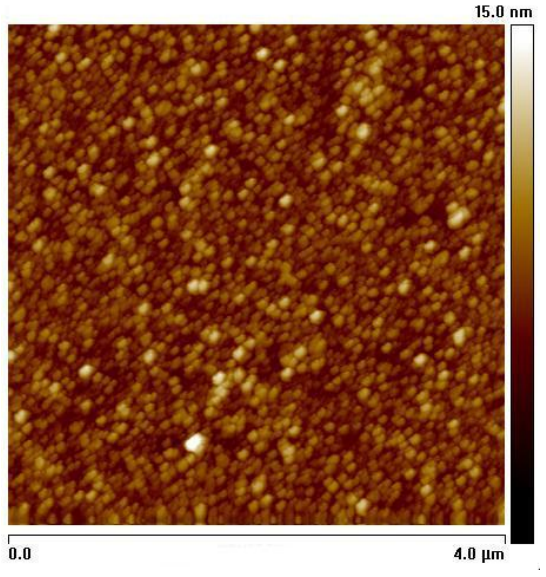


Figure 4:

(A) Compression curve of a layer of RC-containing membrane fragments on the water-air interface of a Langmuir–Blodgett (LB) trough. Compression was performed by moving the barriers at a rate of 5 mm/min up to a surface pressure of 35 mN/m.



(B) Atomic force microscopy (AFM) image of a layer of RC-containing membrane fragments deposited by the LB method. The topograph was obtained by using tapping mode AFM under ambient conditions. Standard silicon nitride cantilevers were used for imaging, with a spring constant of 2.8 N/m and a resonant frequency of 75 kHz.

mode. The AFM image (Figure 4B) shows closely packed membrane fragments with a fairly uniform height distribution.

The interaction between the monolayer and the underlying electrode was investigated by current sensing AFM, similarly as described in Chapter 2. Current-voltage curves were measured across the of LB film of native RC-containing membranes fragments in the tunneling junction formed by the conductive AFM tip and the gold substrate The cantilever of the AFM used in this case was made of silicon nitride, coated with a thin layer of platinum. The contact force exerted by the probe tip was controlled by AFM feedback in contact mode.

Figure 5A shows a typical I-V curve of (native) RC-containing membranes deposited on a gold electrode, at an applied force of 1 nN. The I-V curve has a pronounced asymmetry, with a small to negligible current at negative potentials, whereas at increasing positive potentials a nonlinear rise of the tunneling current is

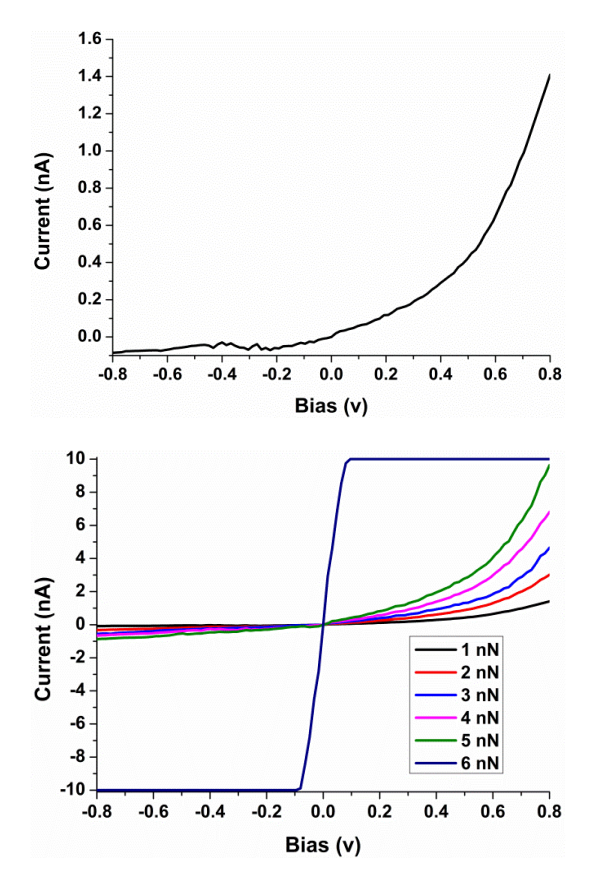


Figure 5:

- (A) Typical current-voltage curve of a RC-containing membrane fragment in a LB-deposited layer on a flat gold electrode. The layer is sandwiched between the gold electrode and a conductive AFM tip. The applied force in this case is 1 nN.
- (B) Current-voltage curves of RCs containing membranes sandwiched between the electrode and AFM tip. A membrane patch was located by tapping mode AFM, the instrument was then switched to contact mode and a voltage ramp was applied between the tip and substrate to record the resulting current. Current-voltage curves were recorded as a function of contact force.

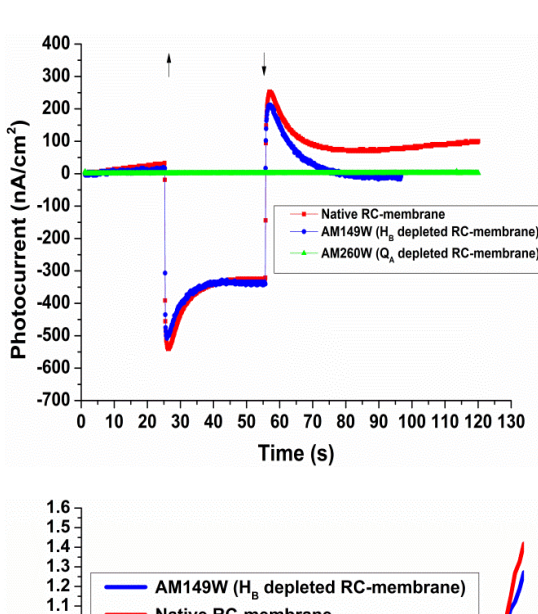
observed. The shape of the curve has the characteristics of a diode junction. The current reaches a value of 1.4 nA at a bias voltage of 0.8 V and a contact force of 1 nN. In Chapter 1 we described a similar asymmetry in the I-V curves of RC-LH1 complexes, although this component was superposed on the contribution of the LH1 complex to the tunneling current. The present experiments confirm the interpretation of this asymmetric component as arising from the RC complex within the LH1 ring. The dependence of the tunneling current on the force exerted on the RC-membrane layer by the tip is shown in Figure 5B, showing an increase of the tunneling current with the applied force. The trend is very similar to that of the asymmetric component in the data shown in Chapter 1 for the 2D-crystals of RC-LH1. Also in the present case we observe a breakdown of the monolayer at higher force, although the breakdown force of about 6 nN is significantly lower than for the 2D RC-LH1 crystals.

4.3.2 Monolayers of RC-variants.

The AM149W and AM260W RC variants each lack a specific cofactor: the AM149W variant does not contain H_B , while the AM260W variant lacks Q_A . (For details of the cofactor composition and arrangement we refer to Chapter 1 of this thesis). We first consider the photocurrent response of surface assembled membrane fragments with these two variants in comparison with that of native RC-containing fragments.

The photocurrent response of native RCs, AM149W and AM260W is shown in Figure 6a. Photocurrents were measured at a potential of –100mv (*vs* SCE), using in all cases the same concentration of Q-0 (800 μM) and cyt *c* (80 μM) and the same light intensity (23 mW/cm², centered at 850 nm, measured at the electrode surface). We also note that the surface density of the RCs in all three cases was very similar, as concluded (and calculated) from the absorption spectra shown in figure 1. Despite very similar measurement conditions, the photocurrent response of the complexes was different. The magnitude of the photocurrent from native RCs membranes and the AM149W variant was very similar, reaching a (peak) value of 550 nA/cm². In the case of the AM260W variant, however, a very different response was observed: in fact no photocurrent was recorded upon light illumination of this particular RC variant.

Current-voltage curves of all three RC-variants were recorded under the same conditions. Figure 6B shows the I-V curves of AM149W, AM260W and native RC-containing membrane fragments deposited on a gold electrode by transfer of the LB monolayer formed at the air-water interface. All the samples were prepared with the same compression rate and surface pressure, and the I-V curves were recorded at the same contact force of 1 nN. The native RC and the AM149W RC-variant have strikingly similar I-V characteristics, whereas AM260W has a completely different character as measured by conductive AFM. The magnitude of the tunneling current for native RCs reached values of 1.3 to 1.4 nA for AM149W at a bias voltage of 0.8 V but no current was recorded for the AM260W variant.



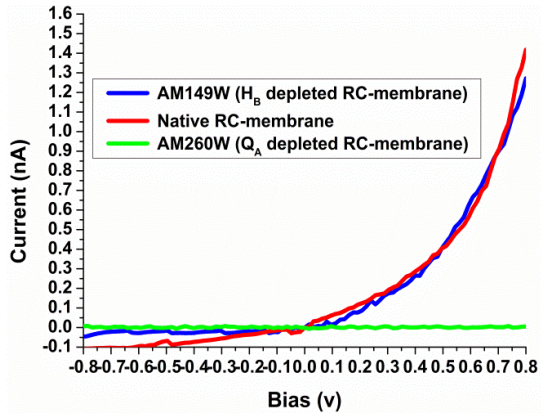


Figure 6.

- (A) Photocurrent RC-containing membrane fragments on gold at a potential of -100 mV (vs SCE), containing, respectively, native RCs (red squares), H_B -depleted RCs (blue circles) and Q_A -depleted RCs (green triangles). Q-0 (800 μ M) and cyt c (80 μ M) were used as redox mediators. Light intensity at the surface was 23 mW/cm². Up/down arrows indicate light being switched on/off
- **(B)** IV-spectroscopy of membrane bound native RCs complexes and mutants with missing cofactors. IV curves of membrane-bound native RCs and mutants were recorded by using conductive AFM in contact mode. I-V curves were recorded at an applied force of 1 nN.

5. Discussion

Bacterial RCs have been previously deposited on electrodes by using various immobilization techniques, including adsorption on functionalized electrodes, genetically modified complexes attached to the surface via linker molecules, Langmuir Blodgett deposition and RCs entrapped in porous material etc. ^{17,35-41} An often used approach to assemble photosynthetic pigment complexes on an electrode or other functional surface is based on an engineered coupling between the complex and the surface, for example by using an interfacial layer or specific molecular linkers. ^{15,38-40} It is usually assumed that it provides an effective way to control the orientation of the protein complex which is important because of the vectorial character of photosynthetic electron transfer. The results in this chapters show that a bare gold electrode also provides a surface for relatively stable adsorption of photosynthetic pigment-protein complexes, that a high surface density can be achieved by simple methods, and that a high degree of orientation can be obtained.

We observed that simple adsorption from solution results in a high surface density of adsorbed RC-complexes on a gold surface. The functionality and activity of the immobilized RCs was verified by measuring the light-induced action spectra of the photocurrent in an electrochemical cell. Since the RC-complexes are adsorbed on the working electrode it is essential to have a mediator in the solution to facilitate electron transport to or from the counter electrode. Optical excitation of the primary donor P in the RC results in reduction of QA and subsequently QB. In nature, the reduced Q_B can be exchanged and replaced by a member of the quinone pool in the photosynthetic membrane. In the experiments described in this chapter, we have Q-0 in solution, and we conclude that it plays a similar role as the quinine pool in nature by accepting electrons from QA, after which it is oxidized at the counter electrode. This is supported by the observation of a photocurrent when only Q-0 is present as mediator, which is in the oxidized form at a potential around -100 mV. It also implies that under those conditions direct electron transfer takes place from the working electrode to the primary donor, at least in a significant fraction of the RC complexes. We stress this last point, because it is quite possible that not all RC complexes were properly oriented on or in sufficiently close proximity to the gold surface for direct electron transfer.

Indeed, we do observe a significant increase of the photocurrent when a second mediator, cyt c, is added to the solution. At negative potentials cyt c is in the reduced state, and capable of electron transfer to the photo-oxidized primary donor, similarly as in nature. This suggests that cyt c assists in the electron transfer from the working electrode to the primary donor. This is consistent with the results of earlier studies 42,43 which showed that cyt c binds in a more or less stable form to gold-adsorbed RC-complexes. It is not clear how such a construct is arranged, but probably cyt c becomes inserted in the free space between or near RC complexes and the gold surface. The stability of such a construct could be the result of the interaction of cyt c with exposed functional groups of the RC complex or the lipid molecules on one hand and with the gold surface on the other hand. Some support for this conjecture comes from a study of the gold substrate topography on the voltammetry of cyt c adsorbed on self-assembled monolayers (SAMs), showing that surface roughness and SAM defects significantly increased cyt c adsorption and the effectiveness of electronic coupling.

The magnitude of the photocurrent depends on the concentration of two mediators. It increased with the concentration of, both, Q-0 and cyt c, but eventually the increase levels of. The photocurrent became saturated when the Q-0 and cyt c concentrations reached 800 µM and 80 µM, respectively. When the concentration of the mediators was increased the time profile of the photocurrent changed during and following the light on interval. At higher concentrations a transient component was observed, both, when the light was switched on and switched off. The amplitude of these components also increased with increasing mediator concentration. When the light is switched on, the instantaneous photocurrent decays to a more or less steady level at a time scale of seconds. The transient that follows after the light is switched off has a similar shape and amplitude, but an opposite sign. These transients can be attributed to storage of charge in the Q-0 pool in solution, which becomes partially reduced because of diffusion limitations. The electron transfer rate will follow the equilibration of the charge distribution after the light is switched on. The reverse transient is probably due to charge recombination when the light is switched off.

The RC-generated photocurrent is also dependent on the applied potentials. At negative potentials a much higher photocurrent is recorded compared to positive potentials, while the current has opposite directions. For negative potentials the

photocurrent is generated by electron flow from the working electrode to the photooxidized primary donor in the reaction center. Direct electron transfer requires a
close proximity of the primary donor to the gold surface, which suggests that the
contribution to the photocurrent is primarily from RCs that are oriented with the
periplasmic side towards the electrode. From the photocurrent measurements,
however, we cannot determine the fraction of RCs that are in this favorable
orientation. Possibly the reversal of the photocurrent at positive potentials is due to
differently oriented RCs. Photocurrents generated by RCs with different
orientations have also been reported in literature, where the desired orientation was
achieved by using linker molecule between genetically modified protein complexes
and the electrode. Higher photocurrents were recorded in these experiments when
the periplasmic side of the RCs was facing the working electrode, compared to the
opposite orientation. The difference in electron transfer rate was attributed to the
larger tunneling distance when the H subunit is oriented towards the electrode.³⁹

The maximum current response is observed around a potential of -125 mV vs. SCE. This is consistent with the redox properties of the mediators. Cyt c has a midpoint potential of 11 mV vs SCE and is almost fully reduced at a potential of -125 mV. The redox chemistry of ubiquinones, however, is less straightforward, involving one or two reduction steps and different protonation states. No less than 9 different redox and protonation states can be identified. For this discussion, the most important step is the one-electron reduction of the Q_AQ_B pair in the RC. Gunner $et\ al$. have calculated that the corresponding reduction potentials for the formation of $Q_A^-Q_B^-$ and $Q_AQ_B^-$ are, respectively, -271 and -251 mV vs. SCE. The reduction potential of the UQ-0/UQ-0 couple in solution is expected to be more positive than it would be in the Q_B site of the RC, if only for the higher dielectric constant in solution. Thus there is roughly a window of -200 to 0 mV where the two mediators can be effective to sustain a photocurrent in a properly configured cell.

The photocurrent measurements do not provide conclusive information about the orientation of the RCs on the electrode surface, although a sizable fraction of the RCs must be in a favorable orientation. It turns out that I-V spectroscopy by means of conductive AFM gives us a handle on this variable. We performed such measurements on LB-films of RC-containing membrane fragments of native RCs and of the AM149W and AM260W RC-variants. At low contact force of the probe

tip the I-V curves of native RCs have a very asymmetric shape: the current is recorded only for positive applied potential, with a negligible response at negative potentials. The immediate conclusion is that electron tunneling in the RC is highly vectorial, strongly reminiscent of the light-induced electron transfer. This current response is similar to that of a diode, which supports current only in forward biased conditions. These results are similar to the ones that have been reported in the literature for Photosystem I complexes with different orientations on the surface of an electrode. ^{16,17,19,46}

The effect of increasing contact force follows the same trend as we reported in Chapter 2: the shape of the I-V curve remains roughly the same, but the magnitude of the current increases until a critical point is reached where presumably the LB layer is perforated and the tip makes direct contact with the underlying electrode. The increase of the tunneling current is probably due to a decrease of the barrier width as a result of compression of the protein complex. The amplitude of the tunneling current is roughly the same as the RC-associated component in the I-V curves of the RC-LH1 complex described in Chapter 2.

In order to further investigate the role of co factors in electron transfer in bacterial RCs, we have compared the photocurrent generated by membrane fragments containing native RCs with those containing RC-variants in which specific cofactors were missing. The photocurrents generated by adsorbed RCs and the AM149W RC-variant (with depleted H_B) have very similar current the same time profile. This measurement show that H_B does not have any functional role in transmembrane electron tunneling in RCs. However, for the AM260W RC-variant (with depleted Q_A) no photocurrent was recorded, which is evidence of a vital role of Q_A in trans-membrane electron transfer. From these results we surmise that the electron tunneling follows the same path as in light-induced charge separation.

-

 $^{^1}$ Q_A depleted RCs of R. sphaeroides mutations were prepared by introducing mutations close to the Q_A site. Two of them, Ala M260 to Trp and Ala M248 to Trp resulted in Q_A depletion, while abolishing photosynthetic growth of the bacterium. Electron transfer from the primary donor to H_A was retained,. The observations were later confirmed by X-ray crystallography data that showed exclusion of Q_A from the reaction center. It was concluded from the X-ray structural data that the volume of the cavity was reduced and the site was occupied by a chloride ion.

Electron transfer from the electrode then must populate the lowest unoccupied molecular orbital (LUMO) of the special pair, from where it migrates to the quinone acceptor exclusively along the A-branch of the RC. When the Q_A site is empty, as in the AM260W RC-variant, the distance of H_A to the electrode at the cytoplasmic side is too large for electron tunneling.

Photocurrent measurements of the AM149W and AM260W RC-variants in the presence of mediators are in agreement with the I-V spectroscopy data. In the absence of Q_A electron transfer to the Q-0 pool in solution appears to be blocked. We also may conclude that under those conditions the B-branch of the RC remains inactive. This is consistent with earlier reports that no electron transfer along the B-branch is observed by only inhibiting electron transfer along the A-branch of the complex.

The mutation of Ala M149 to Trp (AM149W) leads to the assembly of RCs without the H_B cofactor. The absence of this cofactor does neither affect the capability of the RCs to grow photosynthetically, or impair electron transfer from the special pair to Q_A . X-ray crystallography and FTIR data have confirmed the absence of H_B in the complex²⁴. Our measurements of photocurrent with the AM149W RC support these findings because the magnitude and time profile of photocurrents recorded for adsorbed AM149W and native RCs on gold electrode are very similar, which is evidence of the fact that H_B does not have any functional importance. It may, however, have a structural importance or some other role which is not yet known.

The asymmetry of the I-V response of gold-adsorbed RC-membrane fragments is a significant result: because of vectorial electron transfer the direction of the tunneling current will depend on the orientation of the RC complex in the tunneling junction. Opposite orientations of the RC complex in the tunneling junction will thus elicit distinctly different I-V curves which should be inverted around V=0. What we observe is that, apart from limited (up to 25%) variations in the amplitude, the I-V response from one point to the other is always very similar. This provides conclusive evidence that the large majority of the RC-membrane fragments have the same orientation. Combined with the evidence for direct electron transfer from the flat gold electrode, we conclude that the RC complexes in the LB layers have the same orientation and moreover, that the preferred

orientation corresponds to adsorption of RCs with the periplasmic side facing the gold surface.

6. Conclusion

Membrane fragments containing RCs, AM149W and AM260W RC-variants were deposited on a flat gold electrode by adsorption and LB-deposition. They formed dense monolayers with a high degree of orientation, with the periplasmic side of the RC complexes facing the gold surface. Direct electron transfer from the gold surface to the special pair was observed. IV spectroscopy by conductive AFM showed that electron tunneling in the RC complex follows the same path along the A-branch as light-induced charge separation.

References

- Kellogg, E. C.; Kolaczkowski, S.; Wasielewski, M. R.; Tiede, D. M. Measurement of the Extent of Electron-Transfer to the Bacteriopheophytin in the M-Subunit in Reaction Centers of Rhodopseudomonas-Viridis. Photosynthesis Research 1989, 22 (1), 47-59.
- 2. Paddock, M. L.; Chang, C.; Xu, Q.; Abresch, E. C.; Axelrod, H. L.; Feher, G.; Okamura, M. Y. Quinone (Q(B)) reduction by B-branch electron transfer in mutant bacterial reaction centers from Rhodobacter sphaeroides: Quantum efficiency and X-ray structure. Biochemistry 2005, 44 (18), 6920-6928.
- 3. Allen, J. P.; Feher, G.; Yeates, T. O.; Komiya, H.; Rees, D. C. Structure of the Reaction Center from Rhodobacter-Sphaeroides R-26 the Cofactors .1. Proceedings of the National Academy of Sciences of the United States of America 1987, 84 (16), 5730-5734.
- 4. Deisenhofer, J.; Michel, H. Structures of Bacterial Photosynthetic Reaction Centers. Annual Review of Cell Biology 1991, 7, 1-23.
- 5. Nogi, T.; Miki, K. Structural basis of bacterial photosynthetic reaction centers. Journal of Biochemistry 2001, 130 (3), 319-329.
- 6. de Boer, A. L.; Neerken, S.; de Wijn, R.; Permentier, H. P.; Gast, P.; Vijgenboom, E.; Hoff, A. J. High yield of B-branch electron transfer in a quadruple reaction center mutant of the photosynthetic bacterium Rhodobacter sphaeroides. Biochemistry 2002, 41 (9), 3081-3088.
- 7. de Boer, A. L.; Neerken, S.; de Wijn, R.; Permentier, H. P.; Gast, P.; Vijgenboom, E.; Hoff, A. J. B-branch electron transfer in reaction centers of Rhodobacter sphaeroides assessed with site-directed mutagenesis. Photosynthesis Research 2002, 71 (3), 221-239.
- 8. Frolov, D.; Wakeham, M. C.; Andrizhiyevskaya, E. G.; Jones, M. R.; van, G. R. Investigation of B-branch electron transfer by femtosecond time resolved spectroscopy in a Rhodobacter sphaeroides reaction centre that lacks the Q(A) ubiquinone. Biochim. Biophys. Acta 2005, 1707 (2-3), 189-198.

- 9. Haffa, A. L. M.; Lin, S.; Williams, J. C.; Bowen, B. P.; Taguchi, A. K. W.; Allen, J. P.; Woodbury, N. W. Controlling the pathway of photosynthetic charge separation in bacterial reaction centers. Journal of Physical Chemistry B 2004, 108 (1), 4-7.
- 10. Hartwich, G.; Bieser, G.; Langenbacher, T.; Muller, P.; Richter, M.; Ogrodnik, A.; Scheer, H.; MichelBeyerle, M. E. B-branch electron transfer in bacterial photosynthetic reaction centers by energetically activating A-branch charge separation. Biophysical Journal 1997, 72 (2).
- 11. Kirmaier, C.; Laible, P. D.; Hanson, D. K.; Holten, D. B-side charge separation in bacterial photosynthetic reaction centers: Nanosecond time scale electron transfer from H-B(-) to Q(B). Biochemistry 2003, 42 (7), 2016-2024.
- 12. Laible, P. D.; Kirmaier, C.; Udawatte, C. S. M.; Hofman, S. J.; Holten, D.; Hanson, D. K. Quinone reduction via secondary B-branch electron transfer in mutant bacterial reaction centers. Biochemistry 2003, 42 (6), 1718-1730.
- Marchanka, A.; Savitsky, A.; Lubitz, W.; Mobius, K.; van Gastel, M. B-Branch Electron Transfer in the Photosynthetic Reaction Center of a Rhodobacter sphaeroides Quadruple Mutant Q- and W-Band Electron Paramagnetic Resonance Studies of Triplet and Radical-Pair Cofactor States. Journal of Physical Chemistry B 2010, 114 (45), 14364-14372.
- 14. Davis, J. J.; Morgan, D. A.; Wrathmell, C. L.; Axford, D. N.; Zhao, J.; Wang, N. Molecular bioelectronics. Journal of Materials Chemistry 2005, 15 (22), 2160-2174.
- Kondo, M.; Iida, K.; Dewa, T.; Tanaka, H.; Ogawa, T.; Nagashima, S.; Nagashima, K. V. P.; Shimada, K.; Hashimoto, H.; Gardiner, A. T.; Cogdell, R. J.; Nango, M. Photocurrent and Electronic Activities of Oriented-His-Tagged Photosynthetic Light-Harvesting/Reaction Center Core Complexes Assembled onto a Gold Electrode. Biomacromolecules 2012, 13 (2), 432-438.
- 16. Mikayama, T.; Miyashita, T.; Iida, K.; Suemori, Y.; Nango, M. Electron transfer mediated by photosynthetic reaction center proteins between two chemical-modified metal electrodes. Molecular Crystals and Liquid Crystals 2006, 445, 291-296.
- 17. Reiss, B. D.; Hanson, D. K.; Firestone, M. A. Evaluation of the photosynthetic reaction center protein for potential use as a bioelectronic circuit element. Biotechnology Progress 2007, 23 (4), 985-989.
- 18. Song, H.; Lee, H.; Lee, T. Characterization of the tip-loading force-dependent tunneling behavior in alkanethiol metal-molecule-metal junctions by conducting atomic force microscopy. Ultramicroscopy 2008, 108 (10), 1196-1199.
- Stamouli, A.; Frenken, J. W. M.; Oosterkamp, T. H.; Cogdell, R. J.; Aartsma, T. J. The electron conduction of photosynthetic protein complexes embedded in a membrane. Febs Letters 2004, 560 (1-3), 109-114.
- Xi, W.; Zhang, W.; An, B. K.; Burn, P. L.; Davis, J. J. Tunnelling conductance of vectorial porphyrin monolayers. Journal of Materials Chemistry 2008, 18 (26), 3109-3120.
- 21. McAuley, K. E.; Fyfe, P. K.; Ridge, J. P.; Cogdell, R. J.; Isaacs, N. W.; Jones, M. R. Ubiquinone binding, ubiquinone exclusion, and detailed cofactor conformation in a mutant bacterial reaction center. Biochemistry 2000, 39 (49), 15032-15043.
- Ridge, J. P.; van Brederode, M. E.; Goodwin, M. G.; van Grondelle, R.; Jones, M. R. Mutations that modify or exclude binding of the QA ubiquinone and carotenoid in the reaction center from Rhodobacter sphaeroides. Photosynthesis Research 1999, 59 (1), 9-26.

- 23. Wakeham, M. C.; Goodwin, M. G.; McKibbin, C.; Jones, M. R. Photo-accumulation of the P+QB- radical pair state in purple bacterial reaction centres that lack the QA ubiquinone. FEBS Lett. 2003, 540 (1-3), 234-240.
- 24. Watson, A. J.; Fyfe, P. K.; Frolov, D.; Wakeham, M. C.; Nabedryk, E.; Van Grondelle, R.; Breton, J.; Jones, M. R. Replacement or exclusion of the B-branch bacteriopheophytin in the purple bacterial reaction centre: The H-B cofactor is not required for assembly or core function of the Rhodobacter sphaeroides complex. Biochimica et Biophysica Acta-Bioenergetics 2005, 1710 (1), 34-46.
- Jones, M. R.; Heerdawson, M.; Mattioli, T. A.; Hunter, C. N.; Robert, B. Site-Specific Mutagenesis of the Reaction-Center from Rhodobacter-Sphaeroides Studied by Fourier-Transform Raman-Spectroscopy - Mutations at Tyrosine M210 do Not Affect the Electronic-Structure of the Primary Donor. Febs Letters 1994, 339 (1-2), 18-24.
- 26. Wakeham, M. C.; Breton, J.; Nabedryk, E.; Jones, M. R. Formation of a semiquinone at the QB site by A- or B-branch electron transfer in the reaction center from Rhodobacter sphaeroides. Biochemistry 2004, 43 (16), 4755-4763.
- 27. van Baarle, G. J. C.; Troianovski, A. M.; Nishizaki, T.; Kes, P. H.; Aarts, J. Imaging of vortex configurations in thin films by scanning-tunneling microscopy. Applied Physics Letters 2003, 82 (7), 1081-1083.
- Straley, S. C.; Parson, W. W.; MAUZERAL.DC; Clayton, R. K. Pigment Content and Molar Extinction Coefficients of Photochemical Reaction Centers from Rhodopseudomonas-Spheroides. Biochimica et Biophysica Acta 1973, 305 (3), 597-609.
- 29. Semchonok, D. A.; Chauvin, J. P.; Frese, R. N.; Jungas, C.; Boekema, E. J. Structure of the dimeric RC-LH1-PufX complex from Rhodobaca bogoriensis investigated by electron microscopy. Philosophical Transactions of the Royal Society B-Biological Sciences 2012, 367 (1608), 3412-3419.
- 30. Alegria, G.; Dutton, P. L. Langmuir-Blodgett Monolayer Films of Bacterial Photosynthetic Membranes and Isolated Reaction Centers Preparation, Spectrophotometric and Electrochemical Characterization .1. Biochimica et Biophysica Acta 1991, 1057 (2), 239-257.
- 31. Lu, Y.; Xu, J.; Liu, B.; Kong, J. Photosynthetic reaction center functionalized nano-composite films: effective strategies for probing and exploiting the photo-induced electron transfer of photosensitive membrane protein. Biosens. Bioelectron. 2007, 22 (7), 1173-1185.
- 32. Yasuda, Y.; Hirata, Y.; Sugino, H.; Kumei, M.; Hara, M.; Miyake, J.; Fujihira, M. Langmuir-Blodgett-Films of Reaction Centers of Rhodopseudomonas-Viridis Photoelectric Characteristics. Thin Solid Films 1992, 210 (1-2), 733-735.
- 33. Yasuda, Y.; Sugino, H.; Toyotama, H.; Hirata, Y.; Hara, M.; Miyake, J. Control of Protein Orientation in Molecular Photoelectric Devices Using Langmuir-Blodgett-Films of Photosynthetic Reaction Centers from Rhodopseudomonas-Viridis. Bioelectrochemistry and Bioenergetics 1994, 34 (2), 135-139.
- 34. Zaitsev, S. Y.; Kalabina, N. A.; Zubov, V. P.; Lukashev, E. P.; Kononenko, A. A.; Uphaus, R. A. Monolayers of Photosynthetic Reaction Centers of Green and Purple Bacteria. Thin Solid Films 1992, 210 (1-2), 723-725.
- 35. Lu, Y. D.; Xu, J. J.; Liu, B. H.; Kong, J. L. Photosynthetic reaction center functionalized nano-composite films: Effective strategies for probing and exploiting the photo-induced electron transfer of photosensitive membrane protein. Biosensors & Bioelectronics 2007, 22 (7), 1173-1185.

- 36. Lukashev, E. P.; Nadtochenko, V. A.; Permenova, E. P.; Sarkisov, O. M.; Rubin, A. B. Electron phototransfer between photosynthetic reaction centers of the bacteria Rhodobacter sphaeroides and semiconductor mesoporous TiO2 films. Doklady Biochemistry and Biophysics 2007, 415 (1), 211-216.
- 37. Nakamura, C.; Hasegawa, M.; Yasuda, Y.; Miyake, J. Self-assembling photosynthetic reaction centers on electrodes for current generation. Applied Biochemistry and Biotechnology 2000, 84-6, 401-408.
- 38. Trammell, S. A.; Wang, L. Y.; Zullo, J. M.; Shashidhar, R.; Lebedev, N. Orientated binding of photosynthetic reaction centers on gold using Ni-NTA self-assembled monolayers. Biosensors & Bioelectronics 2004, 19 (12), 1649-1655.
- 39. Trammell, S. A.; Spano, A.; Price, R.; Lebedev, N. Effect of protein orientation on electron transfer between photosynthetic reaction centers and carbon electrodes. Biosensors & Bioelectronics 2006, 21 (7), 1023-1028.
- Trammell, S. A.; Griva, I.; Spano, A.; Tsoi, S.; Tender, L. M.; Schnur, J.; Lebedev, N. Effects of distance and driving force on photoinduced electron transfer between photosynthetic reaction centers and gold electrodes. Journal of Physical Chemistry C 2007, 111 (45), 17122-17130.
- 41. Ueno, T.; Hara, M.; Kamo, N.; Fujii, T.; Miyake, J. Control of the unidirectional topological orientation of a cross-linked complex composed of the bacterial photosynthetic reaction center and horse heart cytochrome c reconstituted into proteoliposomes. Journal of Biochemistry 1998, 124 (3), 485-490.
- 42. den Hollander, M. J.; Magis, J. G.; Fuchsenberger, P.; Aartsma, T. J.; Jones, M. R.; Frese, R. N. Enhanced Photocurrent Generation by Photosynthetic Bacterial Reaction Centers through Molecular Relays, Light-Harvesting Complexes, and Direct Protein-Gold Interactions. Langmuir 2011, 27 (16), 10282-10294.
- Lebedev, N.; Trammell, S. A.; Spano, A.; Lukashev, E.; Griva, I.; Schnur, J. Conductive wiring of immobilized photosynthetic reaction center to electrode by cytochrome c. Journal of the American Chemical Society 2006, 128 (37), 12044-12045.
- 44. Leopold, M. C.; Bowden, E. F. Influence of gold substrate topography on the voltammetry of cytochrome c adsorbed on carboxylic acid terminated self-assembled monolayers. Langmuir 2002, 18 (6), 2239-2245.
- 45. Zhu, Z. Y.; Gunner, M. R. Energetics of quinone-dependent electron and proton transfers in Rhodobacter sphaeroides photosynthetic reaction centers. Biochemistry 2005, 44 (1), 82-96.
- Lee, I.; Lee, J. W.; Greenbaum, E. Biomolecular electronics: Vectorial arrays of photosynthetic reaction centers. Physical Review Letters 1997, 79 (17), 3294-3297.

Summary

Natural photosynthesis relies on the interplay between various types of energyharvesting protein complexes, structurally well-defined biopolymers with embedded light absorbing chromophores which are held in exact geometries. The primary photo-conversion reactions within a photosynthetic system involve light absorption, energy transfer and charge transfer, and can reach intrinsic quantum efficiencies near unity. Recent decades have accumulated a wealth of knowledge about assembly and functional mechanisms of these protein complexes. There is a growing interest to exploit these complexes not only by mimicking their functionality but also to utilize these and other proteins for various applications, ranging from bioelectronics to biosensors and biosolar fuel cells. The initial steps of light absorption and charge separation performed by photosynthetic complexes are very efficient; the challenge lies in exploiting this process by functionally coupling the proteins to a solid support for alternative ways of energy conversion. To be able to use these complexes for any such application, immobilization of isolated pigment-protein complexes under ambient conditions on conducting surfaces while keeping their functional integrity intact is one of the prerequisites. The electronic communication of pigment-protein complexes with an electrode will depend on the electron-transfer efficiency from protein complex to the electrode and vice versa.

In the work described in this thesis, we studied different preparations and various methods of interfacing the pigment-protein complexes with a bare gold electrode, and compared the performance of immobilized complexes by measuring light-induced current generation and current-voltage (I-V) characteristics of these complexes, under ambient conditions.

Chapter 1 provides a brief introduction to the protein complexes and experimental techniques used to study these complexes.

For the work described in Chapter 2 we have prepared 2-dimensional (2D) crystals of the pigment-protein complex RC-LH1¹ isolated from *Rhodopseudomonas* acidophila and compared the performance of these complexes with that of detergent-solubilized RC-LH1 complexes by using photo-electrochemistry. Our data show that the photocurrent generation by 2D-crystals of RC-LH1 complexes, a more native-like environment, is higher than from a RC-LH1 layer formed by adsorption from a detergent solution, and out-competes excitation quenching by the gold electrode. Current-voltage spectroscopy of 2D crystals of RC-LH1 complexes was also studied by conductive atomic force microscopy (C-AFM). By AFM feedback the contact force applied by the scanning probe tip can be precisely controlled. At low contact force current-voltage curves show an asymmetric, diodelike behavior which is characteristic of the co-factors of the reaction-center (RC) complex. Additional support for this assignment is provided in Chapter 4 of this thesis. At higher contact forces we observe superposed on this signal a symmetric component. By suitably fitting the data with the Simmons model, the symmetric and asymmetric part of the I-V curves can be resolved quantitatively. The symmetric part can be attributed to the so-called LH1 ring of light-harvesting 1 complexes, which is architecturally similar to the light harvesting 2 (LH2) complexes. For comparison, we have also performed current-voltage spectroscopy of 2D crystals of LH2 complexes embedded in a lipid bilayer, in which case the RC contribution is absent. LH2 exhibits highly symmetric current-voltage curves around V=0, consistent with previous reports. Junction parameters were calculated by fitting the I-V curves with the Simmons model.

In Chapter 3 we report on the investigation of RC-LH1 complex from *Rhodopseudomonas (Rps.) acidophila*, deposited by the Langmuir Blodgett method on a bare gold electrode. By this method we were able to interface the pigment protein complexes with the electrode in a defined orientation. The close proximity

-

¹ The RC-LH1 complex from purple bacteria consists of a reaction center (RC) complex incorporated at the center of a circular array of light-harvesting 1 (LH1) protein subunits. Energy is absorbed by the bacteriochlorophyll pigments contained in the LH1 complex, which is then transferred to the RC complex where it initiates a chain of electron transfer reactions by which the absorbed energy is stabilized and converted to a chemically useful form, serving the metabolism of the bacterial cell.

of the protein complex and the gold electrode, and optimal orientation of the complex resulted in a very high photocurrent with remarkable quantum efficiency. We obtained a photocurrent density of $45~\mu\text{A/cm}^2$ at an incident light intensity of $23~\text{mW/cm}^2$ with internal quantum efficiency of 32~%, which is the highest to date for a monolayer of any photosynthetic protein complex.

In Chapter 4, we examine the role of co-factors in transmembrane electron transfer in bacterial reaction center (RC) complexes. Two mutants of an antenna deficient strain of *Rhodobacter sphaeroides* were studied regarding light-induced current generation and current-voltage spectroscopy, by utilizing photoelectrochemistry and C-AFM. Using the Langmuir-Blodgett method to assemble monolayers of RC-membrane fragments we obtain a dense packing, while the layer is easily transferred to a gold electrode. These layers show a high degree of orientation, with the periplasmic side of the RC complexes facing the gold surface. Direct electron transfer from the gold surface to the RC was observed. Electron tunneling by C-AFM is completely blocked in quinone-depleted reaction centers, while absence of the bacteriopheophytin in the so-called inactive branch has no effect. We conclude that electron tunneling occurs exclusively along the A-branch of the reaction center.

From our data we conclude that the photosynthetic pigment protein complexes, RC-LH1 and RC can be interfaced with a bare gold electrode retaining their functionality of light absorption and electron transfer under ambient conditions. The possibility of controlling the orientation of RC-LH1 complex on bare gold electrode is also demonstrated by exploiting Langmuir Blodgett deposition methods, resulting in the highest ever quantum efficiency of photocurrent generation of 32% measured for a monolayer of protein complexes on a gold electrode, resulting in a relatively high current density. 2D crystals of RC-LH1 provide a native-like environment to the complexes, which improves their performance of energy transfer despite their close proximity to the gold surface.

Samenvatting

Natuurlijke fotosynthese is gebaseerd op de wisselwerking tussen verschillende energie-oogstende eiwitcomplexen, structureel welomschreven biopolymeren met ingebouwde, licht-absorberende pigmenten die ruimtelijk heel precies georiënteerd zijn. De primaire, licht-geïnduceerde reacties binnen een fotosynthetisch systeem leiden tot lichtabsorptie, energieoverdracht en overdracht van lading, met een intrinsiek kwantumrendement van bijna 100%. In de afgelopen decennia is een schat aan kennis opgebouwd over de structuur, de cellulaire architectuur, en de functionele mechanismen van deze eiwitcomplexen. Er is groeiende belangstelling om deze kennis te benutten, niet alleen door het nabootsen van hun functionaliteit, maar ook door het gebruik van deze en andere eiwitten voor diverse toepassingen, variërend van bioelectronica tot biosensoren en (zonlicht-gedreven) biobrandstofcellen. De eerste stappen in het proces van fotosynthetische lichtabsorptie en ladingsscheiding zijn zeer efficiënt; de uitdaging ligt in het benutten van dit proces door de eiwitten functioneel te koppelen aan een vaste drager, en onderdeel te maken van een elektronische schakeling voor alternatieve manieren van energieconversie. Om een dergelijke toepassing te realiseren is immobilisatie van geïsoleerde pigment-eiwitcomplexen op een geschikt oppervlak onder standaard condities noodzakelijk, waarbij behoud van functionele integriteit één van de voorwaarden is. De efficiëntie waarmee elektronen onder invloed van licht kunnen worden overgedragen van het eiwitcomplex naar de elektrode, en vice versa, wordt bepaald door de onderlinge elektronische wisselwerking.

In dit proefschift worden de resultaten beschreven van het onderzoek aan verschillende fotosynthetisch preparaten in combinatie met diverse methoden om de pigment-eiwitcomplexen te koppelen aan een kale goud-elektrode. De eigenschappen van deze gefunctionaliseerde elektrodes werden onderzocht en onderling vergeleken door kwantitatieve metingen van licht-geïnduceerde stroomontwikkeling en van stroom-spanning (I-V) karakteristieken onder standaard condities.

Hoofdstuk 1 geeft een korte beschrijving van de pigment-eiwitcomplexen en van de experimentele technieken die in de loop van dit onderzoek werden gebruikt.

Voor het in hoofdstuk 2 beschreven onderzoek hebben we 2-dimensionale (2D) kristallen het pigment-eiwitcomplex gemaakt van RC-LH1 Rhodopseudomonas acidophila. Na adsorptie van deze 2D kristallen op een goudelektrode werd de activiteit daarvan gemeten met behulp van foto-elektrochemie, en vergeleken met die van een RC-LH1 laag geadsorbeerd uit oplossing. De metingen tonen aan dat in het laatste geval licht-geïnduceerde stroomontwikkeling door RC-LH1 minder efficient is dan met 2D kristallen die een meer natuurlijke omgeving bieden. Electrontunneling werd bestudeerd door de I-V karakteristiek van 2D-kristallen van RC-LH1 complexen te meten met geleidende atomaire krachtmicroscopie (C-AFM). Hierbij wordt een scherpe naald in contact gebracht met een 2D-kristal dat op een goud-elektrode is geadsorbeerd, waarna een spanningsverschil wordt aangelegd tussen de AFM-naald en de electrode. Met AFM kan de kracht die de naald uitoefent nauwkeurig worden geregeld. De grafiek van de stroom als functie van de aangelegde spanning is in het algemeen asymmetrisch rond V=0, en is samengesteld uit een symmetrische en een asymmetrische component. De symmetrische component kan worden toegeschreven aan de bijdrage van het LH1 complex, en is karakteristiek voor electrontunneling door een smalle energiebarriere. Deze interpretatie wordt ondersteund door metingen aan 2D-kristallen van LH2, die eveneens een symmetrische I-V karakteristiek geven; LH2 heeft een vergelijkbare structuur als LH1, maar er is geen RC aanwezig. De asymmetrische component in de RC-LH1 metingen, die alleen een significante stroom laat zien bij positieve spanningen, wordt daarom toegeschreven aan de bijdrage van het RC. Deze conclusie wordt ondersteund door het werk dat in hoofdstuk 4 wordt beschreven. De I-V karakeristiek van de RC component is kenmerkend voor het gedrag van een diode. De relatieve bijdragen van de symmetrische en antisymmetrische componenten kan kwantitatief worden bepaald met behulp van het Simmons model voor electrontunneling. In beide gevallen neemt de stroom toe met de uitgeoefende kracht, maar bij lage kracht wordt alleen de RC bijdrage gemeten.

In hoofdstuk 3 rapporteren we over het onderzoek aan het RC-LH1 complex van Rhodopseudomonas (Rps.) acidophila, gedeponeerd op een kale goud-elektrode

met behulp van de Langmuir-Blodgett techniek. Met deze werkwijze konden we de pigment-eiwitcomplexen in een gedefinieerde oriëntatie binden aan de elektrode. De korte afstand tussen de eiwicomplexen en de goud-elektrode, in combinatie met een optimale oriëntatie, resulteerde in een zeer hoge licht-geïnduceerde stroom met een opmerkelijk hoge kwantumefficiëntie. Wij maten een stroomdichtheid van 45 μ A/cm² bij een invallende lichtsterkte van 23 mW/cm², overeenkomend met een intern kwantumrendement van 32%, het hoogste dat tot op heden is gemeten voor een monolaag van fotosynthetische eiwitcomplexen.

In hoofdstuk 4 onderzoeken we de rol van co-factoren in membraan-overspannende elektronoverdracht in bacteriële RC complexen. Twee mutanten van een antennedeficiënte stam van Rhodobacter sphaeroides werden onderzocht met betrekking tot licht-geïnduceerde stroomontwikkeling en I-V karakeristieken, door gebruik te maken van fotoelectrochemie en stroom-geleidende atomaire kracht microscopie (C-AFM). Met behulp van de Langmuir-Blodgett methode werden monolagen van RC-bevattende membraanfragmenten gevormd, waardoor een dichte pakking werd verkregen, terwijl de laag gemakkelijk kon worden overgedragen op een goudelektrode. Deze lagen toonden een hoge mate van oriëntatie, met de periplasmatische kant van de RC complexen tegenover het goud-oppervlak, of omgekeerd. Onder invloed van een aangelegde spanning tussen de AFM-naald (in contact met de bovenkant van de monolaag) en de goud-electrode werd directe elektronoverdracht van het goud-oppervlak naar het RC waargenomen. Electrontunneling, gemeten met C-AFM, is echter volledig geblokkeerd in chinonverarmde reactie centra, terwijl het ontbreken van bacteriofeofytine in de zogenaamde inactieve tak van het RC geen effect heeft. We leiden daaruit af dat elektrontunneling uitsluitend plaats vindt langs de A-tak van het reactie centrum, zoals ook in het natuurlijke, licht-geïnduceerde proces wordt waargenomen.

Uit onze gegevens concluderen wij dat de fotosynthetische pigment-eiwit complexen, RC-LH1 en RC, effectief kunnen worden gekoppeld met een kale goudelektrode onder standaard condities, met behoud van hun functionaliteit wat betreft lichtabsorptie en electronoverdacht. Door gebruik te maken van Langmuir-Blodgett depositiemethoden kan de oriëntatie van RC-LH1 complexen op de goudelektrode worden gecontroleerd, waardoor het hoogste tot dusver gemeten kwantumrendement werd waargenomen voor een monolaag van fotosynthetische

eiwitcomplexen, met een relatief hoge stroomdichtheid. Twee-dimensionale kristallen van RC-LH1 bieden een natuurlijke omgeving voor deze complexen, die - wanneer gekoppeld aan een geschikte elektrode - de efficiëntie van energieoverdracht en stroomontwikkeling kan verbeteren, ondanks de wisselwerking met de goudlaag, die in principe aanleiding kan geven tot niet-functionele energiedissipatie.

Acknowledgments

I wish to acknowledge the contributions of a number people who provided me with technical support and assistance during my stay in the lab: Federica Galli for helping out with scanning probe techniques, Marcel Hesselberth and Daan Boltje for assisting with thin film deposition, Armand Tepper for setting up the electrochemistry experiments, Ruud Kuyvenhoven for help with computer-related problems, and Yvonne Kerkhof for administrative matters.

Part of the work presented in this thesis was performed in the laboratory of Raoul Frese at the Free University, Amsterdam, with the help of David Delgado and Vincent Friebe.

A big thanks to my lab fellows including Razvan, Fan-Tso, Namik, Nusrat, Mohsen, Miqyas, Saptaswa, Maria, Mihaela, Ankur, Bishwajit and Lionel for their enjoyable company in and outside the lab.

I am very grateful to my parents and brothers for their encouragement and unconditional support throughout my career.

Curriculum Vitae

Muhammad Kamran was born on March 15th, 1981, in Rawalpindi, Pakistan. After completing the high school curriculum with pre-engineering in 2000, he attended Kahuta College (associated with Punjab University) for a Bachelor of Science degree with Physics and Mathematics as major subjects. The BSc degree was awarded in 2002. Subsequently he studied at Quaid-i-Azam University, Islamabad, where he obtained a MSc degree in physics in 2004. While working as lecturer of physics at Kahuta College he studied at the Quaid-i-Azam University, Islamabad, for a M. Phil. degree in physics which he obtained in 2007.

At the end of 2007 he was awarded a fellowship from the Higher Education Commission (HEC) of Pakistan for pursuing further academic training and education abroad. After successfully completing complementary course work at the Leiden Institute of Physics he started a Ph.D. research project in 2009, supervised by Prof. Dr. T.J. Aartsma. The results of his research are described in this thesis.